INTERCALATION OF CONDUCTIVE POLYMERS INTO LAYERED STRUCTURES

A Thesis

Submitted to the Graduate Faculty

In Partial Fulfillment of the Requirements

For the Degree of

Master of Science

In the Department of Chemistry

Faculty of Science

University of Prince Edward Island

© Stephen F. Scully

Charlottetown, P.E.I

April 2007

Reproduced with permission of the copyright owner. Further reproduction prohibited without permission.

Library and Archives Canada

Published Heritage Branch

395 Wellington Street
Ottawa ON K1A 0N4
Canada

Bibliothèque et Archives Canada

Direction du Patrimoine de l'édition

395, rue Wellington
Ottawa ON K1A 0N4
Canada

Your file Votre référence
ISBN: 978-0-494-32108-9
Our file Notre référence
ISBN: 978-0-494-32108-9

NOTICE:
The author has granted a non-exclusive license allowing Library and Archives Canada to reproduce, publish, archive, preserve, conserve, communicate to the public by telecommunication or on the Internet, loan, distribute and sell theses worldwide, for commercial or non-commercial purposes, in microform, paper, electronic and/or any other formats.

The author retains copyright ownership and moral rights in this thesis. Neither the thesis nor substantial extracts from it may be printed or otherwise reproduced without the author's permission.

AVIS:
L'auteur a accordé une licence non exclusive permettant à la Bibliothèque et Archives Canada de reproduire, publier, archiver, sauvegarder, conserver, transmettre au public par télécommunication ou par l'Internet, prêter, distribuer et vendre des thèses partout dans le monde, à des fins commerciales ou autres, sur support microforme, papier, électronique et/ou autres formats.

L'auteur conserve la propriété du droit d'auteur et des droits moraux qui protège cette thèse. Ni la thèse ni des extraits substantiels de celle-ci ne doivent être imprimés ou autrement reproduits sans son autorisation.

In compliance with the Canadian Privacy Act some supporting forms may have been removed from this thesis.

While these forms may be included in the document page count, their removal does not represent any loss of content from the thesis.

Conformément à la loi canadienne sur la protection de la vie privée, quelques formulaires secondaires ont été enlevés de cette thèse.

Bien que ces formulaires aient inclus dans la pagination, il n'y aura aucun contenu manquant.

Canada

Reproduced with permission of the copyright owner. Further reproduction prohibited without permission.

SIGNATURE PAGE

(i)

REMOVED

Reproduced with permission of the copyright owner. Further reproduction prohibited without permission.

SIGNATURE PAGE

(ii)

REMOVED

Reproduced with permission of the copyright owner. Further reproduction prohibited without permission.

Abstract

The goal of this project was to investigate the host-guest intercalation chemistry of electroactive polymers with two dimensional layered compounds.

Aniline, 2-methylaniline, 2-ethylaniline, and 2-propylaniline were intercalated between the layers of iron oxychloride (FeOCl), an oxidizing structure, whereupon oxidation of the monomer afforded polyanilines between the layers. Electrical conductivity measurements indicate an increase in electrical conductivity of the nanocomposites compared with the pristine layered structure.

Aniline monomers were intercalated between the layers of hydrogen titanate ($HTiO_2$) through an acid-base type interaction. The aniline intercalated titanate was heated in air to oxidize the aniline monomers which resulted in polymerization of the monomers to yield polyaniline intercalated titanate.

Attempts to intercalate ionically conductive polymers between the layers of titanate were unsuccessful but indicated that layered TiO_2 has a strong affinity for intercalation of small positively charged species such as H^+.

The highly ion conducting polymer poly(bis-(methoxyethoxyethoxy)phosphazene) was complexed with lithium triflate and intercalated into graphite oxide. The isolated product appears to be graphite reinforced polymer rather than a true intercalation compound but physical stabilization of the polymer is apparent.

The insertion of lithium ions into natural hectorite has been accomplished and a study of its ion conducting properties has shown good room temperature ion conductivity.

Reproduced with permission of the copyright owner. Further reproduction prohibited without permission.

All materials have been characterized by powder X-ray diffraction, FTIR, TGA, and DSC where suitable. Electrical conductivities were investigated using the four probe van der Pauw technique while ionic conductivity was determined through AC impedance spectroscopy.

Reproduced with permission of the copyright owner. Further reproduction prohibited without permission.

Acknowledgments

I would like to thank Dr. Rabin Bissessur, my supervisor, for providing me with the opportunity to work in his lab over the past four years. It has been a pleasure to work in a materials chemistry lab and the skills that I developed during my time spent there will undoubtedly be priceless in the future.

Dr. Doug Dahn from the UPEI Physics Department also deserves many thanks for all of his time, effort, and help with respect to the physical characterizations of my project and for being my co-supervisor. I always enjoyed visiting his lab and learning about the physics side of my project.

The entire Chemistry Department at UPEI also deserves my thanks as I feel that you have provided me with a very solid background in the basics of chemistry which allows me to confidently approach both teaching and research environments, but also for being friends as well as teachers, a quality which I believe is not present at many other institutions.

A special thanks to Dawna Lund who was instrumental in the completion of my work. I am very gracious to Dawna for taking the time to ensure that I understood how to properly use all instrumentation in the department and was always available to help if there was any kind of technical problem. I must also thank Dawna for the many interesting conversation which we had over the years both in and out of the lab!

I must also acknowledge Dr. Christian LaCroix and his students for their time and help with scanning electron microscopy on my compounds.

Reproduced with permission of the copyright owner. Further reproduction prohibited without permission.

I would like to acknowledge my lab mates including my brother Kevin Scully, and friends Peter Liu and Derek Schipper for making life interesting!

Finally I would like to thank Mr. Lloyd Theuerkauf, my high school chemistry teacher, for guiding me down the path of chemistry and continuing to be a good friend to this day.

Reproduced with permission of the copyright owner. Further reproduction prohibited without permission.

Table of Contents

Reproduced with permission of the copyright owner. Further reproduction prohibited without permission.

Reproduced with permission of the copyright owner. Further reproduction prohibited without permission.

List of Figures

Reproduced with permission of the copyright owner. Further reproduction prohibited without permission.

Reproduced with permission of the copyright owner. Further reproduction prohibited without permission.

List of Tables

Reproduced with permission of the copyright owner. Further reproduction prohibited without permission.

List of Abbreviations

DSC - Differential Scanning Calorimetry

FTIR - Fourier Transform Infra Red

GO - Graphite Oxide

$HTiO_2$ - $H_xTi_{2-x/4}\square_{x/4}O_4 \bullet yH_2O$

MEEP - Poly[bis-(methoxyethoxyethoxy)phosphazene]

PANI - Poly(aniline)

PEG - Poly(ethylene glycol)

PEO - Poly(ethylene oxide)

POMOE - Poly[oxymethylene-(oxyethylene)]

PVP - Poly(vinyl pyrrolidone)

SEM - Scanning Electron Microscopy

TBA - Tetrabutylammonium

TBAOH - Tetrabutylammonium Hydroxide

TGA - Thermo Gravimetric Analysis

XRD - X-ray Diffraction

Reproduced with permission of the copyright owner. Further reproduction prohibited without permission.

Chapter 1: Introduction

1.1 Background

Today's society has a thirst for information which is unable to be quenched. There is a huge demand for information to be made rapidly available to us whether it be as simple as what time it is or as complex as the fastest route from your house to a meeting. To suit this undying appetite for information almost every tool and machine which traditionally could only be used in the home or office has been turned into a mobile device. Cell phones, blackberries™, laptops, handheld GPS systems, and Personal Data Assistants (PDA's) are just a few examples of this mobile and wireless revolution. While all of these devices have revolutionized the information industry there is a constant demand for these devices to be made even more advanced and mobile through designing smaller, lighter, and faster machines. The development of these devices continuously pushes the limits of all areas of technology [1].

A common element in all mobile devices is that a battery is required for them to operate. As the devices become smaller the batteries which power them must also become smaller without compromising the power which can be delivered. As such, the advancement of mobile technology also pushes the boundaries of battery development.

1.1.1 The Voltaic Cell

The battery is a relatively new device in terms of human history. It is only recently that we have "mastered" the use of electricity and its storage in devices such as batteries. The Greeks first observed static electricity around 600 BCE but it was Otto von Guericke who first studied it in the 1660's. Alessandro Volta pioneered the field of

Reproduced with permission of the copyright owner. Further reproduction prohibited without permission.

batteries in 1800 with the discovery that when certain metals were immersed in specific solutions electricity was generated [2].

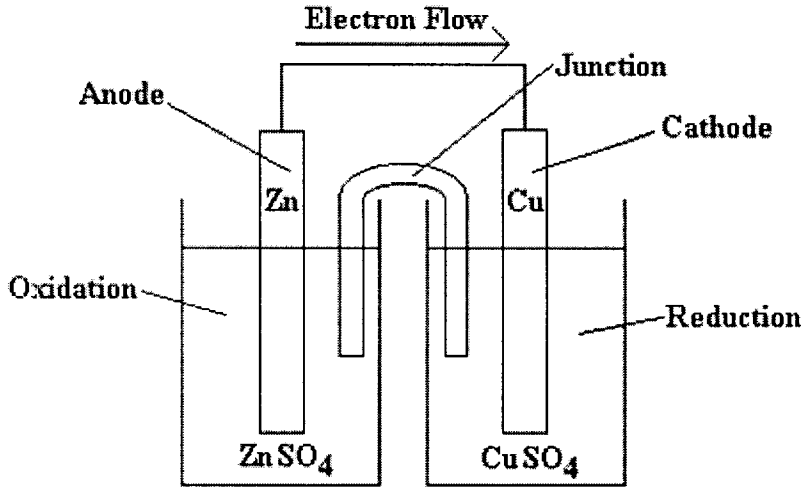

Figure 1 - Voltaic Cell [3]

The voltaic cell was of relatively simple design. Electricity was generated via a redox reaction between two metals called the electrodes. The two metals are called the anode and cathode where oxidation and reduction occur, respectively. Upon oxidation of the anode the metal is ionized resulting in ion migration into solution while the electrons travel through the wire to the cathode. Metal ions in solution around the cathode are reduced and deposited on the surface of the cathode. For this process to occur the electrodes must be bathed in a solution of one of their salts called an electrolyte solution. Finally, for the cell to function the two electrolyte solutions must be connected via a junction commonly called a salt bridge which facilitates charge balance in the cell. The discovery of the voltaic cell sparked a frenzy of research and discovery in the area of electricity and batteries which has lead to the invention of our current battery technologies.

Reproduced with permission of the copyright owner. Further reproduction prohibited without permission.

1.2 Current Battery Chemistries

Today there are five or six different battery chemistries which dominate the battery market. The major chemistries in use today are the lead acid, nickel cadmium, nickel-metal hydride, reusable alkaline, lithium ion, and lithium ion polymer systems. A brief comparison of these battery systems follows.

1.2.1 The Lead Acid Battery

The lead acid battery is the first example of a rechargeable battery released for public use. The chemistry was invented in 1859 by Gaston Plante and involves lead, lead oxide and sulfuric acid. During discharge lead is oxidized by sulfuric acid to yield lead sulfate and water, releasing energy in the form of electricity in the process. This process can be reversed by the addition of an electric charge to the cell resulting in regeneration of the sulfuric acid and lead, also known as charging. The reaction which occurs in the cell is shown in scheme 1.

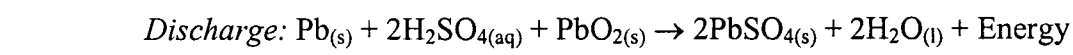

Discharge: $Pb_{(s)} + 2H_2SO_{4(aq)} + PbO_{2(s)} \rightarrow 2PbSO_{4(s)} + 2H_2O_{(l)} + \text{Energy}$

Scheme 1 – Discharge of lead acid batteries

The lead acid battery is very common where large power and current demands exist, such as in cars and uninterrupted power supplies. While the lead acid battery is capable of delivering a lot of power, it is very bulky and heavy resulting in low energy density, the amount of power per unit volume or mass. The lead acid battery has advantages in that it is cheap and requires low maintenance, but lacks in the area of

Reproduced with permission of the copyright owner. Further reproduction prohibited without permission.

cycling. Full discharge of lead acid batteries is severely detrimental to their operation to the extent that they may no longer function if completely discharged. They are also very poor with regards to environmental friendliness. These batteries are generally used in "stand-by" applications where discharge of the cells is rarely required [3].

1.2.2 The Nickel Cadmium Battery

The first example of a Ni-Cd battery was its invention in 1899 by Waldmar Jungner. It was not until the mid 1900's that methods for completely sealing and containing gases emitted during discharge of the cells were developed enabling construction of the batteries we know today. The chemistry of Ni-Cd batteries involves the oxidation of NiOOH by Cadmium metal in KOH solution as depicted in scheme 2 [4].

$$\textit{Anode}: Cd_{(s)} + 2OH^-_{(l)} \rightarrow Cd(OH)_{2(l)} + 2e^-$$

$$\textit{Cathode}: NiOOH_{(s)} + H_2O_{(l)} + e^- \rightarrow Ni(OH)_{2(s)} + 2OH^-_{(l)}$$

$$\textit{Overall}: Cd_{(s)} + 2NiO(OH)_{(s)} + 2H_2O_{(l)} \rightarrow Cd(OH)_{2(l)} + 2Ni(OH)_{2(s)}$$

Scheme 2 – Discharge of Nickel Cadmium Battery

The Nickel Cadmium battery is a real workhorse battery. It can take relatively severe punishment and still operate perfectly with no loss of performance. Contrary to the lead acid chemistry, Ni-Cd's can be discharged fully with minimal impact to their performance. In fact, it is actually beneficial to fully discharge and charge these batteries periodically to prevent a "memory" effect which in essence is a decrease in capacity for the cell. The Ni-Cd battery also differs from the lead acid battery in the area of charging in that it can be charged at a much higher rate which adds to its popularity as a

Reproduced with permission of the copyright owner. Further reproduction prohibited without permission.

commercial rechargeable battery. The Ni-Cd battery really performs well in all areas displaying good charge rates, performance characteristics, shelf life, cost, and availability. The major drawbacks of this chemistry are the memory effects which plague the battery, followed by sub par energy density compared with new batteries, the toxicity and environmental impacts of the cadmium metal in particular, and the self discharge which occurs over time. Today's major applications of these batteries include portable communication devices such as two way radios, portable power tools, and professional camera equipment. While these batteries dominated the rechargeable battery market for many years, newer battery technologies have recently been cutting into the nickel cadmium market [2].

1.2.3 The Nickel-Metal Hydride Battery

Research on the nickel-metal hydride (NiMH) battery stems from research on a very closely related battery system called the nickel hydrogen battery. Pioneering work was started in the 1950's but it wasn't until the 1980's when new discoveries in the area of hydrogen storage made the idea feasible. In fact, NiMH batteries are very closely related to Ni-Cd batteries with the exception of the anode. In NiMH batteries a mixture of metals is used for the anode. The Cadmium anode was replaced with mixture of metals in varying concentrations which had the ability to store hydrogen. The discharge chemistry of the battery is depicted in scheme 3 [5].

Anode: $(1/n)MH_{n(s)} + OH^-_{(aq)} \rightarrow (1/n)M_{(s)} + H_2O_{(l)} + e^-$

Cathode: $NiOOH_{(s)} + H_2O_{(aq)} + e^- \rightarrow Ni(OH)_{2(s)} + OH^-_{(aq)}$

Overall: $NiOOH_{(s)} + (1/n)MH_{n(s)} \rightarrow Ni(OH)_{2(s)} + (1/n)M_{(s)}$

Scheme 3 – Discharge of Nickel Metal Hydride Battery

Reproduced with permission of the copyright owner. Further reproduction prohibited without permission.

The NiMH battery when compared to Ni-Cd batteries is slightly better in almost every way. The overall potential of the cell is identical to that of Ni-Cd batteries but the NiMH batteries have higher energy density giving them a slight edge. They also do not suffer the memory effect anywhere close to what the Ni-Cd batteries experience and perhaps most importantly they are far less toxic to the environment. The only drawbacks to the NiMH system are that deep discharging of the cell can lead to premature failure and that charging is more complex due to thermal issues which can develop if charge rates are too high. The cost of these cells is also slightly more compared to the Ni-Cd cells. The only battery to which the NiMH falls short is the lithium/lithium-ion battery [2].

1.2.4 The Lithium/Lithium ion Battery

The newest and current technology of choice for batteries is by far that of the lithium, or more precisely lithium-ion battery. While pioneering work on lithium battery systems began in 1912 with the work of G. N. Lewis, it was not until the 1970's that lithium battery technology was commercialized. Using lithium in batteries was a logical step as it is the lightest metal and yields the highest energy for its mass. The obvious obstacle for using lithium in a battery is its extreme reactivity. The reactivity of lithium did turn out to be a large and crippling obstacle. While lithium batteries were used in mobile devices for a short time, an incident in Japan in 1991 occurred where a battery in a cell phone exploded causing severe burns to a man's face. The result of this incident was a recall of all lithium batteries for public use.

The problem with lithium batteries was discovered to be a thermal runaway issue where during discharge of the cell, the temperature would rise to a critical point where

Reproduced with permission of the copyright owner. Further reproduction prohibited without permission.

the lithium anode would reach its melting point. From here reactions within the cell would lead to explosive and flammable gases being produced which are severely dangerous to anyone using the batteries. Later that same year Sony released a revised battery chemistry based on lithium called the lithium-ion battery [6].

The lithium ion battery is very similar to every other type of battery on the market as far as its composition. In general, the construction of a lithium ion battery consists of a lithium intercalated anode and a metal oxide cathode separated by some electrolyte material which varies depending on the type of lithium ion battery. The basic structure of a lithium ion cell is shown in figure 2.

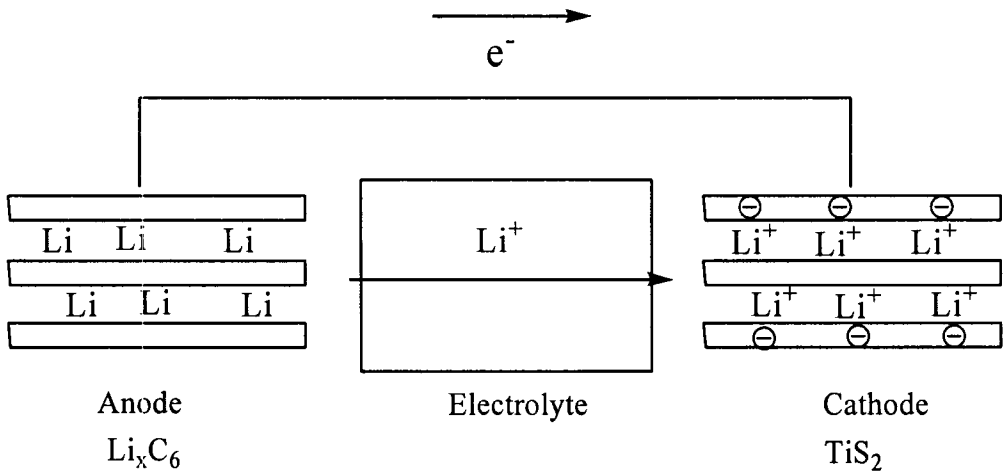

Figure 2 - Classical Lithium Ion Cell

When the battery is fully charged the anode is electron rich and contains many lithium ions for charge balance. During discharge, a spontaneous redox reaction occurs between the anode and cathode via electron flow external to the cell through the load or device being powered. Lithium ions flow through the electrolyte from the anode to the cathode resulting in an overall lower energy system. The free energy evolved through this

Reproduced with permission of the copyright owner. Further reproduction prohibited without permission.

process is harnessed to do work or power the device. The end result, as in the beginning, is a cell with an overall neutral charge.

Overall the lithium ion battery performs very well when compared to other battery chemistries. As a battery, it is lighter and smaller than its counterparts while maintaining superior energy density (exactly what the mobile market needs). While the lithium ion battery does not have increased capacity when compared to other battery chemistries, it compensates for this fact by providing up to three times the voltage for a single cell that other cells can provide. This means that a single lithium ion cell can do the job of three alternate cells which is part of the reason that lithium ion batteries can be made so small. The negative to lithium ion batteries is a small protection circuit must be included in every battery to prevent thermal runaway conditions from occurring which makes the cells more costly than the alternatives [7].

1.3 Research on Lithium Ion Batteries

Due to the superiority and utility of the lithium ion battery, there is a large amount of research with regards to further development of this system. This research has focused on the three major components of the lithium ion battery, namely the anode, cathode, and electrolyte.

1.3.1 The Anode

The anode is the source of both electrons and lithium ions in a lithium ion battery. Upon the discovery that lithium was not a feasible anode material for everyday lithium batteries the carbon anode was introduced for lithium ion applications. The first example of an anode material was lithium intercalated graphite. Graphite was an excellent choice

Reproduced with permission of the copyright owner. Further reproduction prohibited without permission.

for anode materials as it displays a flat discharge curve and has very high reversibility with respect to lithium intercalation.

Graphite has long served as the anode for lithium ion batteries, but new technology is demanding higher cell capacities which have put a severe strain on the ability of the carbon anode. The search for new materials to replace carbon anodes has been intensive but not fruitful. Carbon is hard to replace as an anode due to its low cost and high availability. Adding to the perseverance of carbon is its well understood chemistry and excellent electrochemical behavior [8].

Work on potential anode systems other than carbon can be traced back as far as 1966 but none have outperformed carbon in long term applications [9,10]. There have been many systems which show promise to increased capacity when compared to carbon such as those of silicon but upon cycling they display large changes in volume which results in cracking of the electrode and loss of capacity [11]. The problem of excessive volume change in the anode remains to be a major issue even today [12]. Recent work with metal oxides has also shown promise as possible replacements for carbon but the work is in early stages and still requires development [13,14,15].

1.3.2 The Cathode

The cathode is the site of reduction in the battery and is also where lithium ions end up during discharge. As such cathodes must be good conductors of both lithium ions and electricity. Much research has been performed in the area of cathodes primarily due to the fact that existing cathode systems such as $LiCoO_2$ are toxic and expensive [7]. The low cost of carbon has made improvements of batteries through new anodes difficult and as a result research has focused more on the cathode for cell improvement.

Reproduced with permission of the copyright owner. Further reproduction prohibited without permission.

The main elements of a good cathode were recently outlined in a review by M. Stanley Whittingham and are outlined as follows:

1. Presence of a redox active species such as a transition metal
2. Reversible intercalation of lithium ions
3. Reaction with lithium has high free energy
4. Fast reaction with lithium
5. Good electrical conductivity
6. Stable
7. Low Cost
8. Environmentally friendly

Early cathodes were composed of layered materials such as TiS_2 and $LiCoO_2$. Recent work has focused on non-layered materials such as $LiFePO_4$ and other similar transition metal phosphate systems which offer a cheaper alternative to their layered counterparts [16].

1.3.2.1 Layered Cathodes

In the early 1970's it was discovered that intercalation of electron donating species into tantalum disulfide caused an increase in the superconducting temperature of the material by a factor of three [17]. These results prompted research which led to the discovery that intercalation reactions could be promoted in electrochemical cells [18, 19].

Titanium disulfide was the first choice for research as a cathode material primarily due to it being the lightest dichalcogenide [20-23]. Another advantage of the TiS_2 system was the lack of a phase change upon lithium intercalation. The lack of a

Reproduced with permission of the copyright owner. Further reproduction prohibited without permission.

phase change ensured that lithium could be both removed from the structure, and removed quickly [24]. Titanium disulfide cathodes displayed both good cycling and reversibility and as such Exxon commercialized small batteries from 1977-1979 using it as the cathode [25].

Researchers later began to investigate layered oxides, beginning with V_2O_5 and MoO_3. Molybdenum trioxide showed early promise due to a lithium loading of about 1.5 lithium ions per molybdenum but was abandoned when it displayed low reaction rates [26-28]. Vanadium pentoxide was also dismissed as a cathode material due to multiple phase transitions leading to a broad potential range over its discharge curve coupled with poor cyclability [29]. Recently, new research has focused on vanadium oxide compounds and xerogels where some improvements have been seen with regard to capacity; although rate is still a limiting factor [30-34].

Goodenough first showed that $LiCoO_2$ could be used as a cathode when he demonstrated electrochemical lithium removal [35]. Sony coupled the $LiCoO_2$ cathode with the carbon anode in 1991 to yield the first commercial lithium ion battery whose chemistry is still used to this day [36, 37]. While the $LiCoO_2$ cathode has enjoyed long term use, it has faced several issues including low capacity and variable conductivities across lithium content and temperature reaching upwards of six orders of magnitude [38]. Recently, Cho revealed that coating $LiCoO_2$ with metal oxide or phosphate compounds can increase the capacity of the cathode material enhancing its utility [39-43]. One of the major driving forces for continued research in the area of cathodes has been that $LiCoO_2$ cathodes are limited to smaller cells used for devices such as cell phones. This limitation arises from limited cobalt stocks which in turn drives the cost up. A large number of

Reproduced with permission of the copyright owner. Further reproduction prohibited without permission.

alternate layered cathodes have been investigated but none have been found to be superior enough to the $LiCoO_2$ system to warrant its replacement [16].

1.3.2.2 Iron Containing Cathodes

Cathodes based on the olivine structure, a 3D versus the usual 2D or layered structure, have received much attention recently due to the discovery of their favorable properties in 1997. In particular $LiFePO_4$ has been the focus of research as it displays good cell potential, cyclability, and capacity. Iron containing cathodes are of interest due to the abundance of iron and low cost of materials. This low cost combined with the promising electrochemical properties of $LiFePO_4$ make it a strong candidate for the replacement of the more traditional $LiCoO_2$ cathode [44]. Due to this promise, much research has been invested in the development of the $LiFePO_4$ system [45-57]. One downfall of the $LiFePO_4$ is its low electrical conductivity. As such much of the research on the $LiFePO_4$ has focused on improving the electrical conductivity. A breakthrough in this area was the discovery that doping the material with certain elements can increase the conductivity by up to eight orders of magnitude [56].

Some research has focused on the cobalt, manganese, and nickel derivatives of the $LiMPO_4$ olivine structure system but have all proven inferior to $LiFePO_4$ [58]. Some alternate iron phosphate systems such as $Li_3Fe_2(PO_4)_3$ [46, 59, 60] and $FePO_4 \bullet nH_2O$ [61-63] have also been investigated as well, however yielding more disappointing performances.

Reproduced with permission of the copyright owner. Further reproduction prohibited without permission.

1.3.3 The Electrolyte

The electrolyte is perhaps one of the most important areas of battery research today. The electrolyte serves a dual purpose in a battery, both being very important to the performance of the overall system. The first purpose of the electrolyte is to electrically isolate the anode and the cathode from one another so that the cell does not short circuit. This electrical isolation forces the electrons to go external to the cell and power the desired device. The second purpose of the electrolyte is to facilitate ion flow or transport from the anode to the cathode in order to maintain overall charge balance in the cell. In order for these materials to be effective they must display very high resistance to electrical flow but very high and fast ionic conductivity as the current which can be delivered by the battery is related to how fast ions can be transferred through the electrolyte [64-65]. Relative to the electrodes, little research has been invested into electrolyte materials. Most electrolytes are variations on existing systems primarily due to the fact that it is cheaper to use what is already available. This is an important fact due to the low profit margins in the battery industry. While the adaptation of existing electrolytes allows for increased profit, it is at the sacrifice of battery performance. A large amount of growth has occurred in the lithium ion market in the past few years. In 2000, Japan controlled 94% of the battery market but as a result of the global growth their dominance has fallen to 65%. This rapid growth in the battery industry has created increased demand for battery separators (electrolytes) resulting in increased separator research [66].

There are two main classes of electrolyte that have evolved, namely the liquid organic electrolyte and the polymer electrolyte.

Reproduced with permission of the copyright owner. Further reproduction prohibited without permission.

1.3.3.1 Liquid Organic Electrolytes

Due to the potential range of lithium ion batteries, aqueous electrolytes are not an option as they would decompose. An alternative is the use of lithium salts dissolved in organic solvents. This system can be used provided that it is stable across the potential range of the cell and remains in the liquid phase across the range of operating temperatures. The ionic conductivity of an electrolyte is a function of the number and mobility of the lithium ions. Therefore, viscous liquids are disfavored over more fluid solvents [67].

Some groups have investigated the effect of using mixed solvent electrolytes [68, 69]. While many different combinations of organic liquids have been tested in batteries, the effect of the dissolved lithium salt on cells has also been a major focus of research [70-72]. From this research it has been found that $LiPF_6$ tends to perform the best and as a result is often used for liquid electrolyte systems [67]. One major drawback of all liquid electrolyte batteries is the effort that must be made to prevent the electrolyte from leaking from the cell. Also, some liquids are electrically conductive and require an electrical barrier be placed between the electrodes to prevent short circuits. Both of these points lead to increased volume, weight, and cost of battery construction.

1.3.3.2 Polymer Electrolytes

Recently there has been increasing interest and research into the development of polymer based electrolyte systems. The use of polymers as electrolytes is exciting for several reasons. Firstly, polymer used for ion transport would be electrically insulating, electrically isolating the two electrodes, yet facilitating ion flow. Secondly, and perhaps more importantly, polymers are much easier to contain than liquids and as such the cell

Reproduced with permission of the copyright owner. Further reproduction prohibited without permission.

construction could be simplified reducing volume, cost and weight [73]. The preferred characteristics of modern polymer electrolytes are as follows:

1. High lithium ion conduction between -20°C and 60°C
2. Electrically insulating
3. Environmentally friendly
4. Mechanically, thermally, and electrochemically stable between -20°C and 60°C

The theory of the polymer electrolyte is that if you have electron rich functionalities within the polymer chain, they will coordinate lithium ion and aid in the migration of lithium from one electrode to the other. Polymers are either amorphous or crystalline and while it has generally been believed that the amorphous phase contributes to ionic conductivity there has been some dispute as to which phase is responsible for conduction.

The mechanism for ion transport through polymers is thought to be a phenomenon known as segmental motion. Segmental motion is essentially flexing of the polymer chains and it is through this flexing which lithium ions are thought to be moved along the length of a polymer. Lithium transport through segmental motion is illustrated in figure 3.

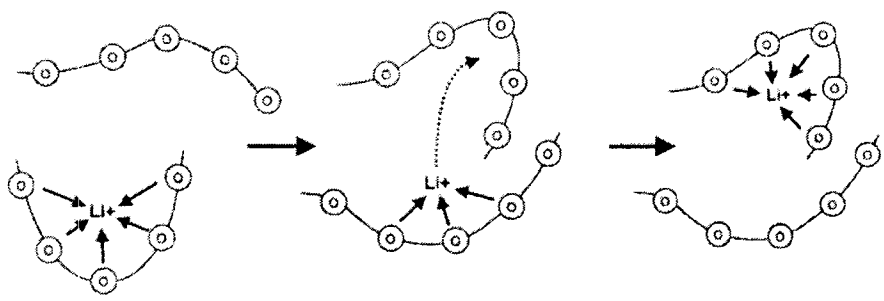

Figure 3 - Ion Transport via Segmental Motion [1]

Reproduced with permission of the copyright owner. Further reproduction prohibited without permission.

The glass transition temperature of a polymer is an important property which can be described as the temperature at which a polymer changes from a crystalline phase to an amorphous phase. Theoretically, the lower the glass transition temperature of the polymer, the better it should facilitate ion flow. While the glass transition temperature of a polymer is analogous to a melting point it is important to note that after its glass transition temperature the polymer does remain a solid, but as a rule of thumb the lower the transition the gummier the polymer [1]. Polymer electrolytes can be divided into three categories: Solid polymer electrolytes, gel polymer electrolytes, and composite polymer electrolytes.

1.3.3.2.1 Solid Polymer Electrolytes

Ionic conduction in solids was first documented by Faraday in 1834 when he reported the conduction of silver ions through silver sulfide [74]. The use of a completely solid polymer electrolyte in a battery is yet to be realized commercially but is being heavily researched. The solid polymer electrolyte would offer the highest possible energy density, easiest packaging, and lowest cost of manufacturing [75]. The advantages of solid polymer electrolytes are clear, yet the challenge is inadequate ion conduction. The diffusion of ions through a completely solid medium is understandably difficult and in order to be a feasible electrolyte conductivities must be of the order of 10^{-3} S/cm or higher at 25°C [76].

The first ion conduction in a polymer was shown by Wright in 1973 when he observed conduction of alkali metals salts in poly(ethylene oxide) (PEO) [77, 78]. It was not until 1978 that Armand proposed the use of these ion conducting polymers in batteries but his proposal sparked a new field of research which has essentially dominated

Reproduced with permission of the copyright owner. Further reproduction prohibited without permission.

electrolyte research ever since [79]. For PEO based systems high room temperature conductivities have been elusive, most being in the range of 10^{-6} S/cm.

Possibly the best candidate yet for a solid polymer electrolyte has been poly(bis-(methoxyethoxyethoxy)phosphazene) (MEEP), which displays a room temperature conductivity of 4 x 10^{-4} S/cm when complexed with lithium triflate ($LiCF_3SO_3$) in the ratio $(MEEP)_{4.0}LiCF_3SO_3$ [80]. The problem with MEEP and most other polymers which display good room temperature conductivities is they tend to be mechanically unstable or fluid. This creates the potential for the polymers to leak out of the cell over time destroying the battery. To counter this problem measures could be taken to seal the cell but this is counterproductive in regards to the goal of solid polymer electrolytes. Some modern research has focused on methods of increasing the mechanical stability of these polymers so that leakage is not a problem. A reasonable degree of success has been obtained in this area upon the incorporation of fine ceramic powders into the polymer [6].

1.3.3.2.2 Gel Polymer Electrolytes

Gel polymer electrolytes consist of ionically conductive polymers which are mixed with organic liquids called plasticizers. This type of electrolyte was first demonstrated in 1975 by Feullade and Perche [81]. The addition of plasticizers allows for increased segmental motion coupled with liquid like properties which accounts for the increased conductivities [67]. Abraham and Alamgir have been able to attain conductivities in the order of 1.7 x 10^{-3} S/cm at 25°C and 1.1 x 10^{-3} S/cm at -10°C using a poly(acrylonitrile) polymer mixed with ethylene carbonate, propylene carbonate, and $LiClO_4$ [82]. While these conductivities are in the realm of potential electrolytes, gelled electrolytes face some problems which still must be overcome. Gelled electrolytes are

Reproduced with permission of the copyright owner. Further reproduction prohibited without permission.

subject to a phenomenon known as the syneresis effect where the plasticizers separate from the polymers under long term storage conditions. This causes increased electrolyte viscosity and substantial reduction in cell viability [83, 84].

1.3.3.2.3 Composite Polymer Electrolytes

Solid polymer electrolytes and gelled polymer electrolytes, while showing promise, appear to have too many complications to be viable for use in modern batteries. Composite polymer electrolytes are ion conducting polymers that have been physically mixed with other compounds to engender new properties [85]. Several papers published have indicated that composite polymer electrolytes are the key to achieving solid polymer electrolyte materials [6, 86, 87].

Weston and Steele initially described the effect of adding α-alumina, an electrochemically inert inorganic material, to PEO in 1982 [88]. This work resulted in a significant increase in mechanical stability and ionic conductivity in PEO. Further work has seen the incorporation of ceramic fillers, ionites, zeolites, glasses, and even fiberglass into ionically conductive polymers [6, 86, 87, 89-94]. Observed increases in ionic mobility are attributed to a decrease in crystallization of the polymer matrix [92, 95].

The highest polymer electrolyte conductivities to date were achieved by Wasiucionek and Breiter through the incorporation of electrolyte materials into sol-gels. The incorporation of 0.2 M LiCl in methanol/water into sols yielded ionic conductivity in the area of 1×10^{-2} S/cm, well within the required limits for an electrolyte material [96].

Few reports exist on the incorporation of composite electrolyte materials into batteries although it is interesting to note that increased electrode stability has been observed in the presence of the composite electrolyte systems [75]. The increase in both

Reproduced with permission of the copyright owner. Further reproduction prohibited without permission.

ionic conductivity and electrolyte stability coupled with enhanced electrode stability indicate that the composite electrolyte materials may have a strong foothold in the future of polymer electrolyte battery applications.

1.4 Intercalation Chemistry

Intercalation chemistry was first demonstrated by Schaffäutl in 1841 when he reported the insertion of sulphate ions into graphite [97]. Intercalation chemistry can be defined as the inclusion of a guest species into the structure of some solid [98]. Two-dimensional layered structures can be envisioned as slices of bread stacked in such a way that there is a regular gap between layers. The gap between the layers has many descriptive terms such as gallery space, lamella, and interlayer [99]. Each layer in a 2D structure is composed of the same grouping of atoms separated by some small distance usually termed d. Adjacent layers in such compounds are held together via van der Waals forces. A general representation of a layered material is shown in figure 4.

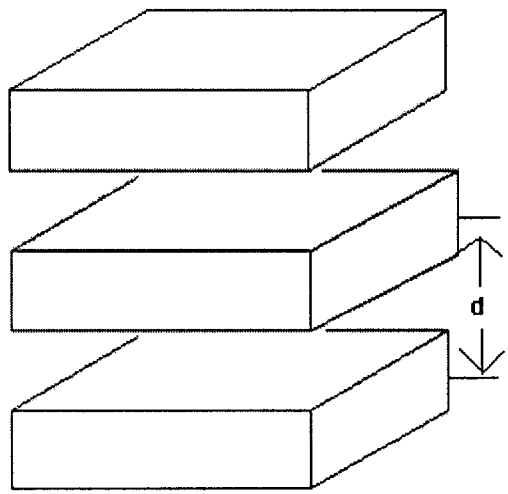

Figure 4 - 2D Layered Structure

Reproduced with permission of the copyright owner. Further reproduction prohibited without permission.

There are many examples of layered compounds, perhaps most common being graphite and clay. Many examples of layered materials containing transition metals have also appeared. The insertion of atoms, molecules, and polymers between the layers of such species has long been of interest due to the interesting properties which emerge upon the intercalation of these moieties [100]. The nanocomposite materials which result from intercalation into 2D structures often display enhanced thermal and mechanical properties, especially in the case of intercalated polymers [99].

1.5 Iron Oxychloride

Iron Oxychloride (FeOCl) was first reported in 1935 by Goldstaub [101]. FeOCl belongs to a group of metal oxyhalides of the form MOX where M = Al, Cr, Fe, In, Ti or V and X = Br or Cl. The chemical structure of FeOCl consists of *cis*-$[FeO_4Cl_2]$ skewed octahedral as shown in figure 5.

Reproduced with permission of the copyright owner. Further reproduction prohibited without permission.

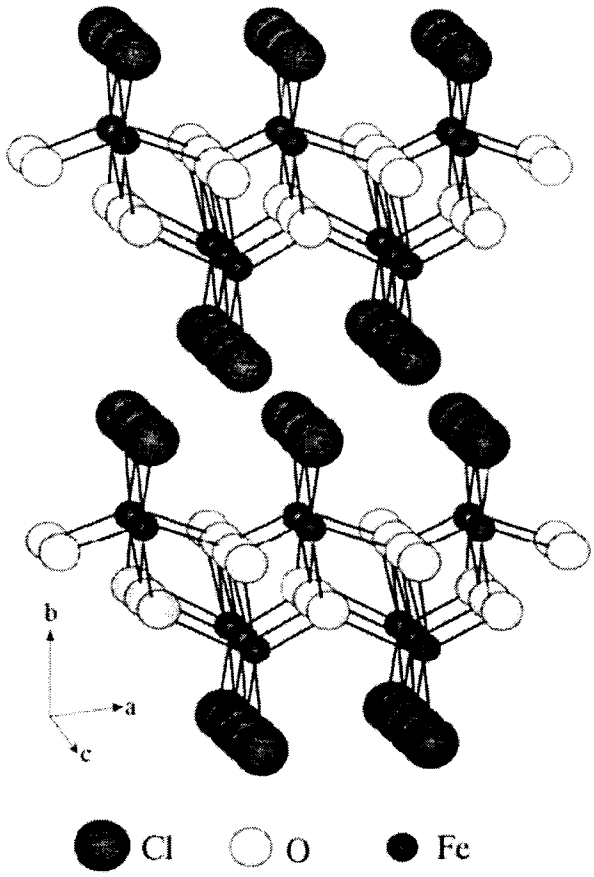

Figure 5 – FeOCl [102]

The intercalation chemistry of FeOCl has been well documented through the insertion of alkali metals, crown ethers, metallocenes, amines, pyridines, phosphines, phosphites, and organophosphates [103-109]. The oxidizing nature of FeOCl has been well known since the 1980's and has offered unique opportunities for intercalation chemistry. Molecules have been inserted into FeOCl and the resulting redox chemistry has been observed on the intercalated molecules [110].

Kanatzidis took advantage of the oxidizing nature of FeOCl to polymerize intercalated pyrrole in 1987 [111]. This was the first instance of a polymerization occurring between the layers of a 2D inorganic structure. The objective of this work was to isolate the polymers in a constrained environment so the structure of the polymers

Reproduced with permission of the copyright owner. Further reproduction prohibited without permission.

could be studied in greater detail. Kanatzidis continued work with the FeOCl system and revealed the polymerization and intercalation of 2,2′-bithiophene in 1989 once again with the premise of understanding the structure of the polymer. It is interesting to note that polymerization of the thiophene monomer does not proceed while the dimer, 2,2′-bithiophene, polymerizes with ease. This was determined to be due to the fact that the anodic potential of thiophene is less positive than that of 2,2′-bithiophene. In fact, it was determined that the redox potential of FeOCl lies between 1.32 and 1.86 volts [112].

The intercalation and polymerization of aniline with FeOCl was reported in 1990, once again by the Kanatzidis group [113]. Further to this communication a full paper was released in 1995 which fully described the aniline/FeOCl system [114]. Kanatzidis revealed a cooperative mechanism between FeOCl and molecular oxygen in the polymerization of aniline. He also showed that intercalated anilinium monomers could be polymerized in the solid product when allowed to sit in air.

Sakaebe et al. tested Kanatzidis' nanocomposites as cathodes for battery applications in 1995 and found promising results with the aniline system. Capacities as high as 210 $mAhg^{-1}$ were observed for some of the aniline composites while the corresponding pyrrole and thiophene composites were poor at 80 $mAhg^{-1}$ or less [115].

FeOCl would be well suited for lithium ion battery applications due to the low cost of iron compounds and the Fe^{3+}/Fe^{2+} redox couple it possesses. While the effect of lithium on FeOCl has been a topic of debate, recent work indicates that chemical lithiation of FeOCl yields a heterogenous product consisting of pristine FeOCl and lithiated FeOCl phases. This work revealed that lithiation of FeOCl leads to a large increase in electrical conductivity of the layered material [116].

Reproduced with permission of the copyright owner. Further reproduction prohibited without permission.

While the intercalation/polymerization of aniline, pyrrole, and 2,2′-bithiophene are well documented for the FeOCl system, there has been no work in the area of substituted derivatives of these materials. Due to the importance of polyaniline we were interested in the investigation of the reactivity of FeOCl towards anilines substituted in the 2 position and the electrical properties of the resulting nanocomposites towards potential cathode materials.

1.6 Titanate

Titanium is surprisingly common on earth's surface ranking ninth in abundance. Of all the forms of titanium which can be found, TiO_2 is the most common. TiO_2 has been used in a variety of applications due to its unique properties. Some areas in which TiO_2 has found applications include photocatalysts, solar cell materials, and various types of coatings [117]. TiO_2 can be found in several forms with the two most prevalent being the anatase and rutile forms. The anatase form of TiO_2 consists of TiO_6 octahedra which share four edges to make an extended 3D structure. The anatase form of TiO_2 is the kinetically favored form and as such when it is heated to 800°C it reverts to the thermodynamic form, rutile. Rutile TiO_2 is chemically equivalent to anatase with the exception that the TiO_6 octahedra share only two edges instead of four. This results in the formation of a layered 2D structure. The transition from anatase to rutile phase maintains a high energy of activation as the conversion is negligible at room temperature [118].

In 1982 the synthesis of titanates with alkali metals within the interlayer was well known. Izawa and coworkers showed that these interlayer alkali metals could be exchanged with protons to yield a protonated phase of TiO_2 [119]. The same research group revealed the acid-base intercalation properties of protonated titanates one year later

Reproduced with permission of the copyright owner. Further reproduction prohibited without permission.

with the intercalation of alkyl ammonium cations [120]. Further research on titanates yielded that suspensions of single layers could be obtained via the reaction of protonated titantate with tetrabutylammonium hydroxide [121, 122].

In 2001 Lerner released a paper which described the intercalation of two polymers between the layers of titanate. The intercalated polymers were poly(ethylene oxide), PEO, and poly(vinyl pyrrolidone), PVP. This was the first instance of the intercalation of a polymer between the layers of titanate [123]. Surprisingly, this has been the only report of intercalation of a polymer between a layered titanate. As a result we were interested in investigating the intercalation properties of TiO_2 with respect to ionically and electrically conductive polymers towards applications in lithium ion battery electrolyte and cathode materials.

1.7 Graphite Oxide

Graphite is a well known allotrope of carbon which is of great importance to society. Due to the favorable properties of graphite, it has found a wide range of applications ranging from golf clubs to pencils and even batteries. Graphite consists of layers of fused benzene rings stacked upon one another. The extended conjugation between the pi orbitals in graphite lead to high electrical conductivity, coupled with its low weight, making it an ideal material for battery applications. The structure of graphite is shown in figure 6.

Reproduced with permission of the copyright owner. Further reproduction prohibited without permission.

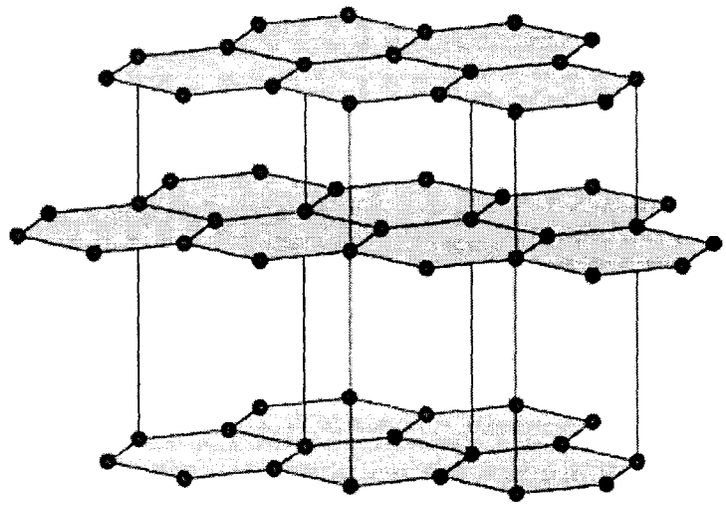

Figure 6 - Structure of Graphite

Graphite has long been used as an anode material for lithium batteries, however the intercalation of polar species into graphite has been dull [124]. The lack of intercalation of polar molecules in graphite is largely the result of the non-polar environment of the interlayer. The intercalation of polar and hydrophilic monomers and polymers is very difficult if not impossible with graphite [125]. The intercalation of chemistry of graphite can be greatly enriched via the oxidation of graphite to graphite oxide.

Graphite oxide is a layered structure which has attracted considerable interest in the areas of fire retardant materials, electrode materials for lithium batteries, and as a biosensor for monitoring DNA hybridization [126-128]. Graphite oxide is synthesized via the chemical oxidation of graphite. The oxidation process leaves the fused benzene ring structure of graphite functionalized with polar groups such as carbonyls, epoxides, and hydroxyls. While the precise structure of graphite oxide is unknown the proposed structure is shown in figure 7.

Reproduced with permission of the copyright owner. Further reproduction prohibited without permission.

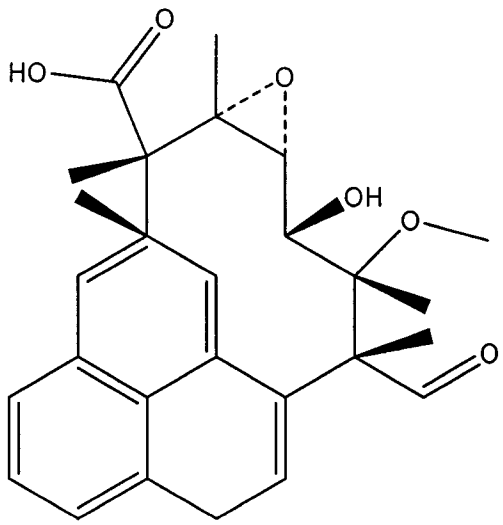

Figure 7 - Proposed Structure of Graphite Oxide [129]

The addition of polar groups to graphite to yield graphite oxide affords a mechanism through which polymers and other polar molecules can be inserted between the layers of graphite oxide. Previous work in the Bissessur group has seen the successful intercalation of polyaniline, polypyrrole, and several ionically conductive polymers between the layers of graphite oxide [130-132]. The intercalation of MEEP within the layers of graphite oxide is as of yet unreported. As such we were interested in the intercalation of MEEP complexed with lithium salts between the layers of graphite oxide and observing the ion conducting properties of the resulting materials.

1.8 Hectorite

Hectorite is a layered aluminosilicate clay mineral which is composed of a corner sharing tetrahedrally coordinated silicon-oxygen network sandwiching an edge-shared octahedral sheet of aluminum. The surfaces of the hectorite layers possess negative

Reproduced with permission of the copyright owner. Further reproduction prohibited without permission.

charges which are countered by sodium and magnesium ions in natural hectorite. The structure of hectorite is shown is figure 8.

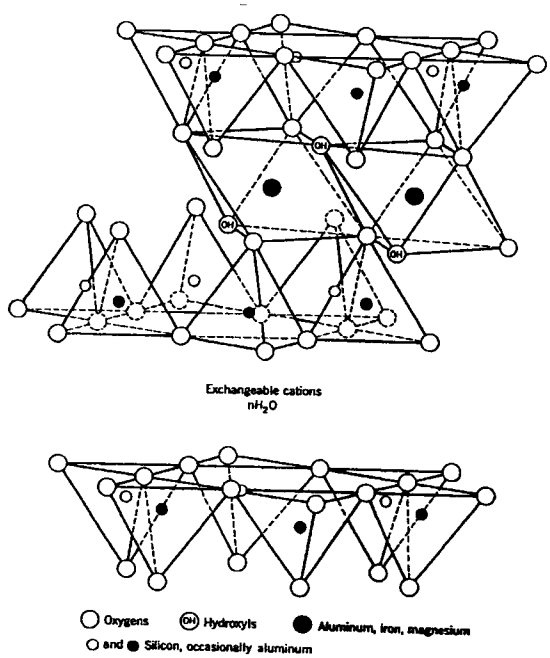

Figure 8 - Structure of Hectorite [133]

One of the favorable properties of hectorite is its ability to exfoliate in water. Mixture of hectorite suspensions with polymers have been shown to create intercalation compounds of hectorite and the polymer [134]. In fact, a very large array of polymers have been intercalated between the layers of hectorite and other similar layered silicates such as montmorillonite. The investigation of the ion conducting properties of polymer/clay nanocomposite materials has been investigated but the focus has been primarily on the PEO and montmorillonite nanocomposite materials [135]. Previous work in the Bissessur group focused on the intercalation of ion conducting polymers between the layers of hectorite. The development of lithium loaded natural hectorite was of

Reproduced with permission of the copyright owner. Further reproduction prohibited without permission.

interest towards the development of electrolyte materials for lithium ion batteries. The intercalation of ion conducting polymers with lithiated natural hectorite could yield highly conductive electrolytes for lithium ion battery applications.

1.9 Mandate of Research

1.9.1 FeOCl

The reactivity of FeOCl towards anilines substituted in the two position was of immediate interest. A systematic study of a series of aniline monomers was to be conducted to describe the effect of substitution of the monomer on both the intercalation and polymerization chemistry of FeOCl. The resulting nanocomposite materials were to be fully characterized and tested for their electrical conductivity to gauge the applicability of the materials towards cathode materials in lithium ion batteries.

1.9.2 Titanate

The exfoliation properties of protonated titanate were to be exploited for the intercalation of ionically conductive polymers. The resulting nanocomposites were to be fully characterized and then screened for their lithium ion conduction ability for application to electrolyte materials for lithium ion batteries.

1.9.3 Graphite Oxide

The intercalation properties of graphite oxide are well established within the Bissessur group although the ion conducting properties have not been investigated. The goal of this project was the intercalation of MEEP complexed with lithium salts between the layers of graphite oxide and the measurement of the ionic conductivity in these materials.

Reproduced with permission of the copyright owner. Further reproduction prohibited without permission.

1.9.4 Hectorite

The goal of the hectorite project was the lithiation of natural hectorite and the intercalation of ion conducting polymers between the layers of the lithium hectorite. Ionic conductivity measurements on these materials could be contrasted to similar layered silicate systems.

Reproduced with permission of the copyright owner. Further reproduction prohibited without permission.

Chapter 2: Experimental

2.1 FeOCl

2.1.1 Reagents and Solvents

Fe_2O_3, $FeCl_3$, and acetonitrile were purchased from Aldrich and used as received without any further purification. Acetone was purchased from Caledon Chemicals and was used with no further purification. Aniline, 2-methylaniline, 2-ethylaniline, and 2-propylaniline were purchased from Aldrich and vacuum distilled using an Aldrich short path distillation apparatus prior to use.

2.1.2 Synthesis of FeOCl

FeOCl was prepared as previously reported [114]. Fe_2O_3 was placed into a Pyrex tube to which 1.4 equivalents of $FeCl_3$ was added. The tube was evacuated and flame sealed using a propane-oxygen flame. Purple crystals were observed after 4 days at 380°C. The contents of the tube were washed over a glass frit with acetone to remove excess $FeCl_3$.

2.1.3 Reaction of Anilines with FeOCl

Freshly distilled anilines were dissolved in acetonitrile to yield 5% (v/v) solutions. The aniline solutions were added to FeOCl such that a ten molar excess of anilines were present compared to FeOCl. The resulting mixtures were stirred via magnetic stirring at room temperature. Samples of the reaction mixtures were pipetted onto glass slides and left to dry in order to probe reaction progress. X-ray diffraction was used to monitor the degree of intercalation of anilines into FeOCl. When the peaks for the pristine FeOCl phase disappeared the reactions were considered complete and the mixtures filtered

Reproduced with permission of the copyright owner. Further reproduction prohibited without permission.

through glass frits under reduced pressure. Products were stored under vacuum prior to characterization.

2.2 Polymers

2.2.1 Poly[oxymethylene-(oxyethylene)]

2.2.1.1 Reagents and Solvents

Dichloromethane, calcium hydride, and potassium hydroxide were purchased from Aldrich and used as received. PEG (MW = 400) was purchased from Aldrich and was dried over molecular sieves (4Å).

2.2.1.2 Synthesis of Poly[oxymethylene-(oxyethylene)]

Poly[oxymethylene-(oxyethylene)] (POMOE) was prepared according to a literature preparation [136]. Dichloromethane was refluxed over CaH_2 for one day to remove moisture from the solvent. The dichloromethane was then distilled under nitrogen. KOH (0.8913 mol) was ground into a fine powder and transferred to a three neck round bottom flask. 2.4 equivalents of the dichloromethane was added to the flask. The flask was stirred mechanically under dry nitrogen purge while one equivalent of PEG was added dropwise from a dropping funnel. The reaction flask was covered with aluminum foil to protect the reaction from light. After two days of stirring, the dichloromethane was removed under reduced pressure and water was added to dissolve the excess KOH. KOH and low molecular weight polymers (<3500) were removed via dialysis until no base could be detected in the dialysis bath. Water was then removed from the pale yellow solution to yield a highly viscous clear polymer.

Reproduced with permission of the copyright owner. Further reproduction prohibited without permission.

2.2.2 Poly[bis-(methoxyethoxyethoxy)phosphazene] (MEEP)

2.2.2.1 Reagents and Solvents

Phosphonitrillic chloride trimer 99.9% ($[PNCl_2]_3$), anhydrous THF, and NaH (95% solid) were purchased from Aldrich and used as received. Di(ethylene glycol) methylether (MEEH) was purchased from Aldrich and dried over 4Å molecular sieves.

2.2.2.2 Synthesis of Poly[bis-(methoxyethoxyethoxy)phosphazene]

Poly[bis-(methoxyethoxyethoxy)phosphazene] (MEEP) was prepared according to a literature method [137]. $[PNCl_2]_3$ was placed into a Pyrex tube which was evacuated and flame sealed. Ring opening polymerization of the trimer occurred through heating the sealed tube in a furnace at 250°C until the molten trimer became viscous over a period of four hours. The tube was removed from the furnace and was allowed to cool to room temperature. The tube was opened under inert atmosphere and the contents transferred to a vacuum sublimator. Excess phosphonitrillic chloride trimer was sublimed at 40°C. The purified poly(dichlorophosphazene) was transferred to a Schlenk flask and dissolved in anhydrous THF (0.0210g polymer/ml THF).

Separately, two equivalents of NaH with respect to the poly-(dichlorophosphazene) repeat unit were placed in a Schlenk flask and dissolved in anhydrous THF (0.0065g NaH/ml THF). This flask was refluxed and a slight excess of MEEH with respect to the NaH was added dropwise via syringe to the mixture. After three hours the reaction mixture turned from a white suspension to a pale yellow solution. This solution was transferred via syringe to the hot poly-(dichlorophosphazene) solution and left to reflux for 24 hours. Volatiles were removed under reduced pressure to yield a viscous gel. Water was added to dissolve the gel and the solution placed in dialysis tubes

Reproduced with permission of the copyright owner. Further reproduction prohibited without permission.

to remove NaCl and low molecular weight polymers (MW<3500). Dialysis was deemed complete when addition of $AgNO_3$ yielded no precipitate. The water was pumped off to leave a pale yellow viscous gel, MEEP.

2.3 Titanate

2.3.1 Reagents and Solvents

Anatase TiO_2, Cs_2CO_3, tetrabutylammonium hydroxide (40 wt. % in water), PEO MW= 100000, and PVP MW= 55000, were purchased from Aldrich and used as received with no further purification. Aniline was purchased from Aldrich and distilled under vacuum using an Aldrich short path distillation apparatus prior to use. $(NH_4)_2S_2O_8$ was purchased from Fisher and was used as received. Concentrated HCl was purchased from Fisher and was used as received. POMOE and MEEP were synthesized as described previously [136, 137].

2.3.2 Synthesis of Protonated Titanate

Synthesis of protonated titanate was performed as per literature method [123]. Anatase TiO_2 (0.0529 mol) was placed in an alumina crucible to which 0.2 equivalents of Cs_2CO_3 was added. The solid mixture was ground to a fine powder and the crucible was capped. The mixture was briefly heated to 800°C in order to remove CO_2 and then reground. The crucible was then placed back in the furnace at 800°C for 20 hours. The white product was reground and then placed back in the furnace for an additional 20 hours. The resulting white material, $Cs_xTi_{2-x/4}\square_{x/4}O_4 \bullet yH_2O$ where $\square$ is a vacancy, was ground to a fine powder.

The protonated form of the titanate was afforded via ion exchange with 1M HCl (0.0108g titanate/ml HCl). The mixture was stirred for 2 days with the HCl being

Reproduced with permission of the copyright owner. Further reproduction prohibited without permission.

replaced every 24 hours. The white protonated titanate, $H_xTi_{2-x/4}\square_{x/4}O_4 \bullet yH_2O$ where x~0.7 and y~1 ($HTiO_2$), was obtained via filtration under reduced pressure.

2.3.3 Exfoliation of Protonated Titanate

Exfoliation of the titanate was afforded via the intercalation of tetrabutylammonium hydroxide (TBAOH). $HTiO_2$ was mixed with aqueous TBAOH such that 0.5 equivalents of the TBAOH was present compared to H^+ in the titanate and 0.0050g of titanate were present per mL of H_2O. The resulting acid-base type intercalation of the alkylammonium ion between the layers of TiO_2 was catalyzed by the sonication of the mixture using a 130W autotune series Cole Parmer ultrasonic processor equipped with a 13mm probe operating at 20 kHz, 30% amplitude for 20 mins. Sonication resulted in the intercalation of TBA^+ ions between the layers which reduces the attraction between the layers sufficiently to induce complete separation or exfoliation of the layers. An exfoliated suspension resulted which remained stable for more than one month.

2.3.4 Intercalation of Polymers

The method of intercalation attempted for the inclusion of polymer chains between the layers of titanate was adapted from the work of Lerner and coworkers [123]. Suspensions of the exfoliated $TBATiO_2$ were taken to which 3 equivalents of aqueous polymer solutions of PEG, PVP, POMOE, and MEEP were added. Upon mixing for several minutes 1M HCl was slowly added to the mixture until gelling of the suspension was observed. After several minutes of stirring the gelled mixtures would be filtered and washed with H_2O. In addition to the method described by Lerner and coworkers, casts of the reaction mixture prior to the addition of acid were attempted. A pH resolved

Reproduced with permission of the copyright owner. Further reproduction prohibited without permission.

experiment was also attempted where the casts of the reaction mixture at varying amounts of added acid were taken to observe the effect of pH on the reaction products. In all cases the product was a white solid material.

2.3.5 Intercalation of Aniline

$HTiO_2$ was placed into an Erlenmeyer flask to which ten equivalents of freshly distilled aniline was added as a 50% (v/v) mixture with H_2O. The resulting mixture was sonicated for four hours on a Fisher brand solid state ultrasonic FS-9 sonicator operating at 75W/45 kHz. Initially aniline and water would make two separate phases but after sonication a stable suspension was created. Upon filtration no intercalation could be observed, however casting yielded a highly oriented intercalated phase. The product was an off-white film which collapsed into a powder.

2.3.6 Polymerization of Aniline-Intercalated TiO_2

The polymerization of aniline intercalated TiO_2 was afforded through oxidation with air. The powdered aniline/titanate nanocomposite was placed in an alumina crucible and placed in a furnace at 140°C for four hours. Upon removal of the crucible the off white powder had became a dark green-black colour.

The polymerization of aniline intercalated TiO_2 was also attempted through the use of $(NH_4)_2S_2O_8$. The method used was similar to that which had been demonstrated by Kanatzidis and coworkers for aniline intercalated MoO_3 [138]. Aniline$_x$TiO2 was placed in an Erlenmeyer flask to which 2 equivalents of an aqueous 0.4M $(NH_4)_2S_2O_8$ cooled to 0°C was added. The reaction was allowed to proceed in a water-ice bath until the reaction mixture began to turn from white to a green-blue colour consistent with the

Reproduced with permission of the copyright owner. Further reproduction prohibited without permission.

polymerization of the aniline monomer. The reaction mixture was then filtered through a glass frit to yield a green powder.

2.4 Graphite Oxide

2.4.1 Reagents and Solvents

Graphite powder and $KMnO_4$ were purchased from Aldrich and used as received without any further purification. H_2SO_4 was purchased from Caledon Chemicals and used as received. H_2O_2 30% was purchased from Fisher Chemicals and used as received.

2.4.2 Synthesis of Graphite Oxide

Graphite oxide was prepared from graphite powder following Hummer's method [139]. 230 mL of concentrated sulfuric acid was placed in a six litre Erlenmeyer flask and cooled to 0°C. Ten grams of graphite powder was added to the flask with magnetic stirring. Thirty grams of the oxidizing agent $KMnO_4$ was slowly added to the flask. After the addition of $KMnO_4$ the flask was allowed to warm to room temperature and 230 mL of H_2O was slowly added. A very rapid increase in temperature was associated with the addition of H_2O and care was taken to keep the temperature below 98°C. Upon completion of the addition of H_2O the flask was left to stir/cool for 15 minutes. 1.4 L of water was then added in a single rapid addition immediately followed by 100 mL of H_2O_2. The addition of the H_2O_2 resulted in some bubbling and the formation of a black material precipitating out of suspension. The supernatant liquid was green in colour and the mixture allowed to sit and settle overnight.

The following day a black solid was observed at the bottom of the flask and the liquid had become clear. Excess supernatant was decanted and the remaining liquid and solid was slurried and transferred into dialysis tubes for dialysis. Dialysis was deemed to

Reproduced with permission of the copyright owner. Further reproduction prohibited without permission.

be complete when no precipitate was observed upon the addition of $BaCl_2$. The water was then removed via freeze-drying to yield a very fine brown powder.

2.4.3 Intercalation of poly[bis-(methoxyethoxyethoxy)phosphazene] into Graphite Oxide

MEEP was synthesized as described previously [137] and mixed with 0.25 equivalents of lithium triflate such that 0.0009g of lithium triflate was dissolved in 1 mL of water. The mixture was sonicated for 20 minutes to dissolve all the polymer. In a separate flask, Graphite Oxide, GO, was dispersed in water such that 0.0009g of GO was dispersed in 1 mL of water. This flask was sonicated for the same period as the flask containing MEEP. The GO suspension was transferred to the MEEP solution and sonicated for an additional 20 minutes. The reaction mixture was stirred for 3 days then placed on the freeze dryer to yield LiMEEP/GO nanocomposite.

2.5 Hectorite

2.5.1 Reagents and Solvents

Sodium hectorite was purchased from the Source Clays Repository and used as received. LiCl was purchased from Fisher and used as received.

2.5.2 Purification of Hectorite

Natural hectorite is a clay mineral mined primarily from Hector California. As such hectorite is laced with impurities. These impurities are primarily in the form of calcite (calcium carbonate), quartz, and other small particles of dirt [140]. As hectorite forms a stable suspension in water the removal of these insoluble impurities is largely accomplished via a sedimentation technique. Typically, 5 grams of hectorite was mixed with 400 mL of water in a 500 mL Erlenmeyer flask which was stirred for one day to

Reproduced with permission of the copyright owner. Further reproduction prohibited without permission.

induce suspension of the hectorite. The flask was then left to sit for three days during which time impurities slowly fell to the bottom of the flask. The resulting pale white translucent supernatant was carefully pipetted to a separate flask which was left to further sediment. This process was repeated until minimal impurities were present in the sample, usually after the third sedimentation.

2.5.3 Lithiation of Hectorite

Purified suspensions of hectorite were centrifuged to yield a hectorite gel. The gels were dispersed in saturated LiCl solutions which were exchanged once a day for three days. After three days the suspension was centrifuged to a gel which was again dispersed in water to help removed excess LiCl. The suspension was centrifuged to a gel and then the dispersion in water was repeated. After centrifuging the resulting gels were placed in a vacuum oven at 100°C for one day. The resulting powder was washed with methanol on a glass frit until no chloride could be detected with the $AgNO_3$ test. The powder was placed in a vacuum oven at 80°C to remove residual methanol.

Reproduced with permission of the copyright owner. Further reproduction prohibited without permission.

Chapter 3 – Results and Discussion

3.1 Instrumentation

Infra-red spectroscopy was run on a Perkin-Elmer 1600 FTIR series instrument or a Bruker Equinox 55 series instrument as pressed KBr pellets.

Powder X-ray diffraction (XRD) was run on a Bruker AXS D8 Advance diffractometer equipped with a graphite monochromator, variable divergence slit, variable antiscatter slit, and a scintillation detector. Cu(Kα) radiation (λ = 1.542 Å) was utilized and the data collection was carried out at room temperature. Samples were loose powders run in air with a scan range of 2 to 60 degrees.

Thermogravimetric analysis (TGA) was performed on a TA 500 instrument under a dry air purge using a heating rate of 10°C/min except for the graphite oxide samples in which a 5°C/min heating rate was used. Differential Scanning Calorimetry (DSC) was performed on a Q100 TA instrument under dry nitrogen purge using a heating rate of 10 °C/min.

Variable temperature van der Pauw electrical conductivity measurements were made using a home built system coupled with a model 350CP CTI Cryogenics closed cycle helium refrigerator. Samples were run as pressed pellets with a diameter of 1.27 cm. Samples were mounted on a copper supported sapphire disk with a weak thermal link to the refrigerating unit. The sample was heated to the desired measurement temperature electrically with temperature control provided by an electronic temperature controller (Lakeshore Cryotronics) utilizing a silicon diode temperature sensor.

Ionic conductivity measurements were made by AC impedance spectroscopy. A Solartron 1250 frequency response analyzer was used to determine the real and imaginary

Reproduced with permission of the copyright owner. Further reproduction prohibited without permission.

components of a sample's impedance and fitted to equivalent circuits using a fitting program called LEVM. LEVM is a free program written by Dr. J. Ross MacDonald at the University of North Carolina and Andiy V. Gorvenko at the National Academy of Sciences of Ukraine and is available for download on the internet at www.jrossmacdonal.com/levminfo.html. The bulk impedance was then extracted from this data whereupon taking the sample geometry into account the ionic conductivity could be calculated. Samples were run either as films cast over painted silver electrodes on glass or as pressed pellets between stainless steel blocking electrodes.

Elemental Analyses were performed at Guelph Chemical Laboratories (Guelph, Ontario).

3.2 FeOCl

FeOCl is not a commercially available compound and therefore had to be synthesized. Reaction of Fe_2O_3 with $FeCl_3$ yields a highly crystalline product. The crystallinity of the product is confirmed by the very strong powder X-ray diffraction pattern as shown in figure 9.

Reproduced with permission of the copyright owner. Further reproduction prohibited without permission.

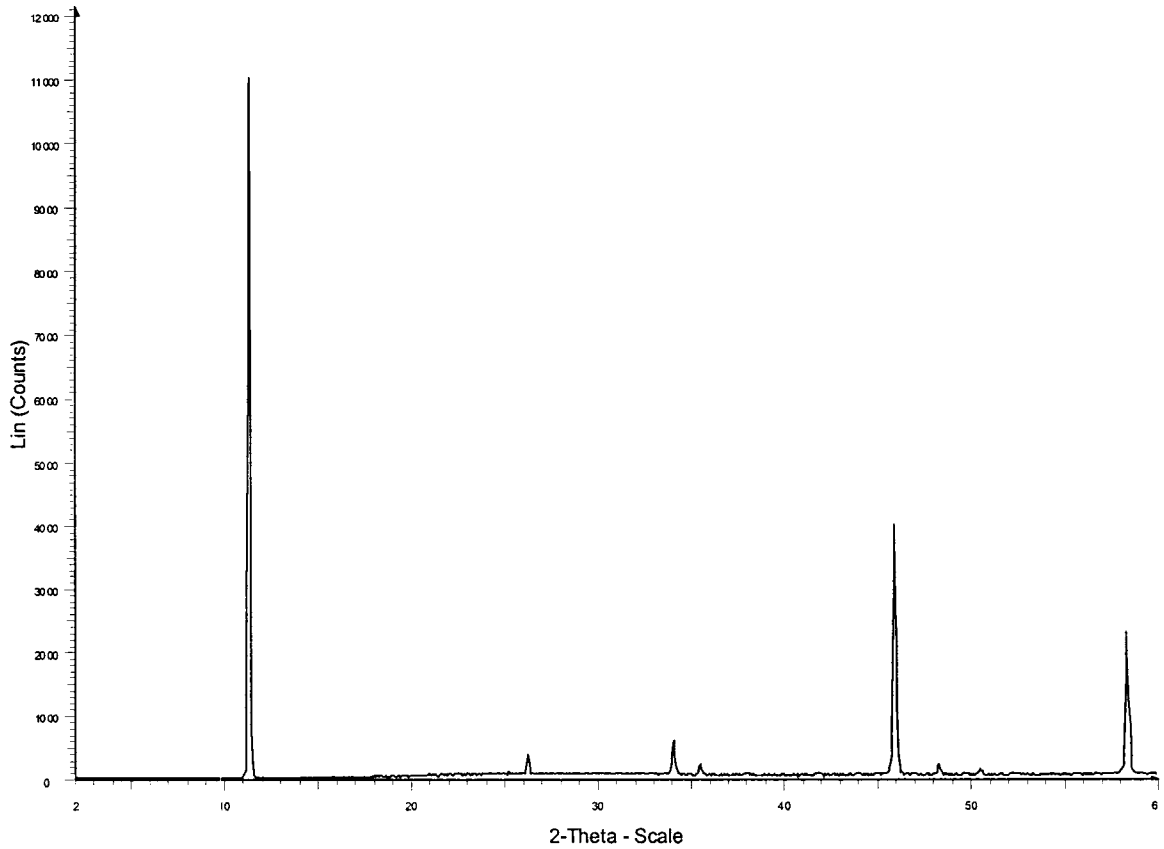

Figure 9 - X-ray Diffraction of FeOCl

The very strong diffraction at low angle indicates an interlayer spacing for pristine FeOCl of 7.8 Å which is consistent with the literature [114]. The FTIR spectrum of FeOCl, shown in figure 10, is relatively featureless with only a mild OH stretch due to intercalated/adsorbed water molecules and strong diagnostic peak at 480 cm^{-1} due to the Fe-O bond stretch. There is also a broad peak at high wavenumbers due to many electronic transitions in the FeOCl framework which make the use of diagnostic IR peaks above 1500 cm^{-1} difficult.

Reproduced with permission of the copyright owner. Further reproduction prohibited without permission.

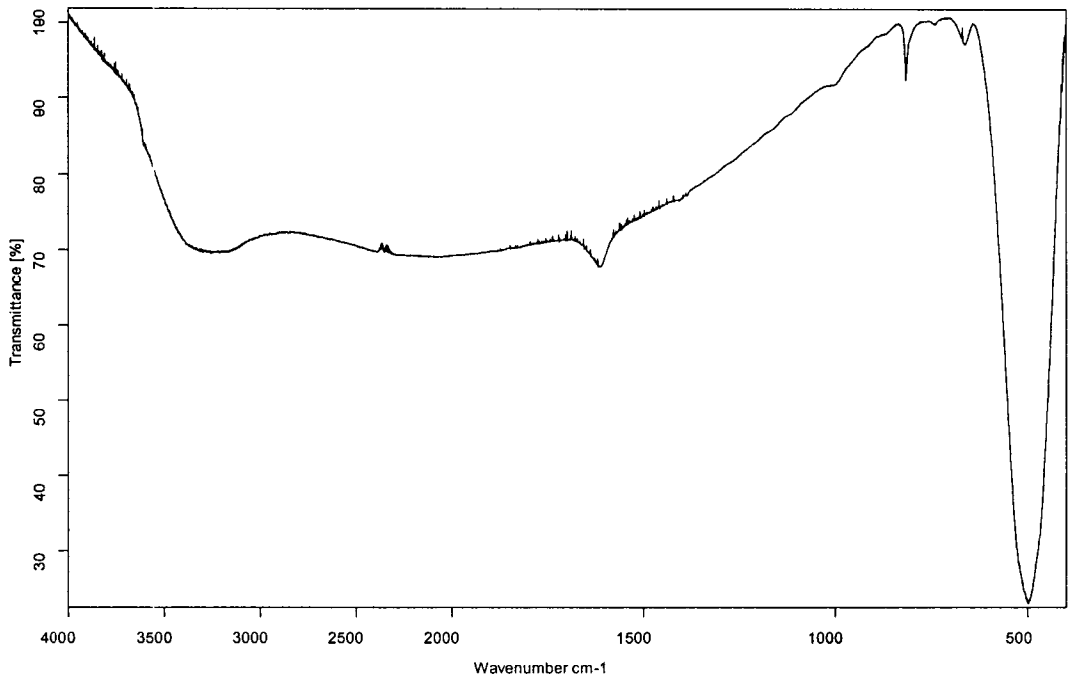

Figure 10 - FTIR of FeOCl

Thermo gravimetric analysis of FeOCl, shown in figure 11, indicates that it is thermally stable in air up to a temperature of 400°C. A rapid decomposition occurs at 400°C which corresponds to the volatilization of $FeCl_3$ from the FeOCl framework. The residue remaining after decomposition of the layered material was determined to be Fe_2O_3 by X-ray diffraction.

Reproduced with permission of the copyright owner. Further reproduction prohibited without permission.

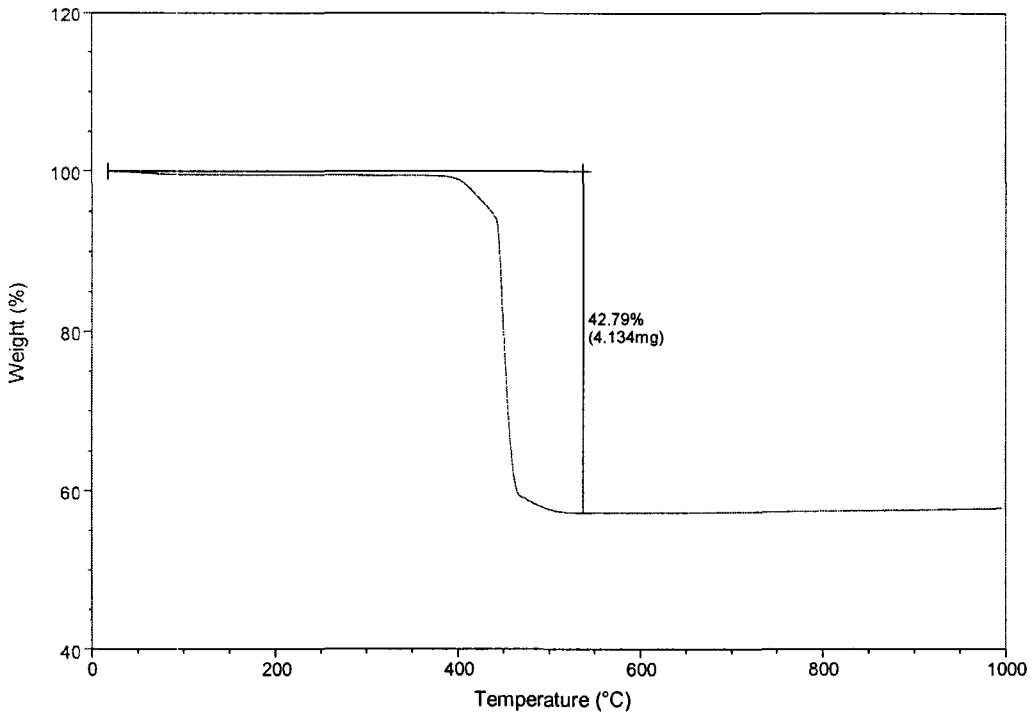

Figure 11 - TGA of FeOCl

The intercalation of anilines into FeOCl is afforded by the reaction of acetonitrile solvated aniline monomers mixed with FeOCl. The FeOCl crystals were ground to a fine powder prior to reaction to maximize surface area of the solid. Mixing with acetonitrile yielded a plain mixture in which the FeOCl would sit on the bottom of the flask. Agitation with magnetic stirring yielded a dark purple mixture. Reactions were run in atmospheric air as reactions in dry solvents under nitrogen usually lead to decomposition rather than intercalated products. It has been proposed that the failure to obtain an

Reproduced with permission of the copyright owner. Further reproduction prohibited without permission.

intercalated product in the absence of air is due to the fact that molecular oxygen is somehow involved in the oxidation of the anilines.

Previous investigation of the aniline/FeOCl system by Kanatzidis showed that if FeOCl was the only oxidizer present then protons released from the aniline monomers upon oxidation should be absorbed by the FeOCl, and that the degree of polymerization of aniline should be reflected by the degree of reduction of the FeOCl layers. An experiment where 0.2 equivalents of aniline were reacted with FeOCl provided insight on the reaction. 0.2 equivalents of aniline being polymerized should result in FeOCl where half of the Fe sites have been reduced from Fe^{3+} to Fe^{2+}. Mossbauer spectroscopy on intercalated materials showed that only about 10% of all Fe sites had been reduced. Further to these findings previous work by Meyer and coworkers revealed that beyond 10% reduction in FeOCl the layers decompose [141].

There is also a lack of H^+ in the recovered intercalated product which indicates that some other moieties must be absorbing the protons. Oxygen is the proposed sink for these protons forming either H_2O or H_2O_2. The mechanism for this process is not well understood and whether the oxygen acts directly on the aniline monomers, or oxidizes the layered structure which in turn oxidizes the monomers is unclear.

FeOCl is also susceptible to hydrolysis in water and by atmospheric moisture. Experimentation by Kanatzidis showed that pristine FeOCl or intercalated FeOCl phases which were left in air for extended periods of time would convert from the FeOCl phase to the FeOOH phase. This change is spectroscopically observed by the disappearance of the strong peak at 480 cm^{-1} in the FTIR spectrum which is replaced by a peak at 680 cm^{-1}.

Reproduced with permission of the copyright owner. Further reproduction prohibited without permission.

At the beginning of the project, aniline was reacted with FeOCl to gain insight into the reactivity of the FeOCl system as previous examples were available in the literature for comparison purposes. Freshly distilled aniline mixed with acetonitrile yielded clear solutions which upon agitation with FeOCl turned purple. Previous work in the literature claimed that the reaction of aniline with FeOCl took approximately one week to go to completion while we observed completion between 2 and 4 days [114]. Reaction progress was monitored by observing relative peak intensities of the pristine FeOCl and the intercalated phase. X-ray diffraction data was collected by casting the reaction mixture on a glass slide and running on the dried film. Upon completion of the reaction a black crystalline powder was obtained by filtration. X-ray diffraction of the product, shown in figure 12, indicated an interlayer spacing of 13.8 Å. This value corresponds to a 6 Å expansion of the FeOCl layers which is consistent with polyaniline chains being intercalated with the rings perpendicular to the layers. This configuration is supported by the channeling effect created by the axial chlorine atoms. The polymer chains would orient such that they lay in the channels created by the chlorine atoms in the interlayer area. The orientation of the polymers between the layers is depicted in figure 13. A small peak can also be observed which corresponds to a minor amount of unreacted FeOCl.

FTIR of the aniline intercalated product, shown in figure 14, clearly shows the FeOCl vibrations are still present indicating that decomposition of the FeOCl framework has not occurred. Of most importance in the FTIR is the appearance of the characteristic fingerprint of polyaniline which provides proof for the polymerization of aniline *in situ* and not just intercalation of the monomer.

Reproduced with permission of the copyright owner. Further reproduction prohibited without permission.

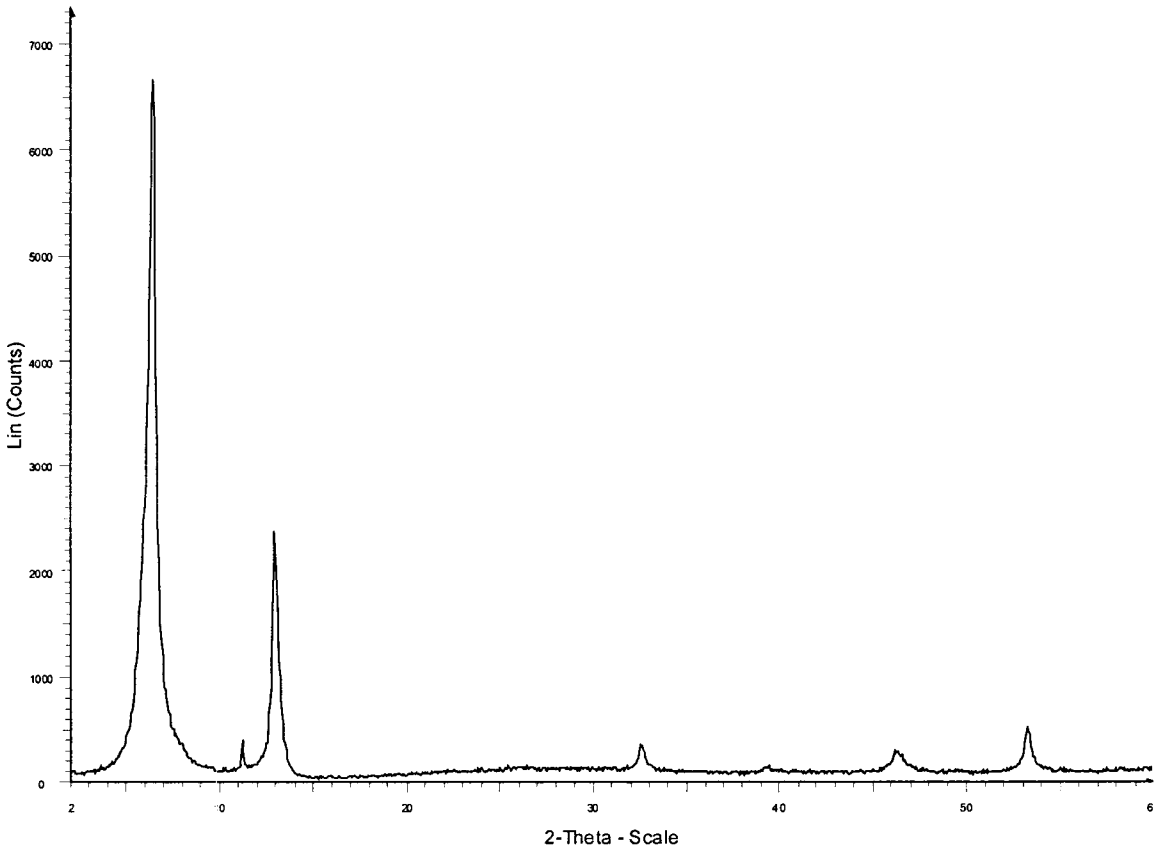

Figure 12 – X-ray Diffraction of Aniline/FeOCl

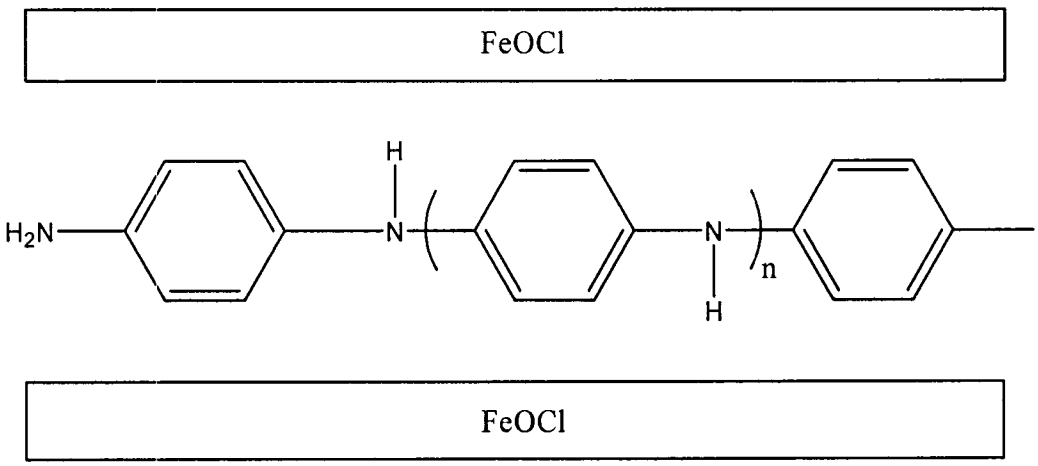

Figure 13 - Orientation of Polyaniline between the Layers of FeOCl

Reproduced with permission of the copyright owner. Further reproduction prohibited without permission.

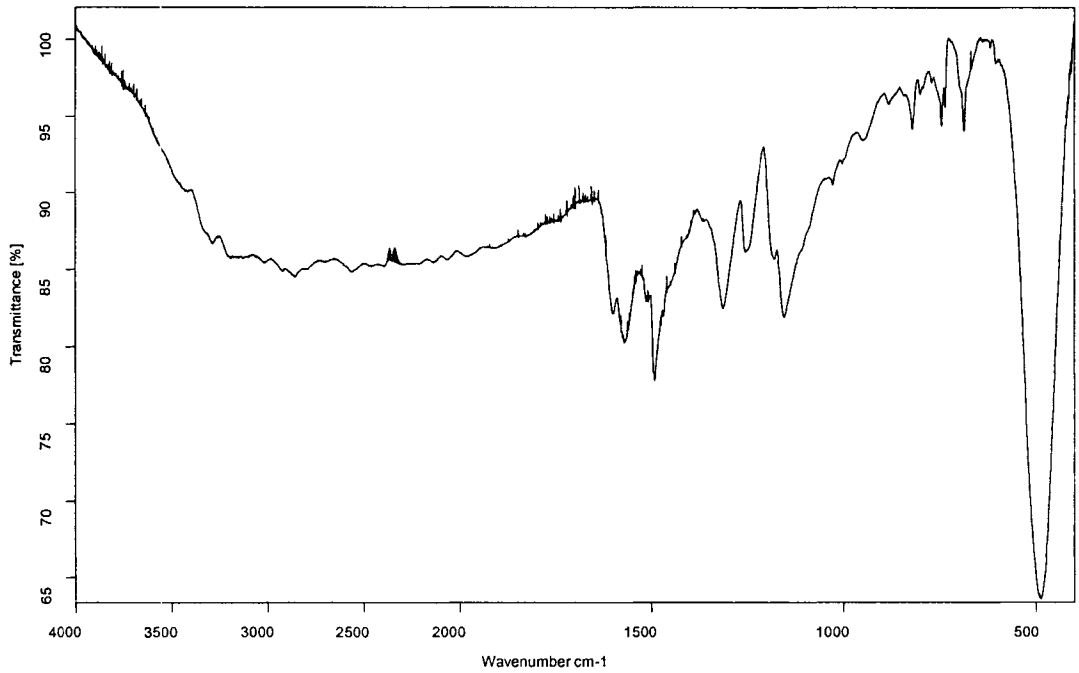

Figure 14 - FTIR of Polyaniline/FeOCl

The N-H band which should be present around 3400 cm-1 is masked by electronic transitions in the FeOCl structure. Aromatic C-H bends and C-N stretches are visible at 2919 and 1296 cm^{-1}, respectively. Quinone C-H and C-N stretches are present at 1460 and 1114 cm^{-1}, respectively.

TGA of the polyaniline intercalated nanocomposite remains largely unchanged from that of the pristine FeOCl. Close inspection of the thermogram shows that a gradual weight loss is present from room temperature to the decomposition temperature of the FeOCl. The gradual weight loss can be attributed to two major decompositions. In the range of 20-100°C surface bound and intercalated solvent would diffuse into the dry gas

Reproduced with permission of the copyright owner. Further reproduction prohibited without permission.

purge. In the range from 100°C to the decomposition of FeOCl the polyaniline would slowly begin to decompose. Unfortunately, the major decomposition of both polyaniline and FeOCl occurs over the same temperature region which makes extraction of useful information from the thermogram difficult. Based on the non-overlapping region a rough estimate of the stoichiometry of the nanocomposite could be made but elemental analysis was chosen to determine the precise stoichiometry of the nanocomposite. The thermograms for both bulk polyaniline and polyaniline intercalated FeOCl are shown in figures 15 and 16 respectively.

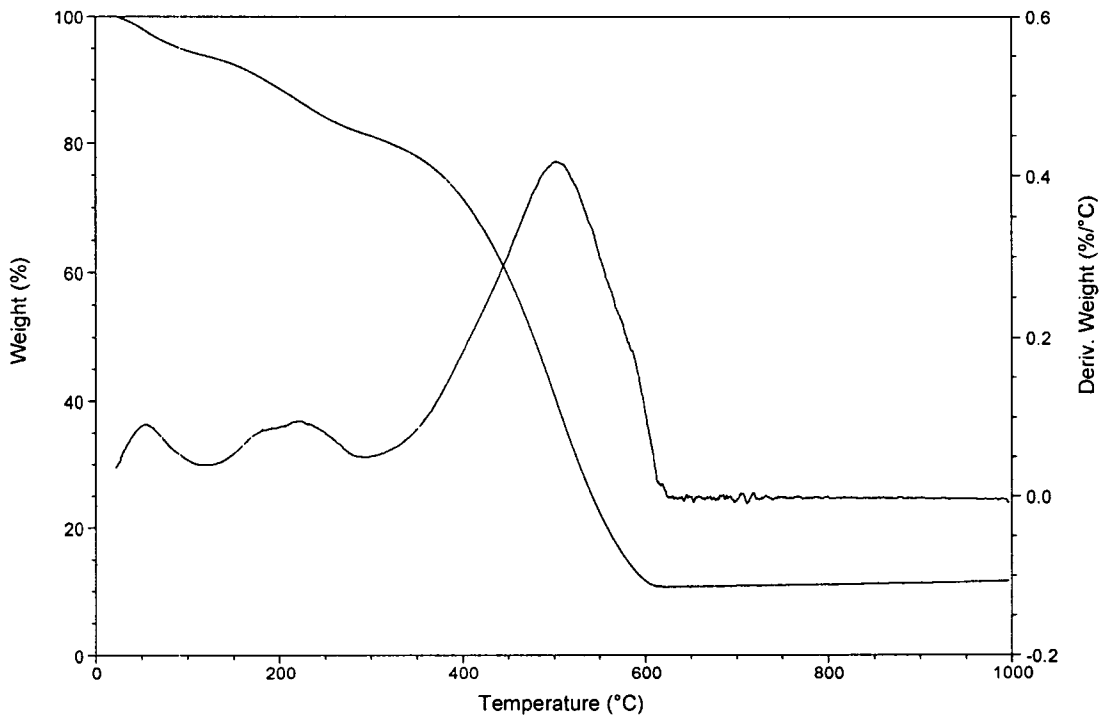

Figure 15 – TGA of Bulk Polyaniline

Reproduced with permission of the copyright owner. Further reproduction prohibited without permission.

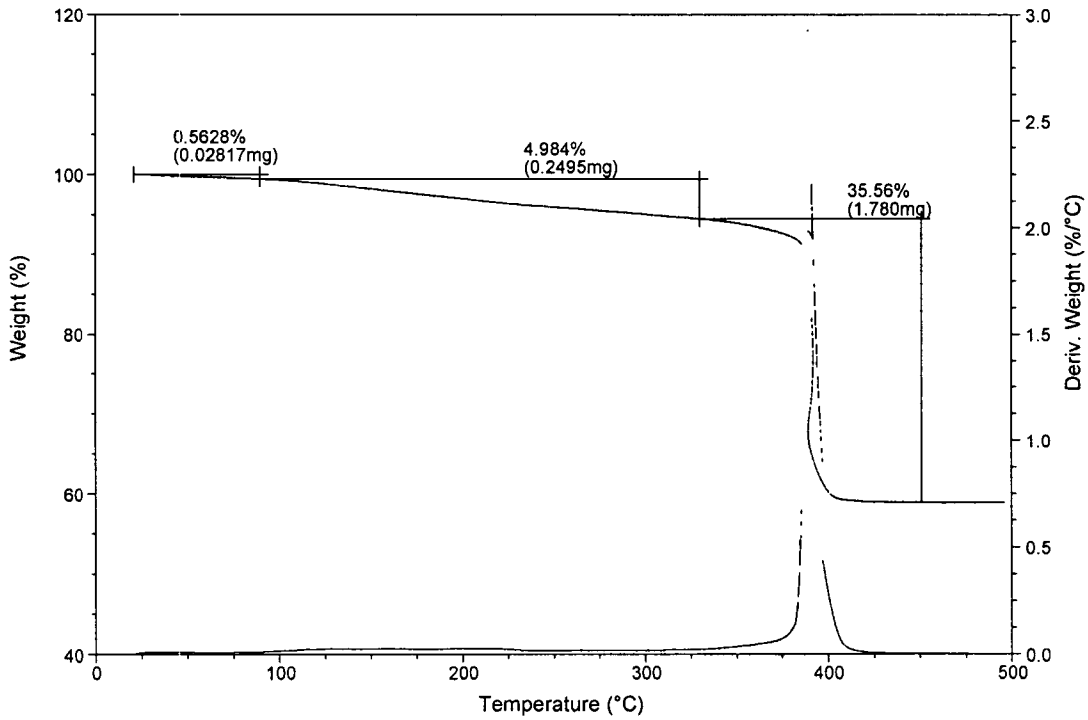

Figure 16 – TGA of Polyaniline/FeOCl

Three major mass losses are observable in the TGA of bulk polyaniline corresponding to water, dopant, and finally the bulk of the polymer chain as the temperature is increased.

The electrical conductivity of these materials was of particular interest as good cathode materials must be good electrical conductors. Variable temperature van der Pauw electrical conductivity measurements were performed on a home built system built by the Dahn research group in the UPEI physics department. Samples were run as pressed pellets. As a result of the samples being pressed pellets the measured conductivity values

Reproduced with permission of the copyright owner. Further reproduction prohibited without permission.

will be lower than the true conductivity of the material. This is due to the fact that the material is microcrystalline and the grain boundaries, or contacts between individual crystals, will lead to lower conductivity than the material truly has. The temperature dependence of the resistivity of FeOCl is shown in figure 17.

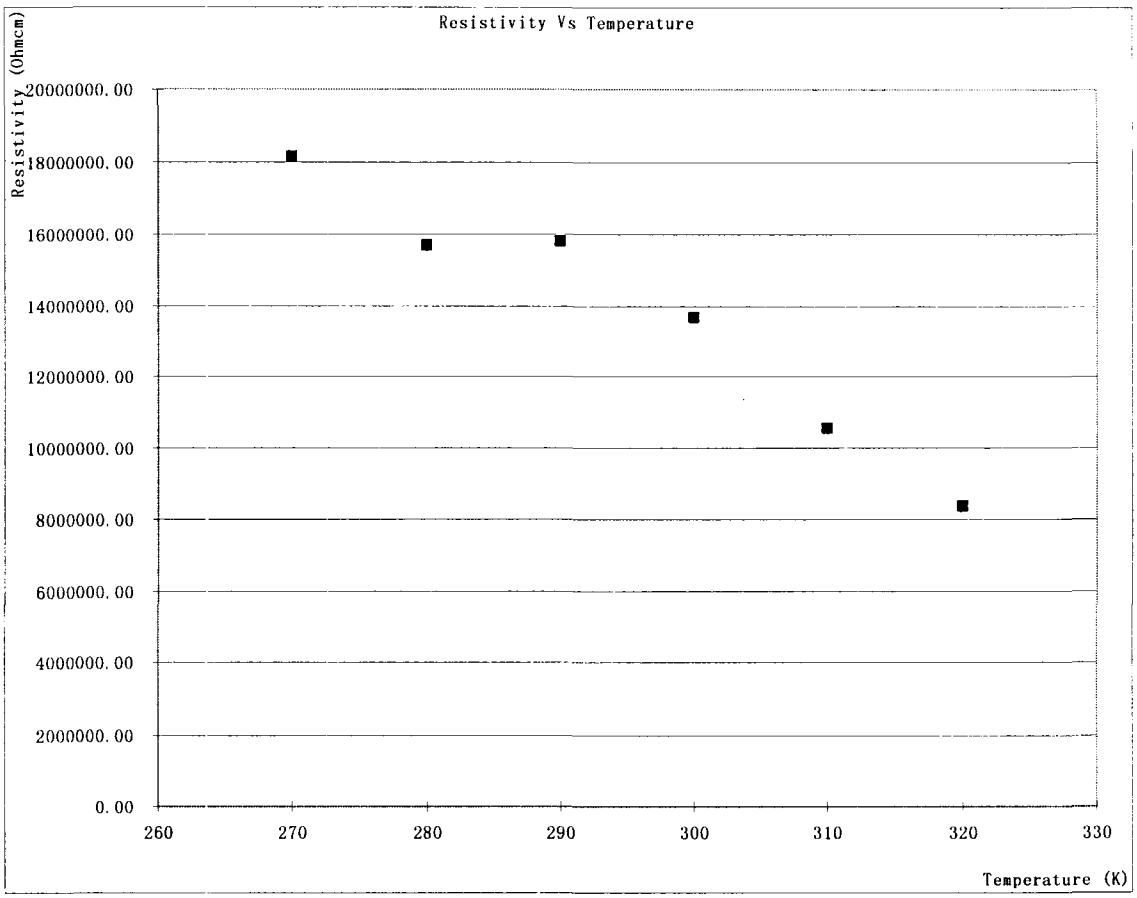

Figure 17 – Resistivity vs. Temperature for FeOCl

The resistivity of the material is impressively high for pristine FeOCl measuring on the order of 8 x 10^8 Ωcm even at elevated temperatures. Its room temperature conductivity is 6.3 x 10^{-8} S/cm, indicating a very poor conductor. The inclusion of aniline and the subsequent polymerization of the monomer should yield the electrically conductive polymer polyaniline. If polyaniline has indeed been created

Reproduced with permission of the copyright owner. Further reproduction prohibited without permission.

then the electrical conductivity of the material should increase accordingly. Electrical conductivity measurements were run on the aniline/FeOCl and the temperature dependence of the resistivity is shown in figure 18.

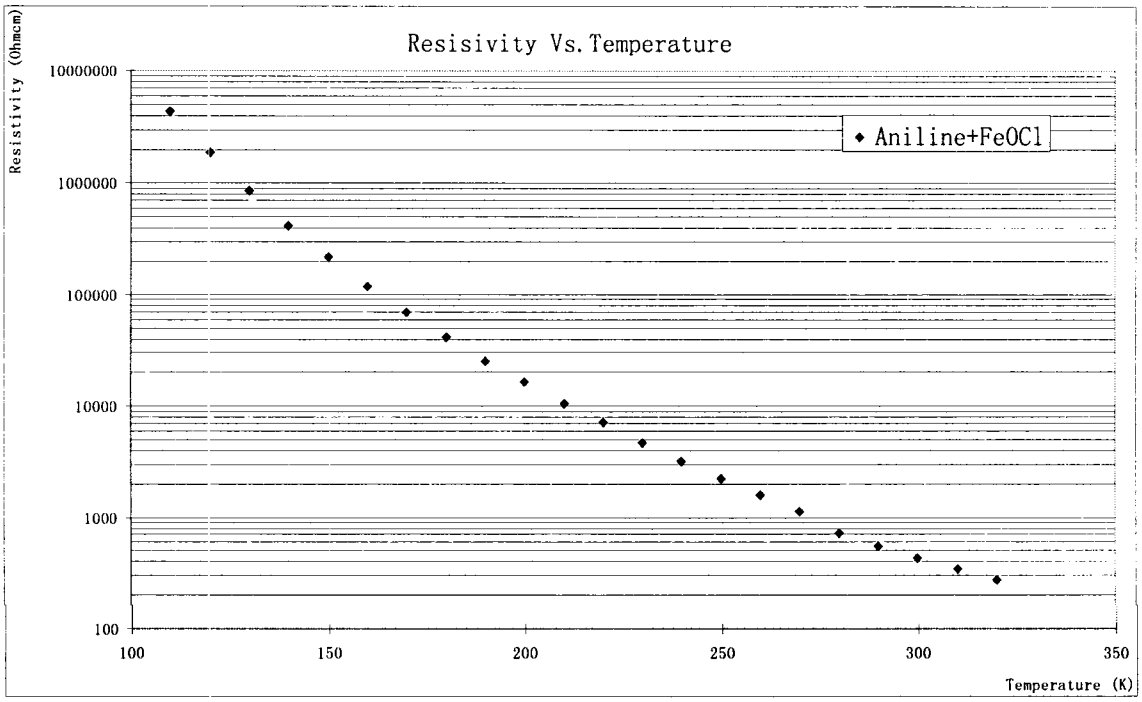

Figure 18 – Resistivity vs. Temperature for Polyaniline/FeOCl

The plot of resistivity vs. temperature for the polyaniline/FeOCl nanocomposite is shown with the resistivity axis on a log scale. This is due to the fact that there is a large range of resistivity values with the resitivity becoming very high at low temperatures. Overall the electrical properties of the polyaniline intercalated FeOCl are much improved with the room temperature conductivity rising to a modest value of 1.8×10^{-3} Scm^{-1}. This is an improvement in conductivity of five orders of magnitude or by a factor of almost 30000 times. It is reasonable to assume that the increase in conductivity is due to the

Reproduced with permission of the copyright owner. Further reproduction prohibited without permission.

polyaniline which has been intercalated between the layers although the reduction of iron sites cannot be overlooked as a contributing factor. In fact, work by Moran and coworkers on lithium FeOCl ($Li_{0.5}FeOCl$) showed room temperature conductivities on the order of 10^{-4} S/cm [116]. These results indicate the measured conductivity is actually a combined effect of increased conductivity of the reduced FeOCl layers and the polymer.

With the intercalation chemistry of FeOCl now well understood, reactions were carried out on the substituted polyanilnes 2-methylaniline, 2-ethylaniline, and 2-propylaniline. Figure 19 depicts all the guest species and the resulting intercalated polymeric form which would be obtained upon oxidation of the monomers. All materials were characterized as mentioned above. The spectra for the remaining nanocompsites can be found in Appendix 1.

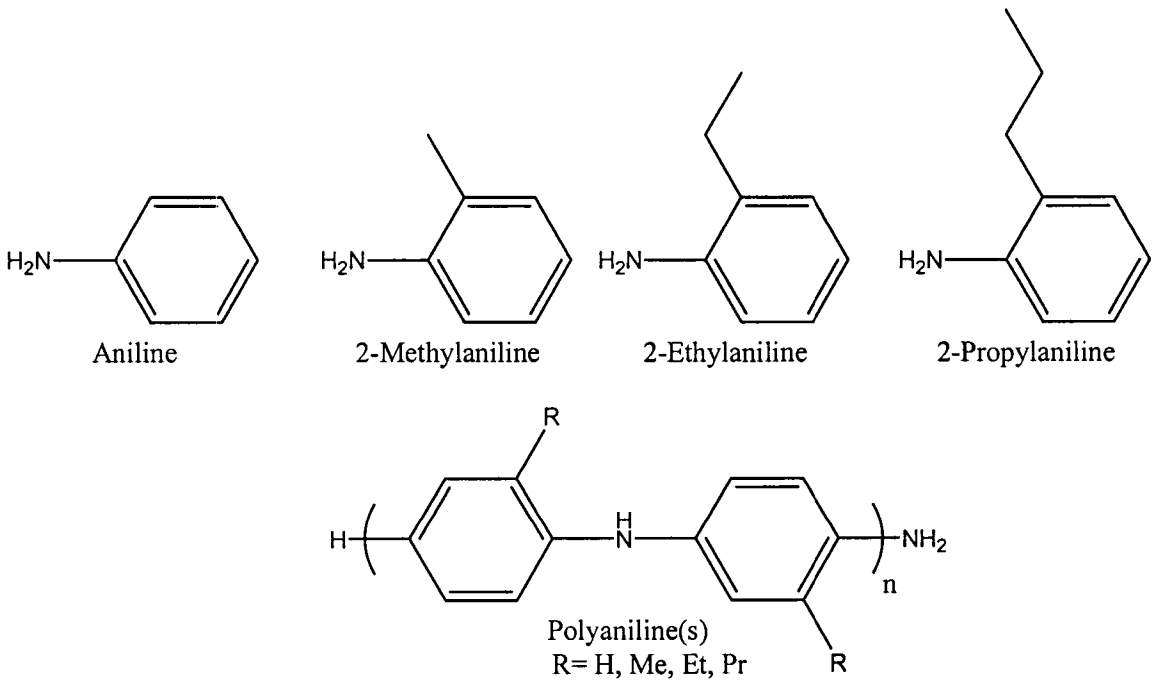

Figure 19 – Structure of Intercalated Anilines/Polyanilines

Reproduced with permission of the copyright owner. Further reproduction prohibited without permission.

The intercalation of the substituted anilines yielded very similar powder patterns to that of the aniline intercalated nanocomposite. A small increase in d-spacing was observable for increased substituent size on the aromatic ring of the monomer.

FTIR remained very diagnostic for the formation of polyanilines between the layers. For all of the nanocomposites the usual fingerprint of the polyaniline backbone was present. The substituted polyanilines also displayed new peaks when compared to aniline just below 3000 cm^{-1}. The appearance of these peaks corresponds to the alkyl substitution and is due to the C-H stretches on the alkyl branch. As the degree of substitution increased the prominence of the absorptions due to the polyaniline appeared to decrease in intensity. As will be seen, this could possibly be due to decreased loading of the polymers between the layers of FeOCl with increased substitution or possibly a lower degree of polymerization of the monomers.

The thermogravimetric analysis of all the nancomposites with intercalated substituted polymers were very similar to that of the polyaniline intercalated material having the slow sloping decomposition from room temperature up to the decomposition of FeOCl. Once again the decomposition of the polymers were overlapped with the decomposition of the FeOCl which made it difficult to extract useful information. In an effort to obtain some information from the TGA, the weight loss between 100°C and the decomposition temperature of the FeOCl was assumed to be the intercalated polymer. From this a rough estimate of the amount of polymer between the layers was able to be calculated to yield an approximate stoichiometry for the materials.

Reproduced with permission of the copyright owner. Further reproduction prohibited without permission.

Electrical conductivity of the substituted polyanilines intercalated in FeOCl were obtained with very similar results. The nanocomposites which contained substituted polymers all displayed lower electrical conductivities than that of the aniline/FeOCl system. This is supported experimentally by previous findings in the Bissessur group who found that increased substitution of the polyaniline chain reduces the electrical conductivity [130]. Another plausible explanation for reduction in electrical conductivity is that as the steric crowding increased around the monomer, polymerization became more difficult leading to shorter chain lengths and as a result lower electrical conductivity. All of the substituted polymer nanocomposites had room temperature conductivities on the order of 10^{-5} Scm^{-1}. A summary and comparison of the room temperature conductivity data is provided in table 1.

Finally, elemental analysis was performed on the nanocomposites to determine the loading of polymer between the layers of FeOCl. Elemental analysis were peformed by Guelph Chemical Laboratories. From elemental analysis data the stoichiometry of the nanocomposites was determined as shown in table 1.

	d (Å)	Expansion (Å)	σ (S/cm, 17°C)	Stoichiometry
FeOCl	7.8	------	6.3×10^{-8}	FeOCl
Aniline/FeOCl	13.8	6.0	1.8×10^{-3}	$(PANI)_{0.09}FeOCl$
Methyl/FeOCl	14.0	6.2	2.9×10^{-4}	$(PMA)_{0.06}FeOCl$
Ethyl/FeOCl	14.3	6.5	5.8×10^{-4}	$(PEA)_{0.03}FeOCl$
Propyl/FeOCl	15.0	7.2	1.8×10^{-4}	$(PPA)_{0.05}FeOCl$

Table 1 -- Summary of Results for Intercalated FeOCl Nanocomposites

From the elemental analyses the ratio between nitrogen and iron was used to determine the stoichiometies of the intercalation compounds. It was also noted that as the

Reproduced with permission of the copyright owner. Further reproduction prohibited without permission.

alkyl group on the polymer was increased the nitrogen to carbon ratio decreased, as expected. The elemental analysis data is shown in table 2.

Sample	Carbon %	Hydrogen %	Nitrogen %	Iron %
Aniline/FeOCl	15.34	0.99	3.59	45.34
Methyl/FeOCl	12.11	1.22	2.22	44.58
Ethyl/FeOCl	7.31	0.82	1.26	47.98
Propyl/FeOCl	9.95	1.06	1.77	44.79

Table 2 – Elemenal Analysis Results for FeOCl Nanocomposites

Further evidence for the intercalation of the polymers was provided by scanning electron microscopy (SEM). Figure 20 shows the highly ordered and crystalline nature of FeOCl.

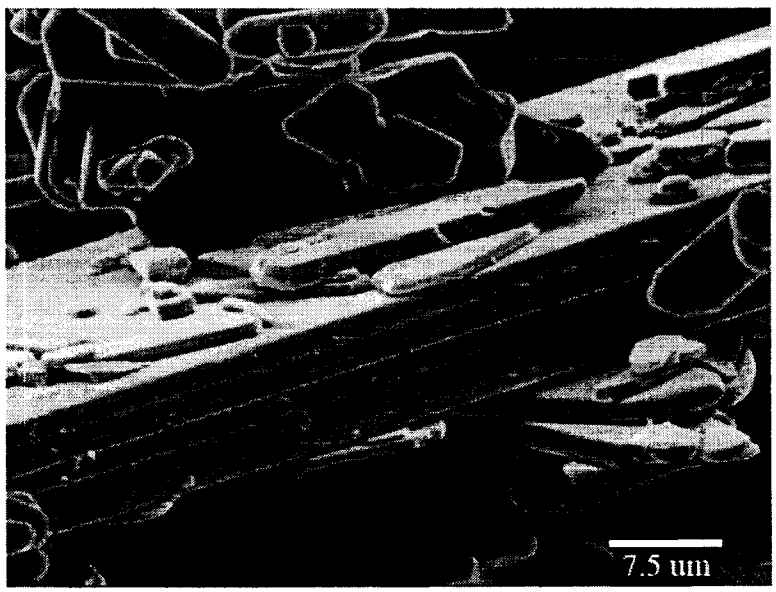

Figure 20 – SEM of Pristine FeOCl (2000x, 45°)

This SEM was taken with the sample placed at a 45° angle such that the edges of the layers could be seen. The layering effect of the material is clearly visible among the large plates. Upon intercalation the X-ray diffraction patterns indicated a substantial loss

Reproduced with permission of the copyright owner. Further reproduction prohibited without permission.

of crystallinity via the decrease in peak intensity and broadening of peak width. The loss of crystallinity of the samples is confirmed by SEM in which substantial disorder of the layered structure can be observed. Figure 21 shows the SEM of polyaniline intercalated FeOCl.

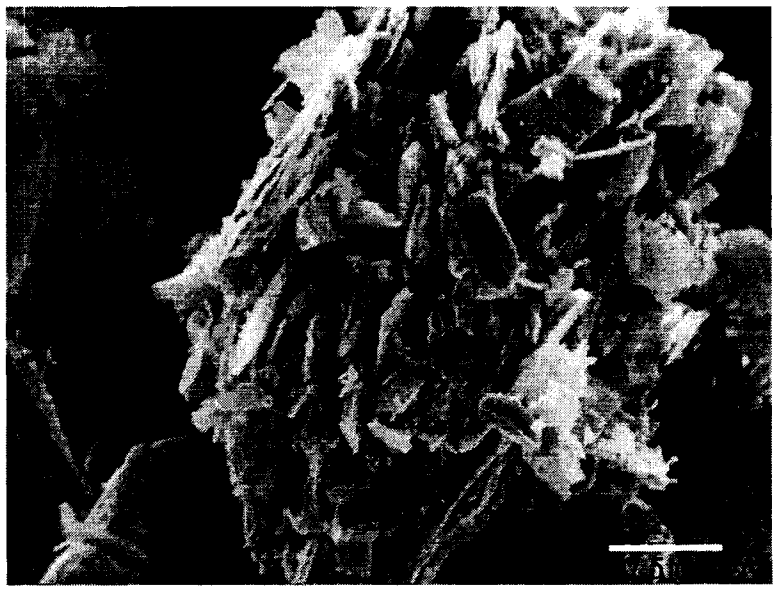

Figure 21 – SEM of Polyaniline/FeOCl (2000x)

While the crystallinity of the FeOCl systems has been substantially reduced as observed in figure 21, it is important to note that the layered structure is still intact. Also important to note is that no amorphous material is present on the surface of the layers indicating that all polymeric material must be intercalated and not just simply adsorbed on the surface. Further SEM data for FeOCl as well as the nanocomposite materials can be observed in appendix 1.

Reproduced with permission of the copyright owner. Further reproduction prohibited without permission.

3.3 Titanate

The layered form of titanate is usually created via the formation of protonated titanate, $HTiO_2$. TiO_2 is a compound usually found in its kinetic product form which has the anatase structure. The thermodynamic product is the layered form which is interesting with respect to intercalation chemistry. Reaction of anatase TiO_2 and Cs_2CO_3 yielded a fine white powder. The reaction of TiO_2 and Cs_2CO_3 at elevated temperatures serves a two-fold purpose. First and foremost, heating of TiO_2 affords the layered form, and the presence of Cs_2CO_3 results in Cs^+ ions being intercalated between the layers of the TiO_2. X-ray diffraction of the Cs intercalated phase surprisingly yielded no peaks indicating that the material is amorphous after heating. Ion exchange of the Cs^+ ions with acid is easily accomplished which results in the desired protonated titanate, $HTiO_2$. The powder X-ray diffraction of the acid exchanged titanate is shown in figure 22.

Reproduced with permission of the copyright owner. Further reproduction prohibited without permission.

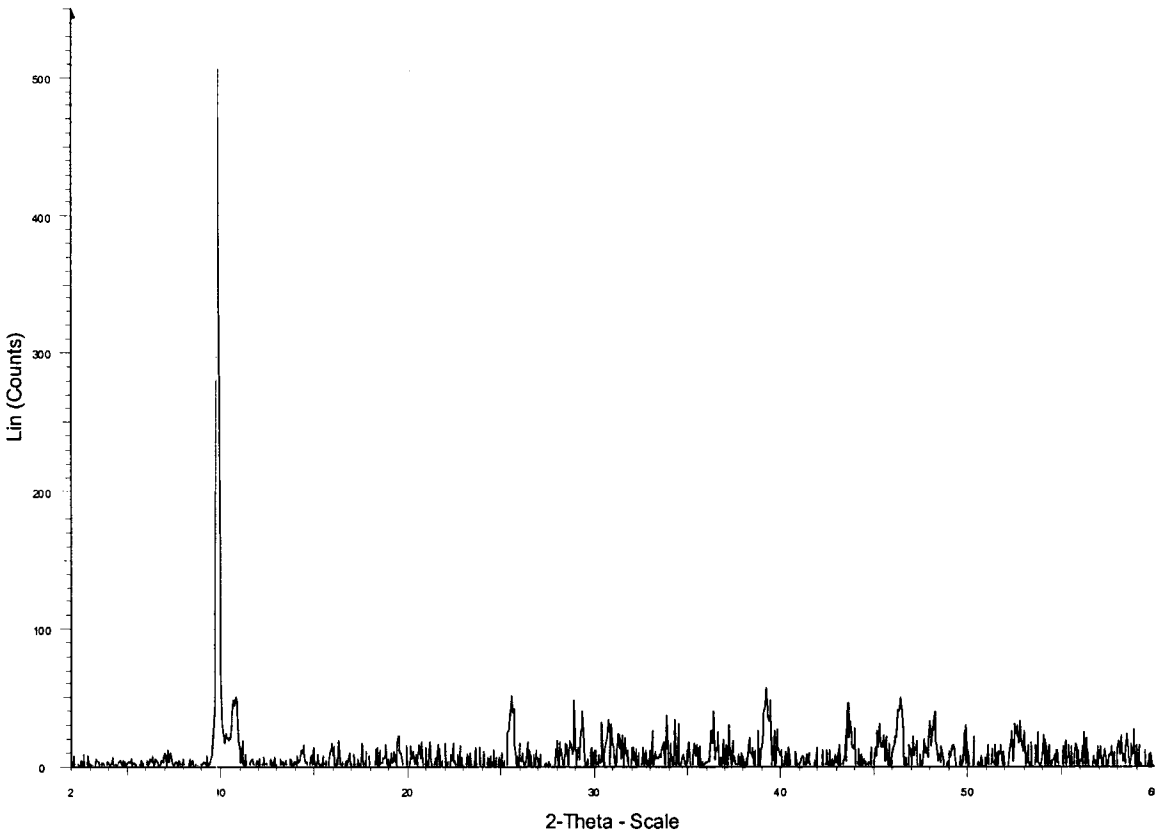

Figure 22 – X-ray Diffraction of $HTiO_2$

The diffraction pattern for $HTiO_2$ clearly shows an ordered of the system with a strong diffraction peak at $2\theta = 9.7°$ corresponding to an interlayer spacing of 9.1 Å. This value corresponds well to previous work with $HTiO_2$ indicating that we have indeed synthesized the desired titanate [123]. Upon close inspection of the powder pattern for $HTiO_2$ a small peak at slightly higher angle can be seen besides the peak corresponding to $HTiO_2$. This peak has not previously been reported in the literature and the source of this diffraction has not yet been determined. This peak does not correspond to any of the starting materials and, as will be discussed later, does not seem to disappear upon

Reproduced with permission of the copyright owner. Further reproduction prohibited without permission.

intercalation of other molecules indicating that it is not a diffraction due to the (00*l*) plane.

The FTIR of $HTiO_2$, as shown in figure 23, is not very diagnostic yielding only a broad peak around 3400 cm^{-1} and a weak peak around 1630 cm^{-1} corresponding to intercalated water molecules, and a relatively strong absorption between 400-1000 cm^{-1} corresponding to Ti-O and Ti=O vibrations.

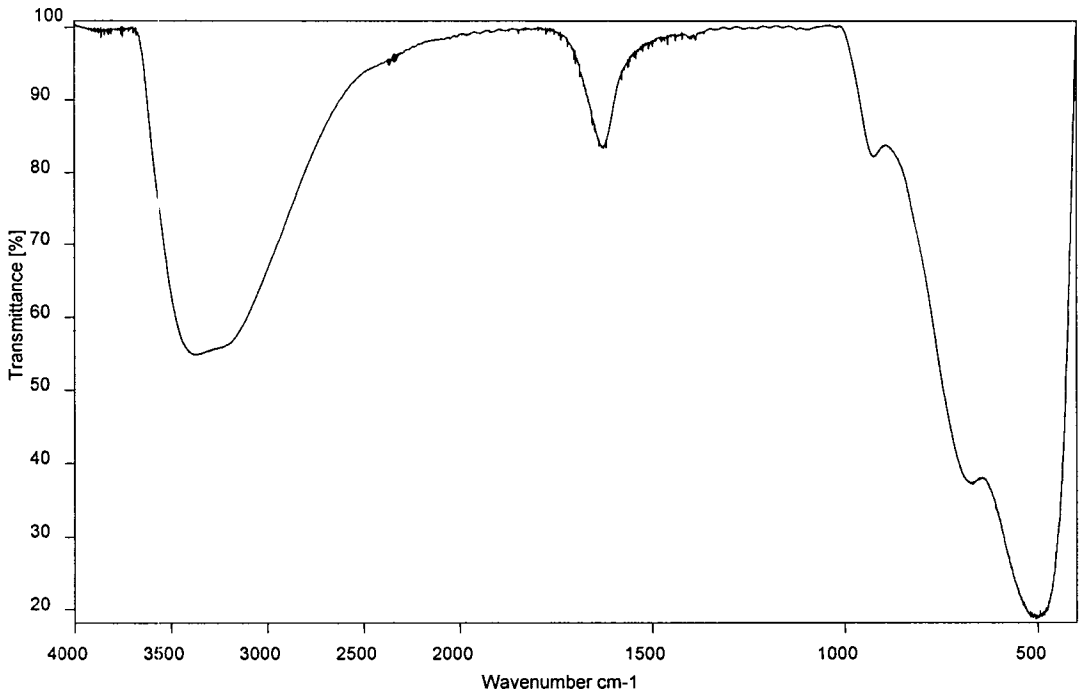

Figure 23 – FTIR of $HTiO_2$

Thermo gravimetric analysis of $HTiO_2$, shown in figure 24, shows no major features except at relatively low temperatures. The major mass loss of $HTiO_2$ is that of adsorbed water from room temperature up to about 120°C. A further minor weight loss is

Reproduced with permission of the copyright owner. Further reproduction prohibited without permission.

attributed to intercalated water. It was determined that upon further heating the layered structure breaks down forming an amorphous material. Further heating of the amorphous material leads to the formation of anatase TiO_2. The reformation of anatase TiO_2 was confirmed by running X-ray diffraction on the residue of a TGA, which gave a diffraction pattern which was identical to the anatase starting material. Figure 25 illustrates the anatase TiO_2 after TGA has been run on $HTiO_2$.

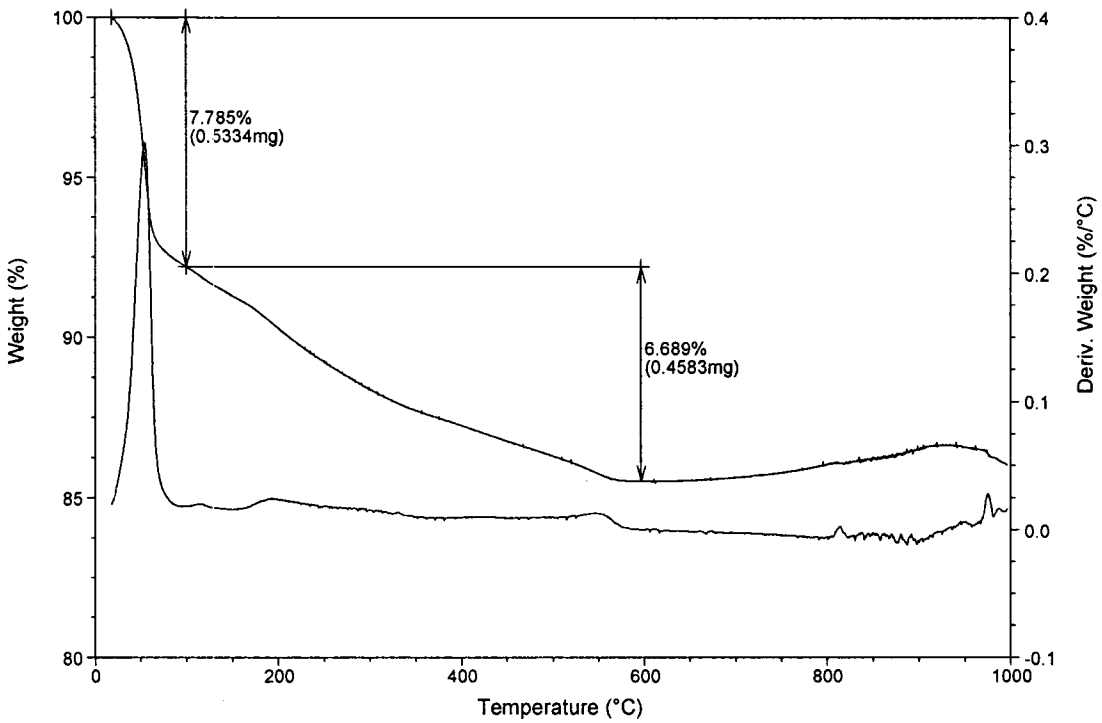

Figure 24 – TGA of $HTiO_2$

Reproduced with permission of the copyright owner. Further reproduction prohibited without permission.

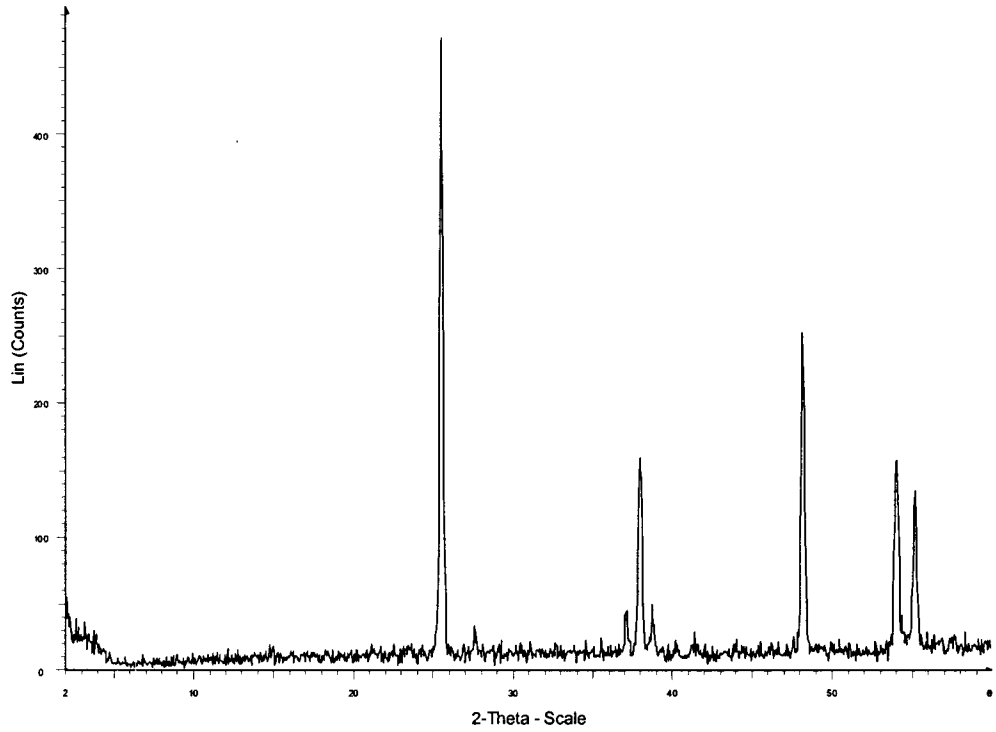

Figure 25 – X-ray Diffraction of $HTiO_2$ Residue after TGA to 1000°C

It was experimentally found that the layers of TiO_2 have very strong attractions for H^+ ions. These attractions make the exfoliation of $HTiO_2$ very difficult even in a polar medium such as water. Mixing $HTiO_2$ with water yielded only $HTiO_2$ powder on the bottom of the flask which could not be exfoliated even after substantial sonication. Due to the fact that protons were intercalated between the layers, previous studies investigated the acid-base properties of the material and indeed it was found that bases could be reacted with $HTiO_2$. Tetrabutylammonium hydroxide (TBAOH) is a base with a very bulky ammonium cation. Upon reaction of a 1:1 ratio of TBAOH to the H^+ in the $HTiO_2$, a $TBATiO_2$ phase was isolated. The X-ray diffraction of the $TBATiO_2$ phase is shown in Figure 26.

Reproduced with permission of the copyright owner. Further reproduction prohibited without permission.

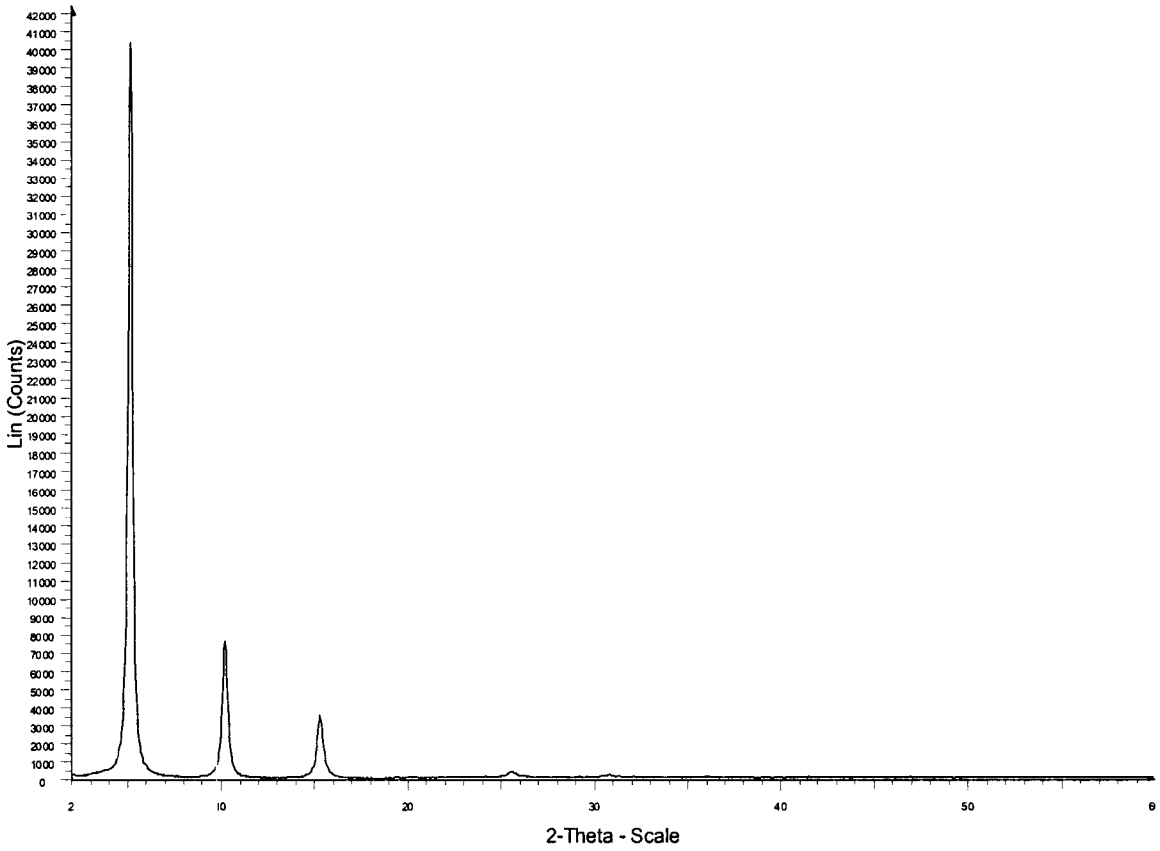

Figure 26 – X-ray diffraction of $TBATiO_2$

Evidence for the intercalation of TBA^+ ion between the layers of TiO_2 is clearly shown by the shifting of the (001) peak to low angle in the powder pattern corresponding to an interlayer spacing of 17.3 Å.

FTIR, as shown in figure 27, provides further evidence for the intercalation of TBA into TiO_2 with the appearance of C-H stretches originating from the alkyl branches on the ammonium ion just below 3000 cm^{-1}. CH_2 bends are also visible just below 1500 cm^{-1}.

Reproduced with permission of the copyright owner. Further reproduction prohibited without permission.

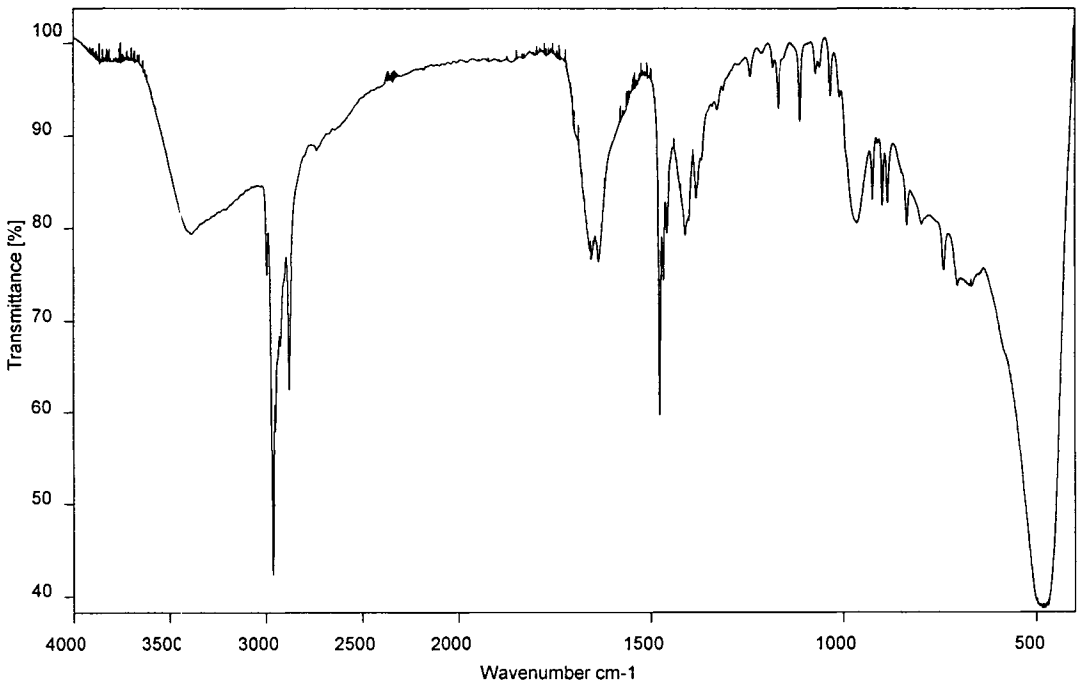

Figure 27 – FTIR of $TBATiO_2$

In solution, the bulky nature of the TBA cation appears to induce substantial swelling of the TiO_2 layers. Upon reaction of the TBAOH with $HTiO_2$ a stable suspension is formed through the delamination or separation of the layers to yield individual sheets of TiO_2. With a stable suspension it was suspected that mixing with solutions of polymers possessing solid electrolyte properties would yield polymer intercalated products which could be studied towards their ion conducting properties.

Initial investigation into TiO_2's intercalation chemistry was through reaction of PEO and PVP whose successful intercalation were reported previously [123]. Mixing of polymer solutions with exfoliated TiO2 layers yielded either very poor or no intercalated phases. Figure 28 depicts the best powder pattern obtained for the direct reaction of PEO with $TBATiO_2$ which shows a very broad peak at low angle presumably due to a mixture

Reproduced with permission of the copyright owner. Further reproduction prohibited without permission.

of both polymer and TBA cation. Also present in the diffraction pattern is considerable amount of $HTiO_2$ phase

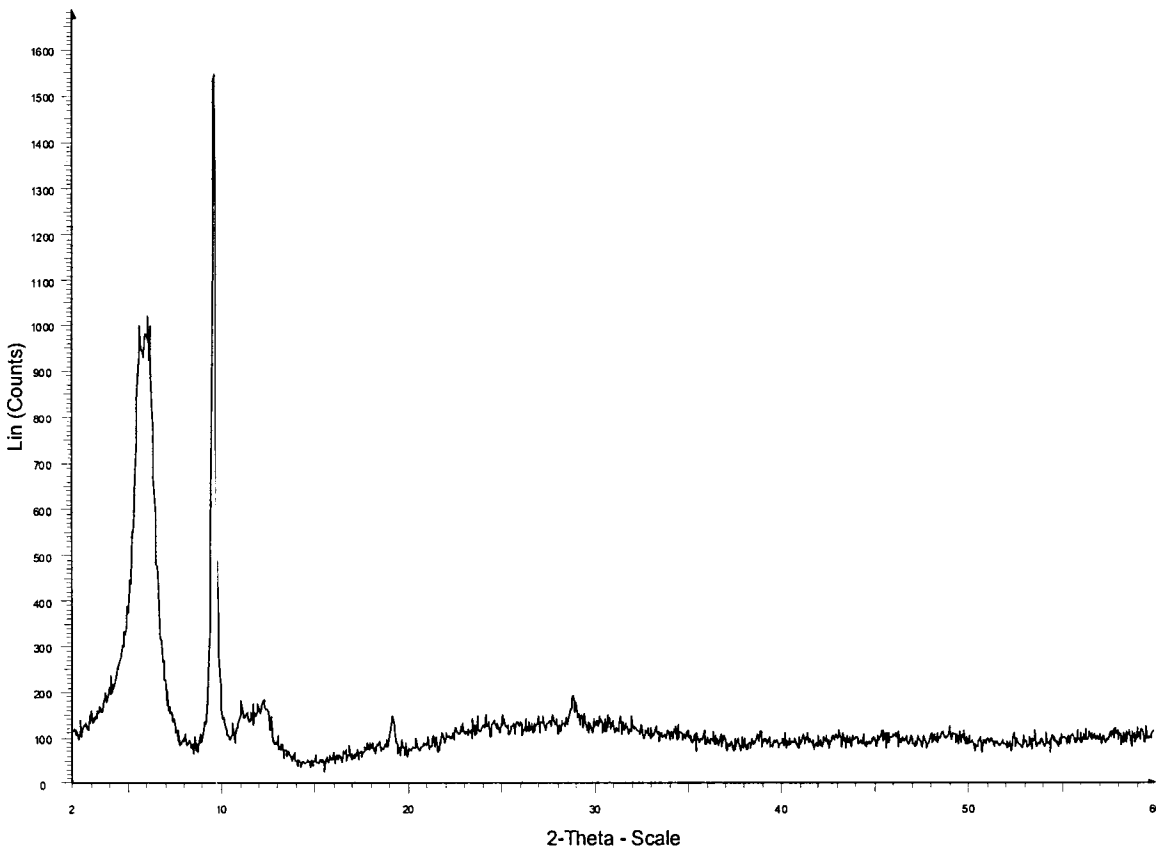

Figure 28 – X-ray Diffraction of PEO/TBATiO_2

The direct reaction of polymer with $TBATiO_2$ was thought to be unsuccessful due to the lack of columbic attraction between the neutral polymer chains and the negatively charged plates of TiO_2. Previous work by Lerner and coworkers used acids to protonate the polymer chains inducing the formation of sandwich compounds [123]. All attempts to duplicate this work resulted in the reformation of the $HTiO_2$ phase with no intercalated material present. After repeated experiments and varying parameters such as different

Reproduced with permission of the copyright owner. Further reproduction prohibited without permission.

reaction times, polymers (PEO, PVP, POMOE, MEEP), concentrations of acid used to protonate the polymers, and multiple other attempts it became very clear that the $HTiO_2$ phase was resistant towards intercalation. The effect of pH on the reaction was also investigated.

A suspension of $TBATiO_2$ was mixed with PEO and the pH was adjusted to a value of >10. 1M HCl was slowly added dropwise and the pH of the system was monitored via alkacid strips. With each addition of acid the pH was measured and casts of the solution on glass plates obtained when the mixture was strongly basic (pH >10), moderately basic, weakly basic, neutral, weakly acidic, and strongly acidic (pH < 2). XRD was run on the dried casts to determine if any intercalation or phase changes had occurred. For basic conditions the $TBATiO_2$ phase appeared to dominate. In a weakly basic solution it appeared that there may be a small degree of intercalation although the peak was very weak. When the solution became neutral it appeared that $HTiO_2$ was regenerated and remained through strongly acidic conditions. We observe that in the presence of any free acid the layers immediately precipitate out of suspension and a white powder is obtained. Since the intercalation of ionically conducting polymers was not well suited for the TiO_2 system, some alternate chemistry was investigated.

The intercalation of alkyl ammonium ions through an acid-base reaction had already been well established with the TiO_2 system. Although many alkyl ammonium cations had been inserted between the layers of TiO_2, we found that aniline had not been previously intercalated. The reaction TiO_2 with neat aniline yielded no intercalation after prolonged sonication. The mechanism for the intercalation of aniline was proposed to be through the protonation of the $-NH_2$ group to yield the positively charged anilinium ion.

Reproduced with permission of the copyright owner. Further reproduction prohibited without permission.

The reaction was attempted in a 50% (v/v) mixture of aniline and water. After four hours of sonication it appeared that the aniline, $HTiO_2$, and water, which at first did not mix, had mixed and suspended the $HTiO_2$. Casting of the product yielded a film. XRD of the film, shown in figure 29, indicated that intercalation of the aniline had indeed occurred.

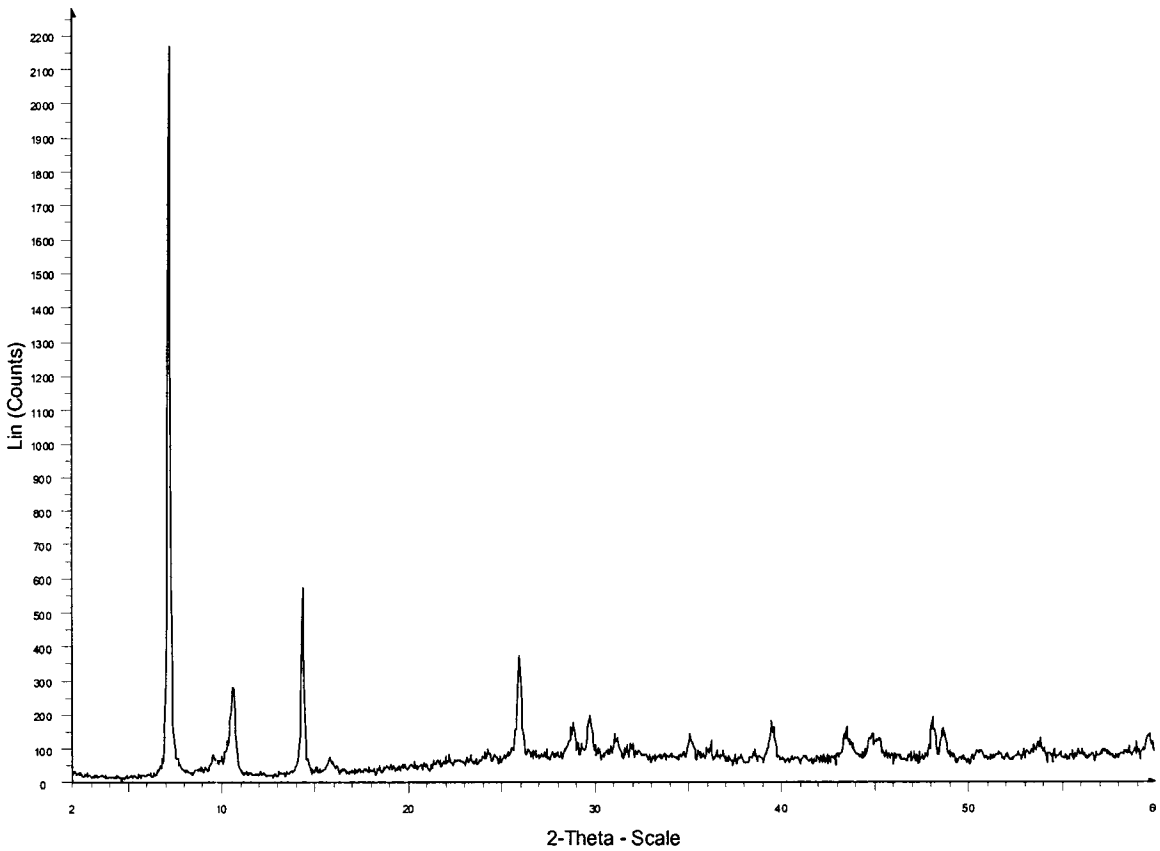

Figure 29 – X-ray Diffraction of Aniline Intercalated TiO_2

The powder pattern for aniline intercalated TiO_2 clearly shows that intercalation of the aniline monomer has occurred and that no $HTiO_2$ phase remains. The first and second diffraction of the aniline intercalated phase are clearly visible with an interlayer spacing of 12.3 Å. The peak at $2\theta = 10.6°$ corresponds to an unknown phase.

Reproduced with permission of the copyright owner. Further reproduction prohibited without permission.

FTIR of the aniline intercalated HTiO2, shown in figure 30, provides further evidence for the intercalation of aniline between the layers.

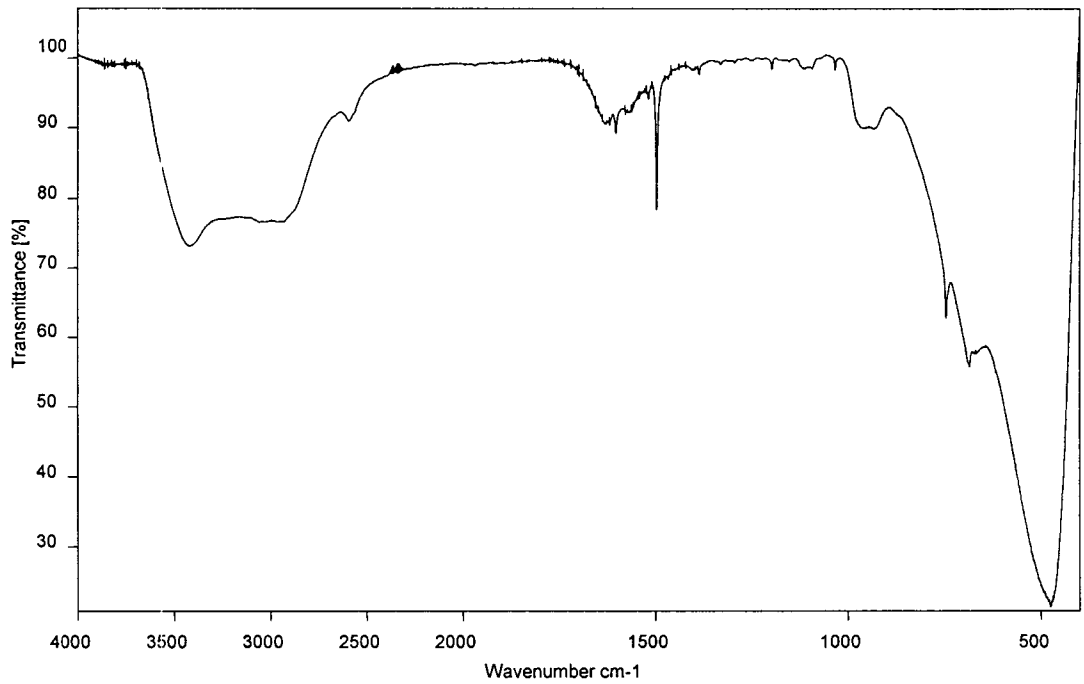

Figure 30 – FTIR of Aniline Intercalated in $HTiO_2$

The TiO_2 structure clearly remains intact but the appearance of peaks just below 3500 cm^{-1} and at 1500 cm^{-1} correspond to N-H stretches and bends, respectively, providing strong evidence for the presence of aniline. Further support for the intercalation of aniline is obtained from TGA, shown in figure 31.

Reproduced with permission of the copyright owner. Further reproduction prohibited without permission.

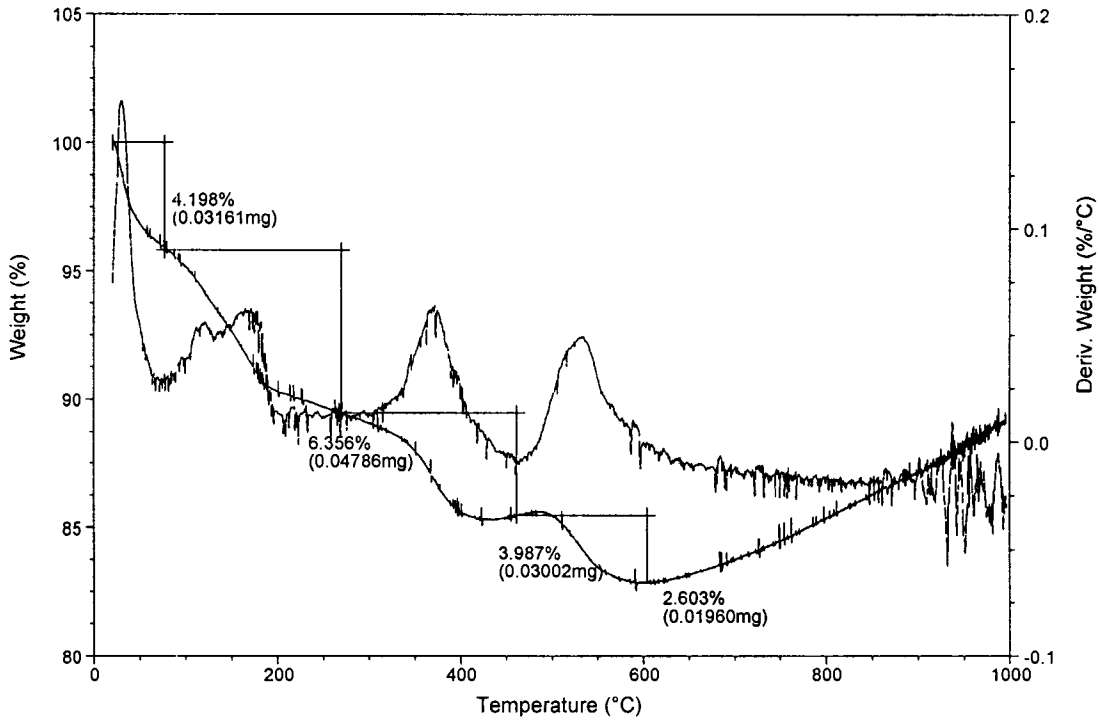

Figure 31 – TGA of Aniline Intercalated in $HTiO_2$

In contrast to $HTiO_2$ which has only one major mass at low temperature and a long sloping mass loss at high temperature, the aniline/$HTiO_2$ show four distinct mass loss regions. The first and second mass losses are assigned to water which is adsorbed and intercalated, respectively. The third and fourth mass losses are attributed to the evaporation/decomposition of adsorbed and intercalated aniline, respectively. The long sloping mass gain at high temperatures is due to the oxidation of the reduced TiO_2 layers.

The polymerization of intercalated aniline to form polyaniline intercalated TiO_2 was attempted through the oxidation of aniline. Several methods were employed for the oxidation of aniline starting with oxidation with air. A sample was placed in the furnace at 140°C for several hours. After four hours the material became very dark in colour. This was promising as it was indicative that some form of oxidation had occurred. X-ray

Reproduced with permission of the copyright owner. Further reproduction prohibited without permission.

diffraction of the heated material, shown in figure 32 indicated that an intercalation compound still existed.

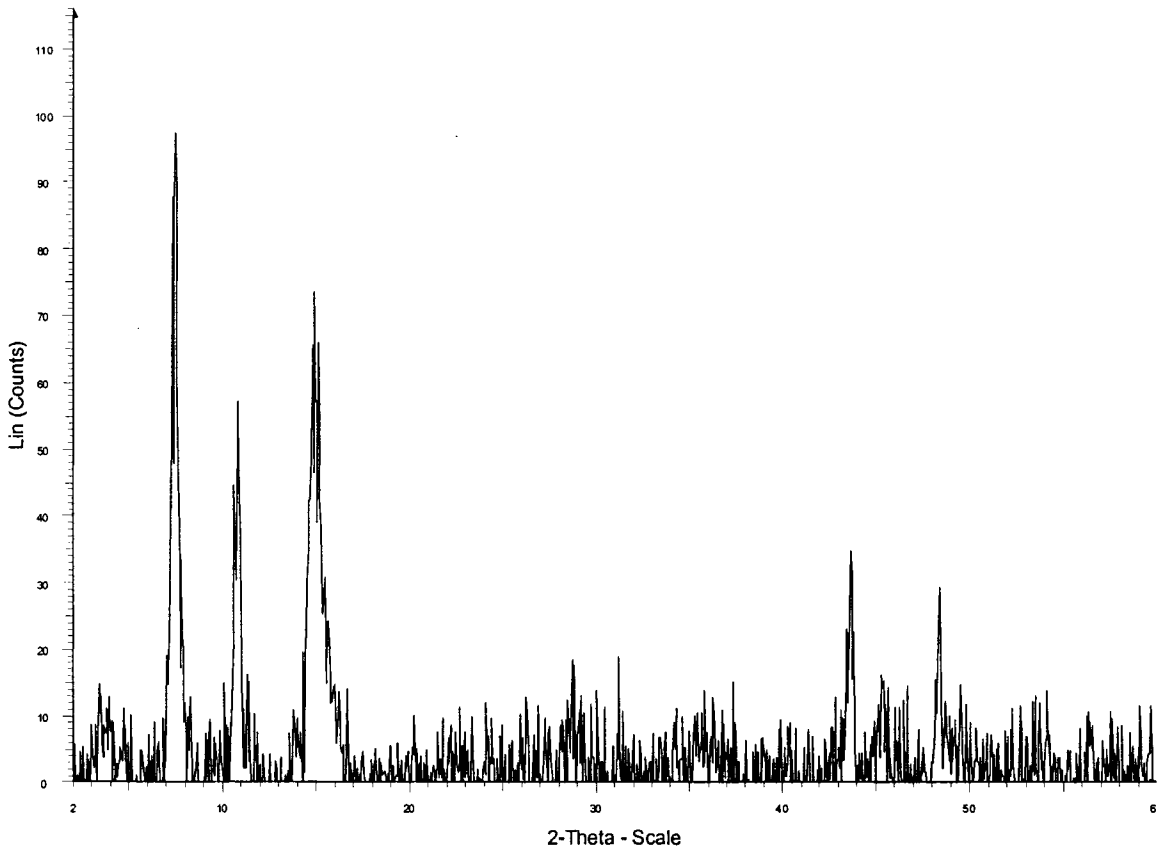

Figure 32 – X-ray Diffraction of Aniline/$HTiO_2$ heated at 140°C (4 Hours)

The first and second diffraction peaks of an intercalated phase corresponding to an interlayer spacing of 11.8 ´ can be observed. The interlayer spacing of the intercalate corresponds to a 2.7 ´ expansion of the layers when compared to $HTiO_2$, but a 0.5 ´ contraction when compared to that of the aniline intercalated phase prior to heating. This could be accounted for by the removal of interlayer water upon heating to yield a nanocomposite with a slightly smaller d value. From the powder pattern (Fig. 32), it is

Reproduced with permission of the copyright owner. Further reproduction prohibited without permission.

clear that the lamellar character of the material is retained, and the development of an emerald-green colour suggests that the aniline has been polymerized to polyaniline. The X-ray data suggests that the polymer is lying with the rings parallel to the layers. FTIR confirms the formation of polyaniline as shown in figure 33.

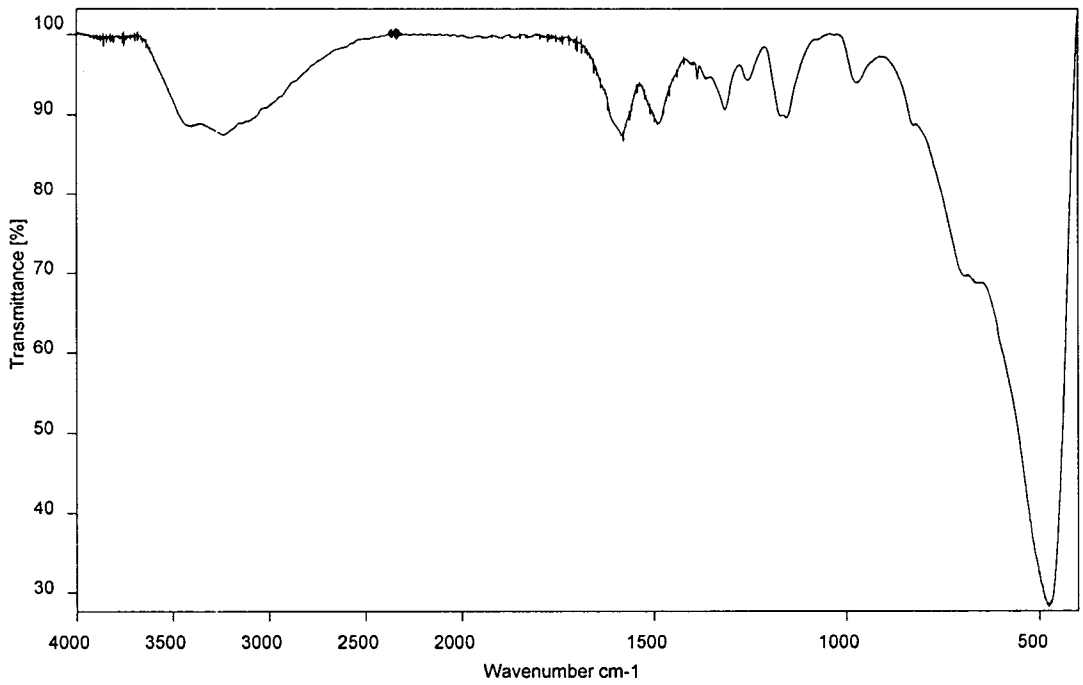

Figure 33 – FTIR of PANI/TiO_2 Heated at 140°C

The FTIR clearly shows the retention of the layered structure as shown by the broad band between 400 and 800 cm^{-1} and the emergence of the characteristic fingerprint of polyaniline. It is interesting to note that when compared to bulk polyaniline, all the peaks in the above IR corresponding to polyaniline are shifted to higher wavenumber or higher energy. This indicates some interaction between the polymer and the layered host. It is proposed that this interaction causes an increase in the reduced mass of the polymer

Reproduced with permission of the copyright owner. Further reproduction prohibited without permission.

thus increasing the energy required to vibrate the molecule which results in shifting of the peaks.

Direct oxidation of the material with $(NH_4)_2S_2O_8$ was also attempted as the formation of polyaniline is well documented with this oxidizing agent. The formation of polyaniline was obvious by the change in colour from an off white mixture to a green-blue mixture, the characteristic colour of polyaniline. Upon filtration a green-blue product was obtained. FTIR of the product again clearly showed the fingerprint of polyaniline further confirming that aniline had been intercalated between the layers of TiO_2 and that indeed polyaniline has been synthesized. Unfortunately, XRD of the polyaniline product indicated that the polyaniline was not intercalated and that in fact, the $HTiO_2$ phase has been regenerated. The powder pattern for the oxidized product is shown in figure 34.

Reproduced with permission of the copyright owner. Further reproduction prohibited without permission.

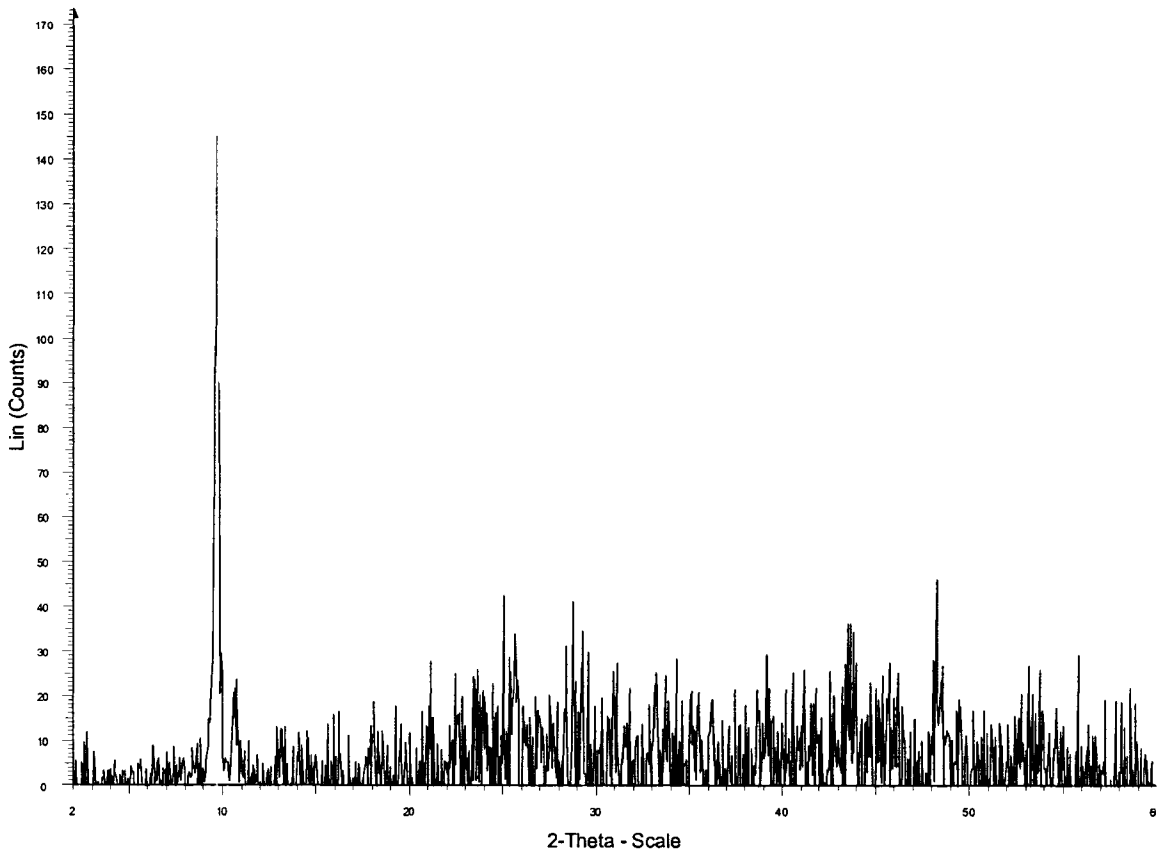

Figure 34 – X-ray Diffraction of Aniline/TiO_2 Oxidized by $(NH_4)_2S_2O_8$

The regeneration of the $HTiO_2$ phase is plausible as protons are liberated from the aniline monomers upon coupling. It is proposed that the protons released during the oxidation of the aniline react to form the stable $HTiO_2$ phase into which the polyaniline chains are not able to intercalate. As a result the final product is a mixture of polyaniline and $HTiO_2$. Several other oxidizing agents such as H_2O_2, and Ce^{4+} were attempted and while they all resulted in polymerization of the aniline, none were successful in making polyaniline intercalated TiO_2. It is proposed that failure to produce polyaniline intercalated TiO_2 in the cases of treatment with oxidizing agents other than air is due to the fact that they were performed in solution. In solution exfoliation of the TiO_2 sheets

Reproduced with permission of the copyright owner. Further reproduction prohibited without permission.

occurs. As the polymerization progresses free protons are liberated in the solution which the TiO_2 sheets coordinate with and form the stable $HTiO_2$ phase.

3.4 Graphite Oxide

The conversion of graphite into graphite oxide is afforded through a relatively harsh oxidation process. Upon completion of the oxidation the graphite oxide is easily characterized as being a considerably different compound. Upon visual inspection it can be seen that the graphite oxide powder is a light brown colour compared to the perfectly black graphite. XRD is the primary characterization tool used to study the conversion of graphite to graphite oxide, and the diffractograms for graphite and graphite oxide are shown in figures 35 and 36, respectively.

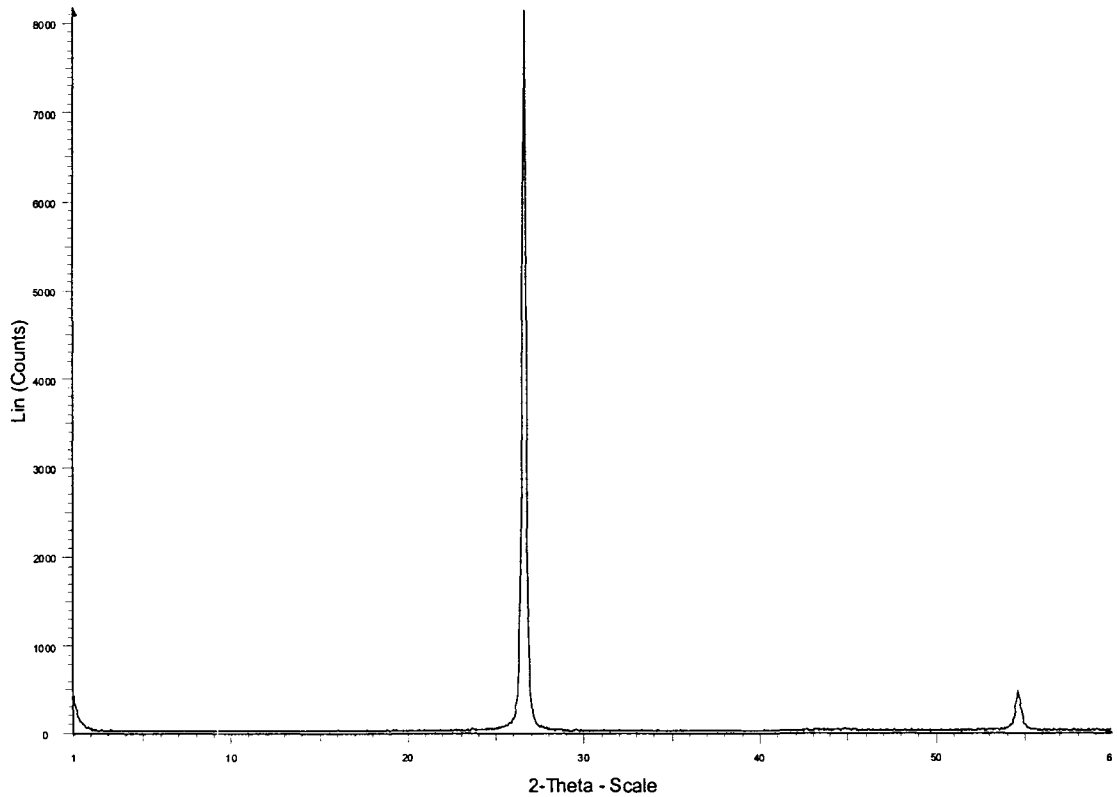

Figure 35 – X-ray Diffraction of Graphite

Reproduced with permission of the copyright owner. Further reproduction prohibited without permission.

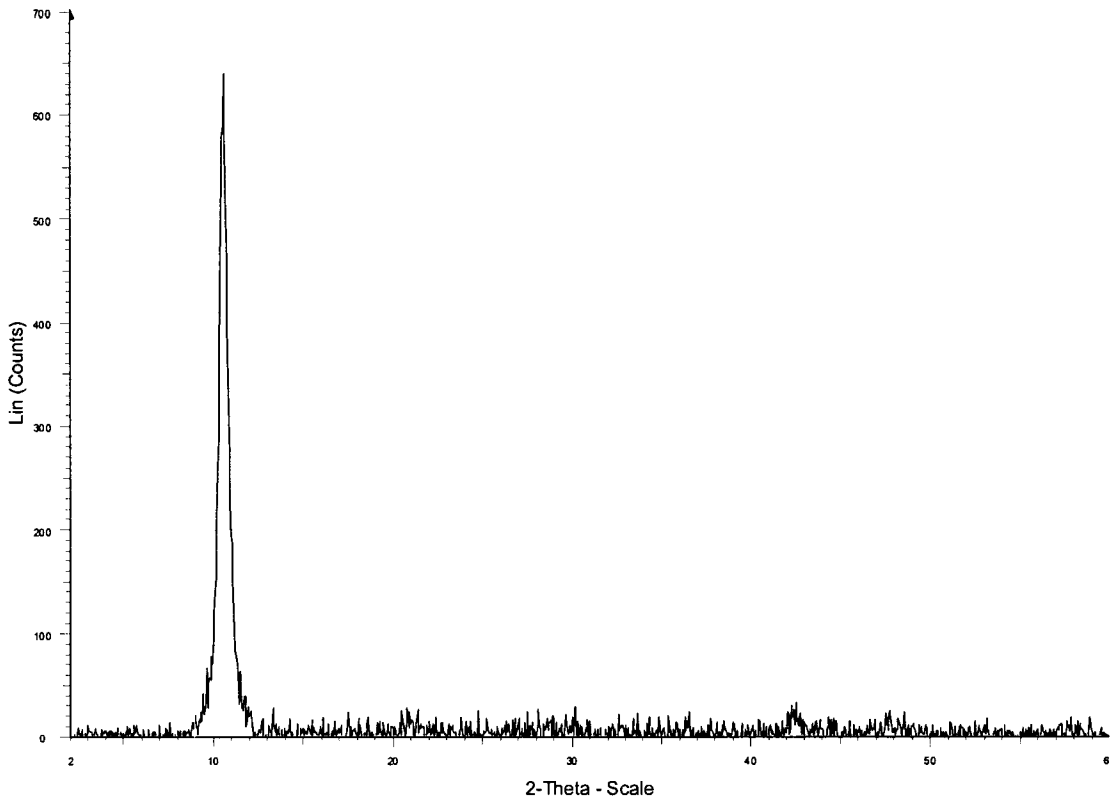

Figure 36 - XRD of Graphite Oxide

The interlayer spacing of pristine graphite is 3.3Å. Upon oxidation the ordering of the layers is severely disrupted resulting in a much less ordered material than that of graphite oxide. The peak for our graphite oxide corresponded to an interlayer spacing of 8.3Å and is consistent with values that have been reported previously [144].

The oxidation of graphite introduces many polar groups into the structure of graphite, such as –OH, -COOH, C=O, and epoxides, as shown in figure 38.

Reproduced with permission of the copyright owner. Further reproduction prohibited without permission.

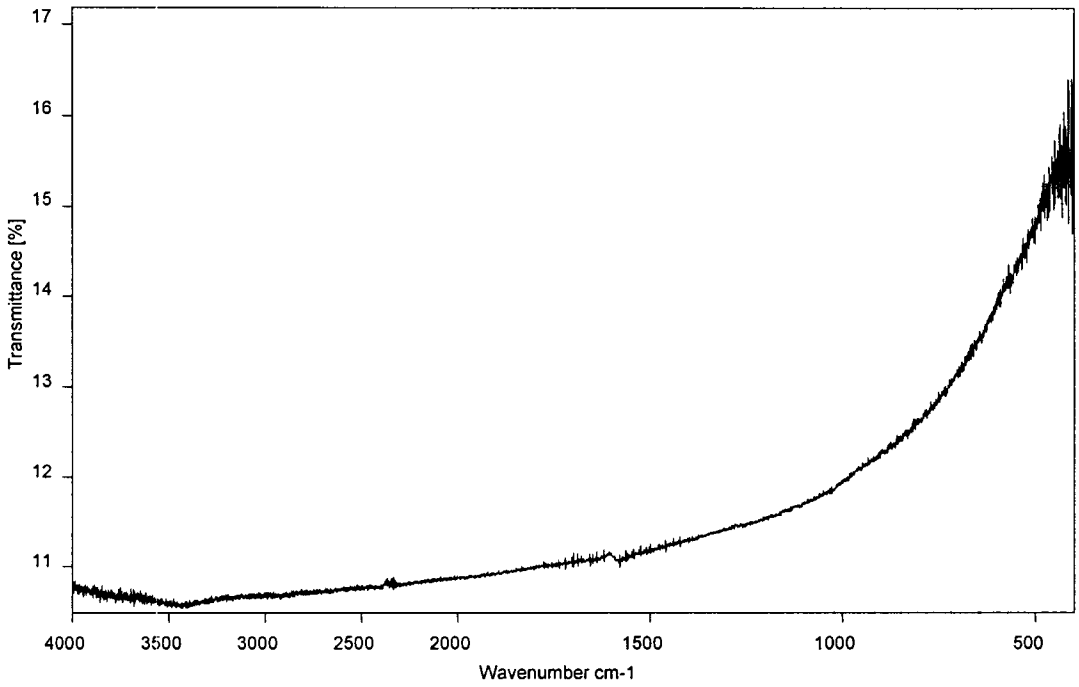

Figure 37 – FTIR of Graphite

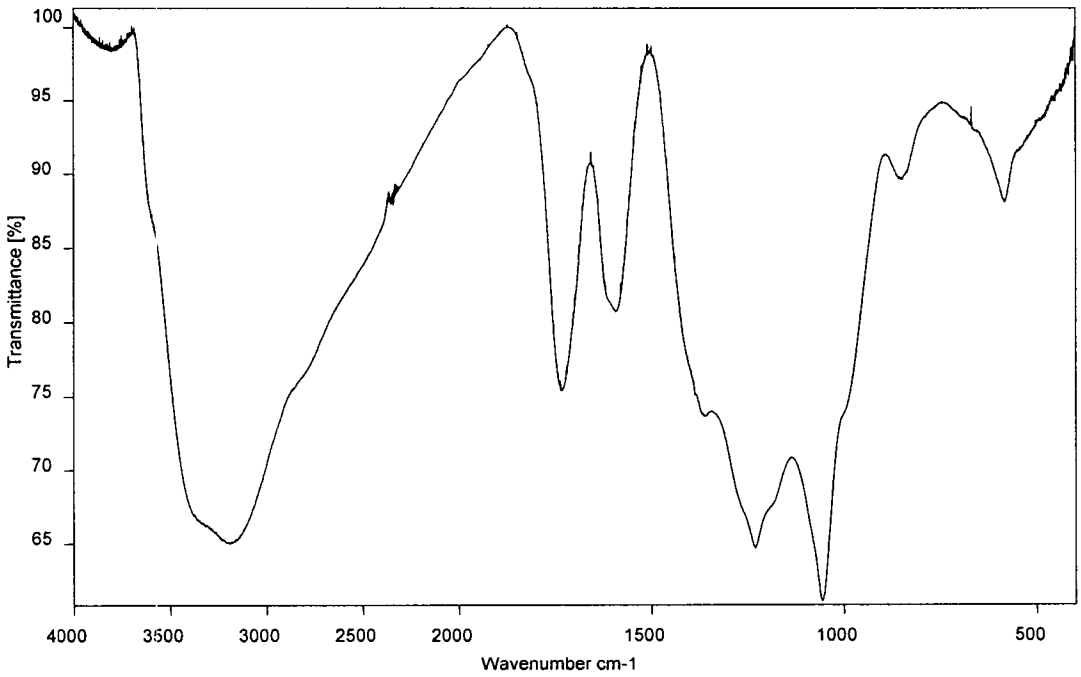

Figure 38 - FTIR of Graphite Oxide

Reproduced with permission of the copyright owner. Further reproduction prohibited without permission.

The FTIR of graphite (Figure 37) is featureless, transmitting almost no radiation making FTIR not interpretively useful for pristine graphite. In comparison the FTIR of graphite oxide is quite rich displaying much functionality. A strong OH peak is visible at 3364 cm^{-1} along with other C-O functionalities such as COOH (1727.8 cm^{-1}) and COC/COH (1383-1065 cm^{-1}). Residual sp^2 character is denoted by the absorption of C=C bonds at 1618 cm^{-1}.

The TGA of graphite oxide is shown in figure 39.

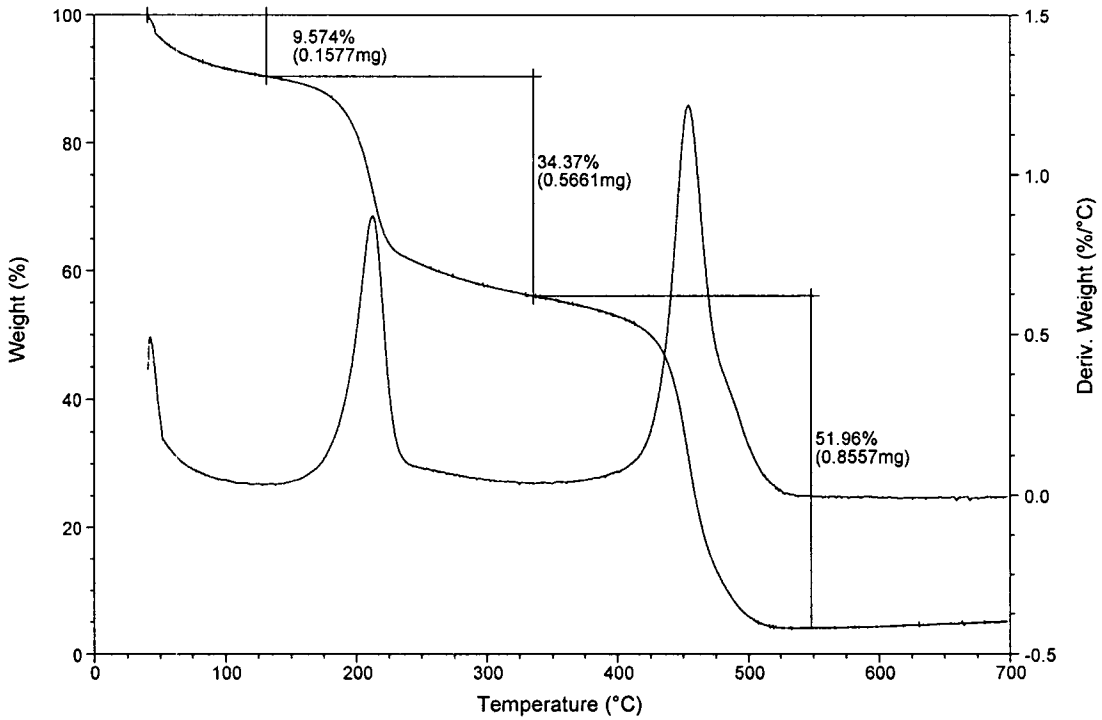

Figure 39 – TGA of Graphite Oxide

TGA of graphite oxide shows three major mass loss regions at 40, 185, and 433°C corresponding to the loss of water, CO and CO_2, and finally the carbon skeleton. Water is liberated from the graphite oxide at relatively low temperature due to diffusion into the

Reproduced with permission of the copyright owner. Further reproduction prohibited without permission.

dry air purge. The evolution of CO and CO_2 is from the oxidation of functional groups on the graphite oxide [142].

DSC of graphite oxide shows a broad endothermic peak around 133°C which corresponds to the evolution of water from between the layers. Upon cooling and reheating no peaks disappears indicating that the water does not penetrate back between the layers. The DSC of graphite oxide is shown in Figure 40.

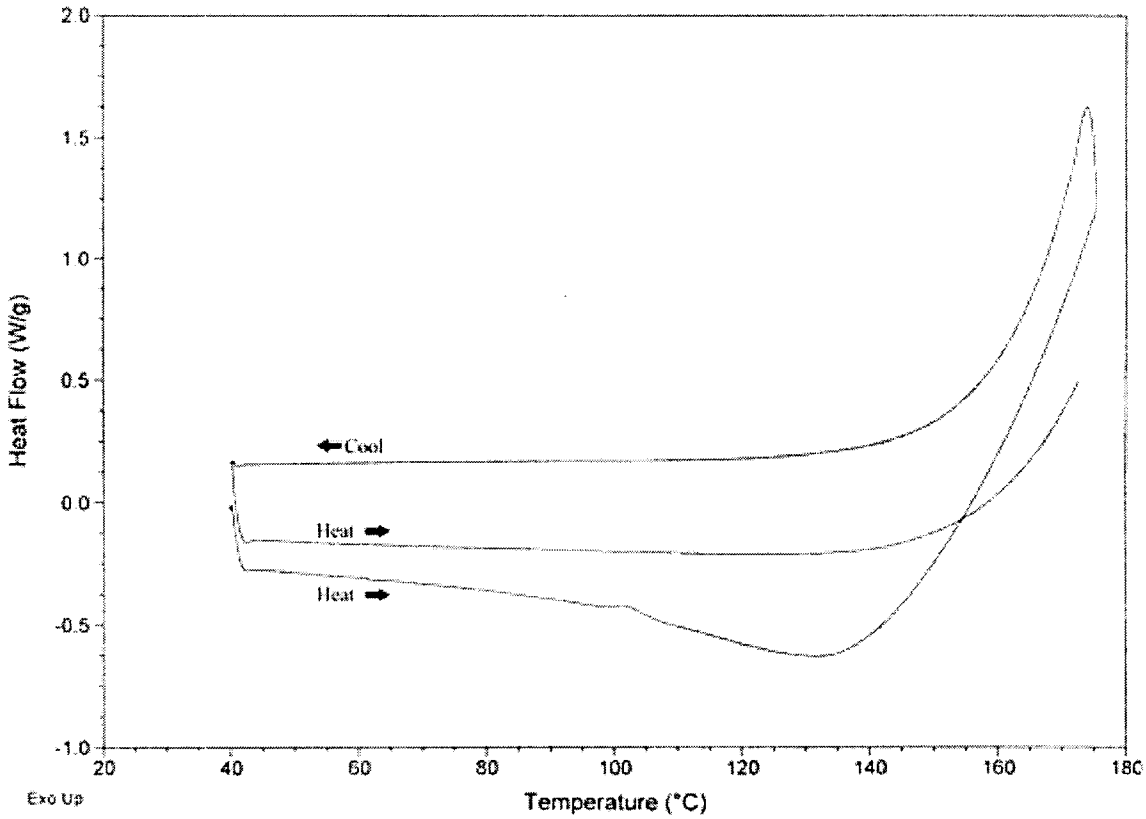

Figure 40 – DSC of Graphite Oxide

Electrical conductivity measurements also indicate that graphite oxide has been formed. Graphite is a good conductor due to the conjugated pi system which it possesses. Upon oxidation of graphite this conjugation is destroyed resulting in a much lower

Reproduced with permission of the copyright owner. Further reproduction prohibited without permission.

electrical conductivity. van der Pauw electrical conductivity measurements found the conductivity of the graphite oxide to be 3×10^{-9} S/cm, 7×10^{7} fold lower than that of pristine graphite.

Previous work in the Bissessur group had shown that intercalation of polar polymers was achievable through an exfoliation and restacking process [139]. Having a well established methodology for the intercalation of polymers into graphite oxide coupled with the poor electrical conductivity of the species led us to experiment with the possibility of using graphite oxide as an electrolyte material for solid state batteries. MEEP is one of the best ionically conductive polymers available and had not been intercalated between the layers of graphite oxide. As such, this species was designated as a target electrolyte material for the Bissessur group.

MEEP was synthesized as described in the experimental section, the DSC of MEEP confirmed the glass transition temperature was around -80°C as shown in figure 41.

Reproduced with permission of the copyright owner. Further reproduction prohibited without permission.

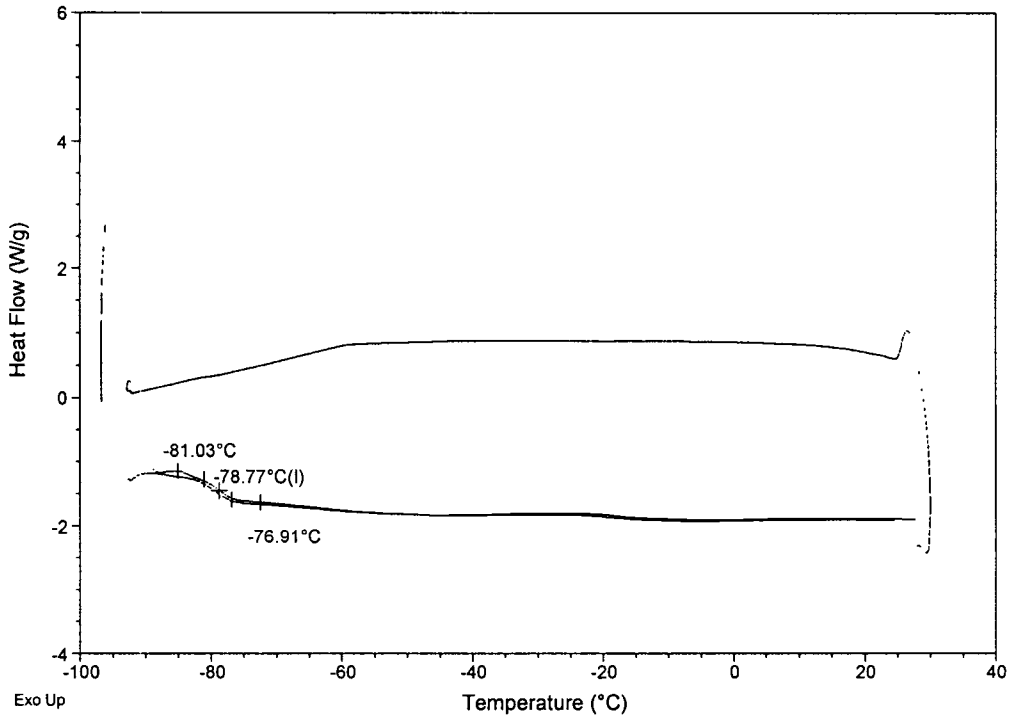

Figure 41 – DSC of MEEP

In order to be useful as an ionic conductor the MEEP must be first complexed with lithium salts. Lithium triflate was used to lithiate MEEP in the ratio $(LiOTf)_1(MEEP)_4$ simply by stirring the salt with the polymer in aqueous solution. Upon isolation of the MEEP complexed with lithium triflate, DSC was ran and the data indicated a shift in the glass transition temperature to a higher temperature of -43°C. This is to be expected as coordination of the lithium ions will reduce the mobility of the polymer chain and is consistent with the literature [143]. The DSC of lithium complexed MEEP is shown in figure 42.

Reproduced with permission of the copyright owner. Further reproduction prohibited without permission.

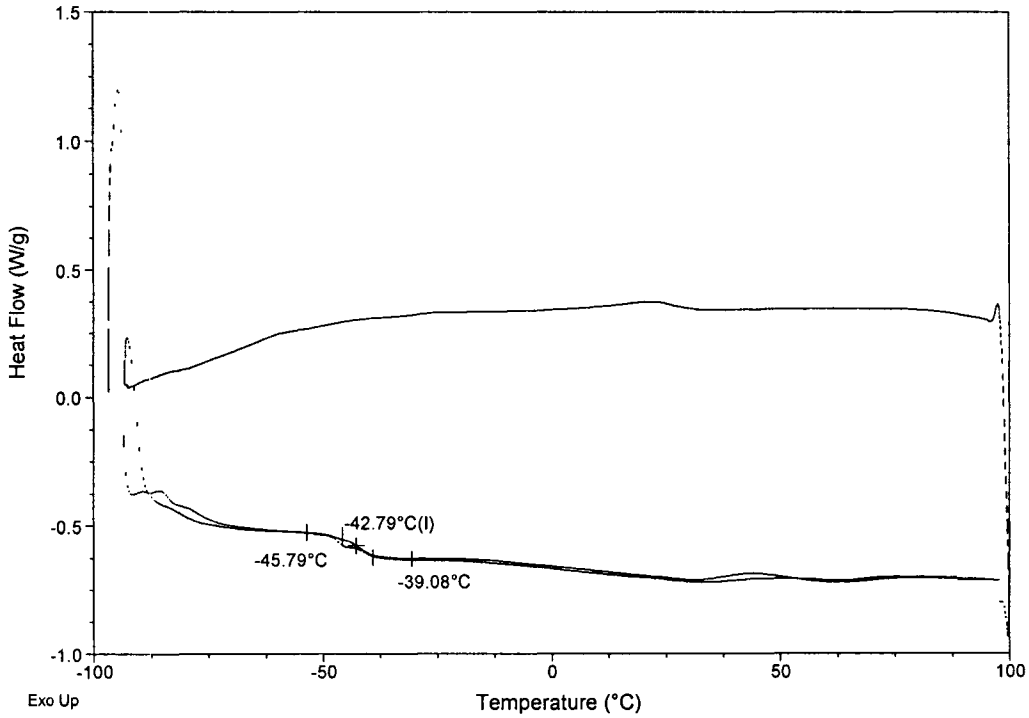

Figure 42 – DSC of LiMEEP

XRD shows the successful intercalation of $(MEEP)_4LiOTf$ into GO as shown in figure 43.

Reproduced with permission of the copyright owner. Further reproduction prohibited without permission.

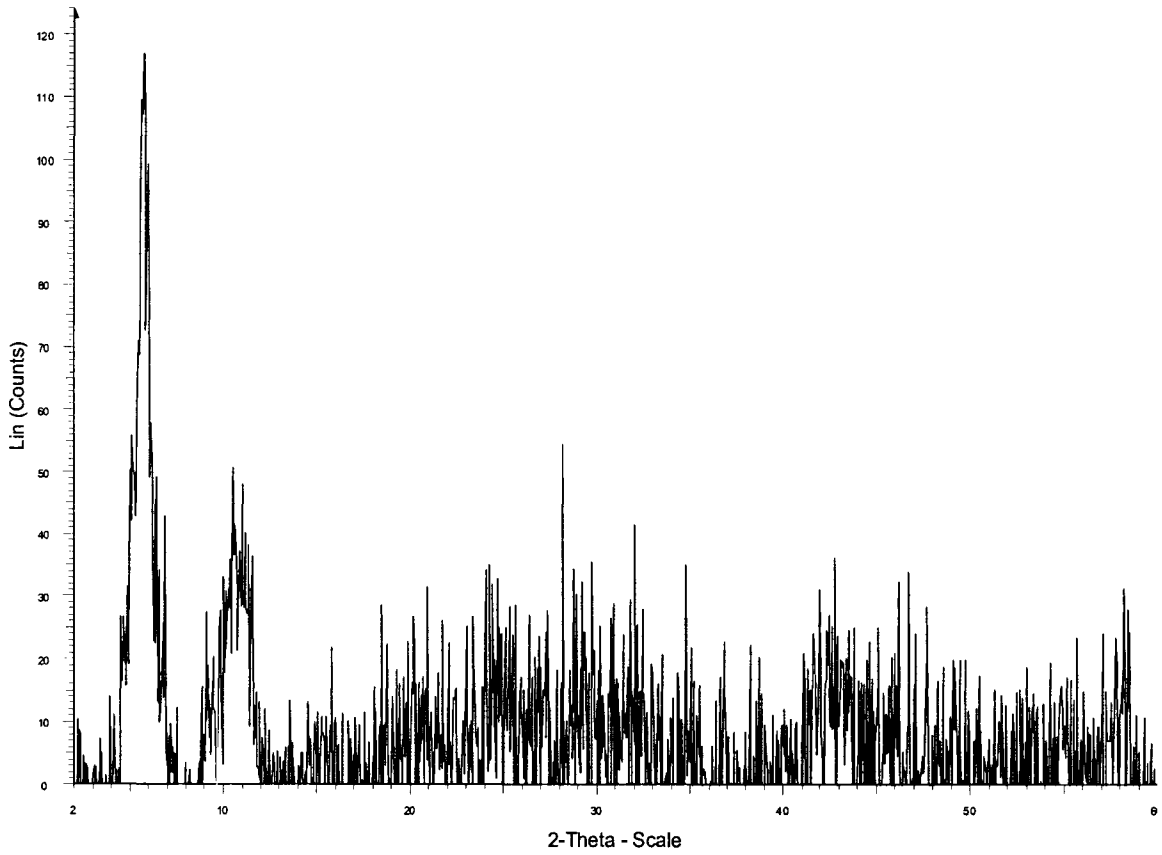

Figure 43 – X-ray Diffraction of LiMEEP/Graphite Oxide Cast on Glass

The interlayer spacing of the intercalated product is 15.5 Å. When compared with GO this indicates an interlayer expansion of 7.2 Å. As was shown previously by DSC, GO contains water molecules between its layers. Previous studies have shown that upon intercalation of polymers these water molecules are largely displaced, and as a result a correction factor of 2.8 Å must be added on to the observed interlayer expansion. 2.8 Å corresponds to the molecular diameter of a water molecule. Applying this correction factor yields the true interlayer expansion of 10 Å for the intercalation of $(MEEP)_4LiOTf$ into GO.

Reproduced with permission of the copyright owner. Further reproduction prohibited without permission.

The solid LiMEEP/GO nanocomposite was obtained through freeze drying. The resulting dark powder was collected and fully characterized. XRD of the material, shown in figure 44, shows very weak peaks which do correspond to the powder pattern obtained from the sample cast on a glass plate.

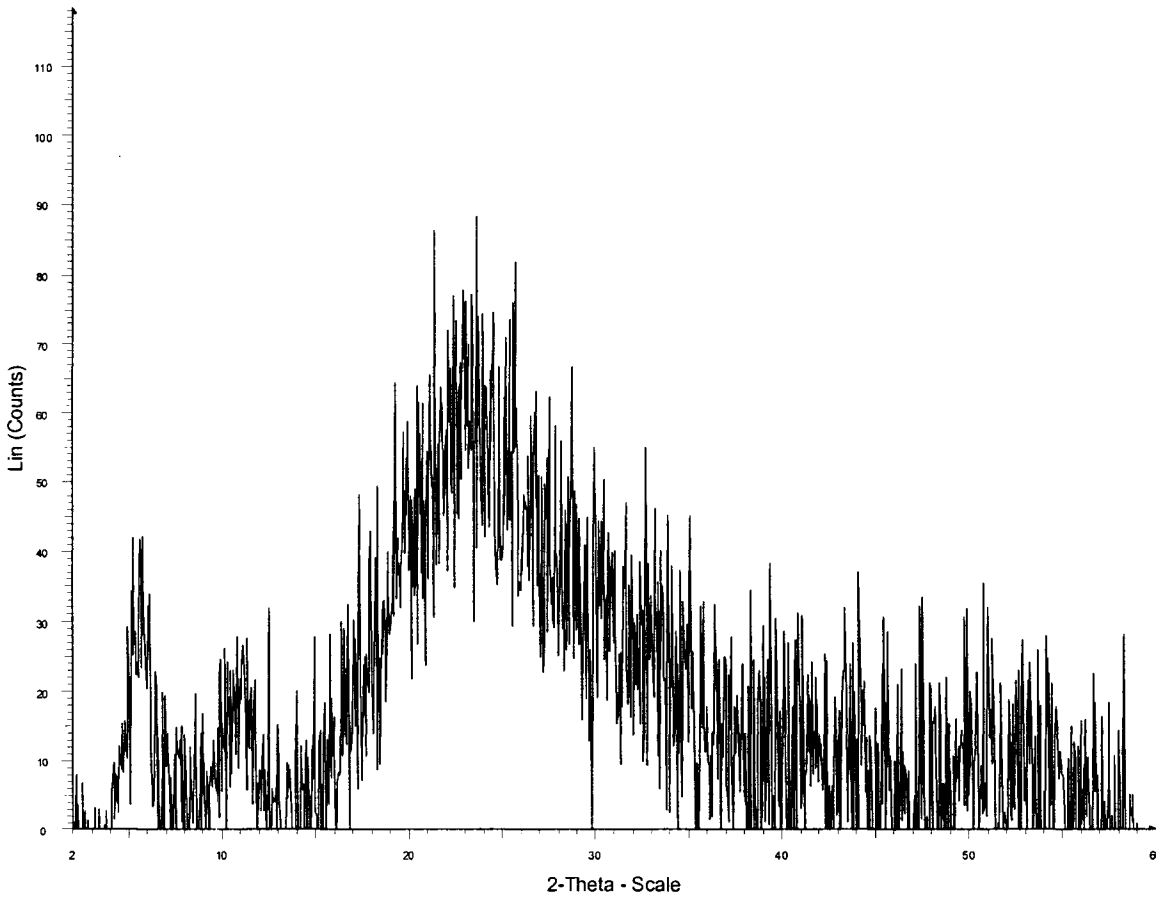

Figure 44 – X-ray Diffraction of Freeze dried LiMEEP/Graphite Oxide

A plausible explanation for the decrease in peak intensity is the non preferential ordering of the layers in the solid state coupled with the low electron density of materials. Preferential orientation of the layers was attempted via pressing the sample into pellets and then running XRD but no improvement of the spectrum was visible.

Reproduced with permission of the copyright owner. Further reproduction prohibited without permission.

FTIR of the nanocomposite, shown in figure 45, clearly shows the peaks of GO are still present along with several new peaks which correspond exactly with the FTIR of MEEP.

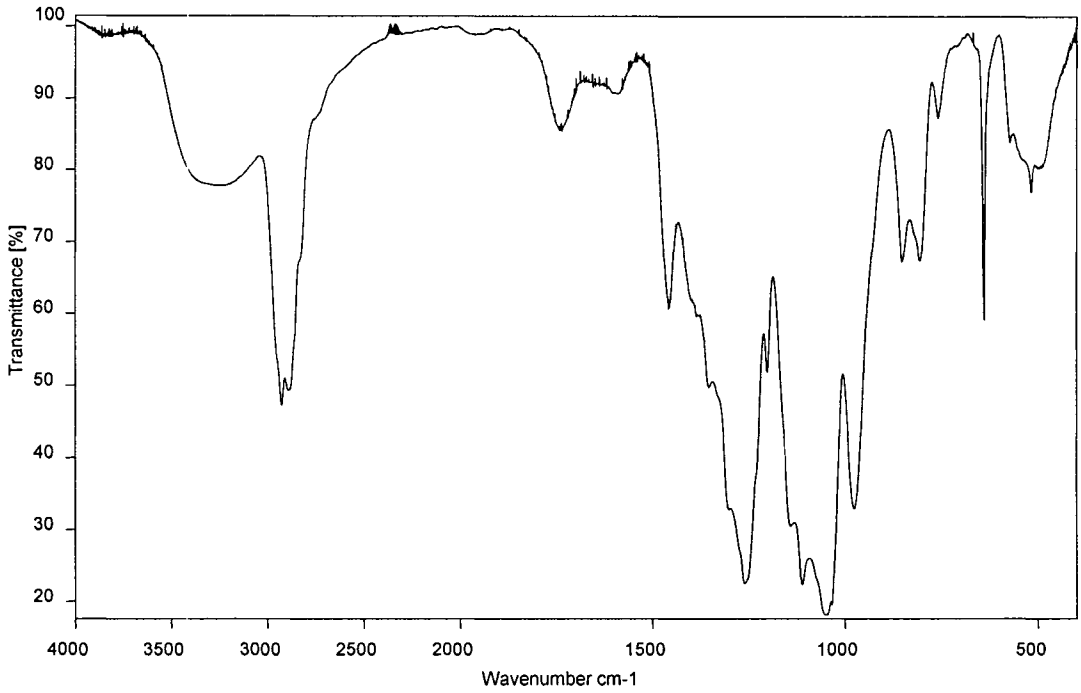

Figure 45 – FTIR of LiMEEP/Graphite Oxide

TGA of the LiMEEP/GO, shown in figure 46, reveals a major mass loss around 200°C and another minor mass loss around 700°C.

Reproduced with permission of the copyright owner. Further reproduction prohibited without permission.

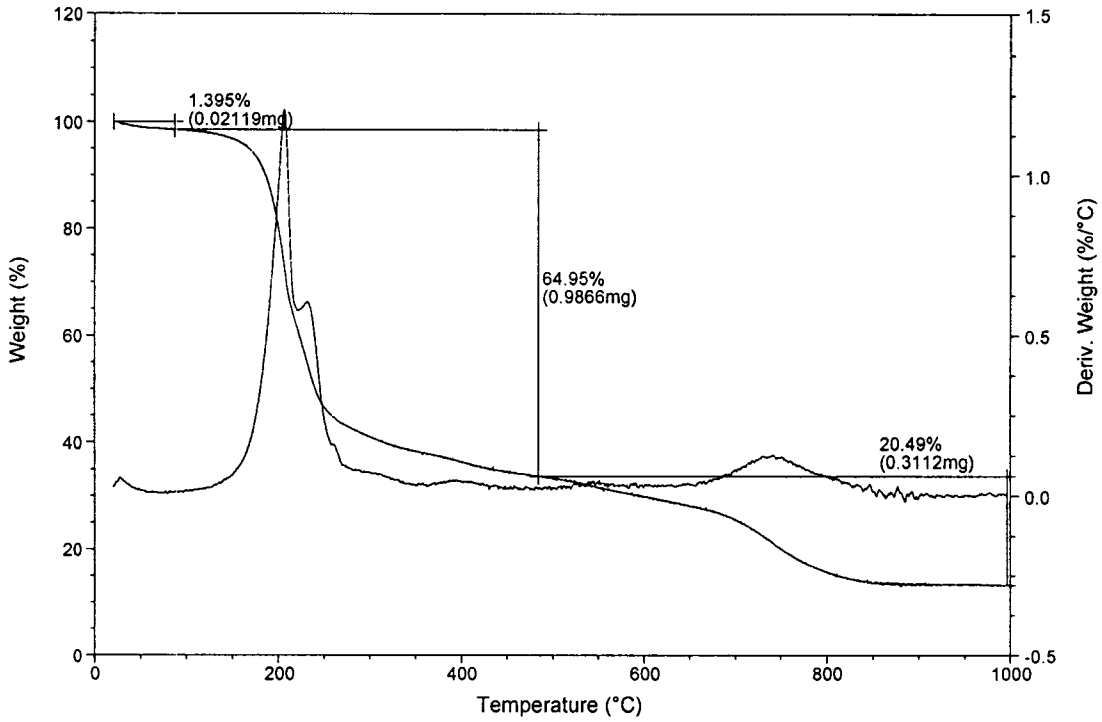

Figure 46 – TGA of LiMEEP/Graphite Oxide

Compared with the thermogram of GO the nanocomposite decomposes much differently and, in fact, appears to be the decomposition of the polymer alone. This indicates that the polymer somehow stabilizes or protects the graphite oxide from thermal decomposition.

DSC of the nanocomposite, shown in figure 47, shows a glass transition temperature corresponding to the lithiated MEEP polymer.

Reproduced with permission of the copyright owner. Further reproduction prohibited without permission.

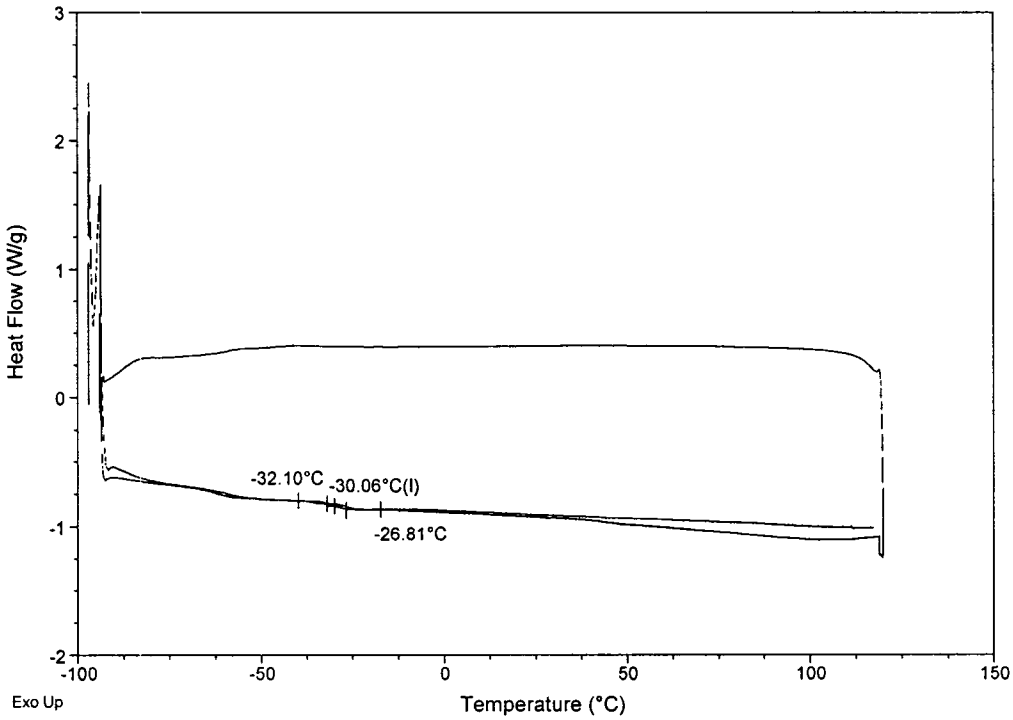

Figure 47 – DSC of LiMEEP/Graphite Oxide

Interestingly, the glass transition temperature for the nanocomposite is shifted to a higher temperature of -30°C compared to that of -43°C for the LiMEEP polymer. This phenomenon has been observed previously with MEEP intercalated smectites and it has been proposed that the rise in glass transition temperature is due to the polymer's environment becoming constrained [145].

Finally, ionic conductivity measurements were taken at room temperature. Measurements were taken on pressed pellets from powder which was previously heated to 100°C under dynamic vacuum to ensure removal of moisture. The pellets were pressed while the powder was still hot and assembled in an airtight measurement cell. While a complete analysis has not yet been obtained, preliminary analysis indicates a room temperature ionic conductivity of 6.8×10^{-6} S/cm, one order of magnitude lower than that

Reproduced with permission of the copyright owner. Further reproduction prohibited without permission.

of unintercalated LiMEEP. This data is encouraging as the measurements were taken perpendicular to the preferred orientation of the layers. It has been shown that ionic conductivity of layered compounds is considerably higher parallel to the preferred orientation of the layers [80]. Based on this previous evidence it is reasonable to assume conduction along the layers will be much higher than that of which has already been measured.

3.5 Lithium Hectorite

Previous work in the Bissessur group involved the insertion of polymers between the layers of hectorite [146]. While many polymers with solid electrolyte properties have been included between the layers of hectorite, the lithiation of natural hectorite had not been explored in the Bissessur group.

The purification of natural hectorite through a sedimentation process is required to remove impurities such as calcite and quartz. After purification by sedimentation is complete a suspension of hectorite is obtained whereby a white fluffy powder can be isolated through freeze drying. XRD of this material, shown in figure 48, clearly displays the layered morphology of hectorite.

Reproduced with permission of the copyright owner. Further reproduction prohibited without permission.

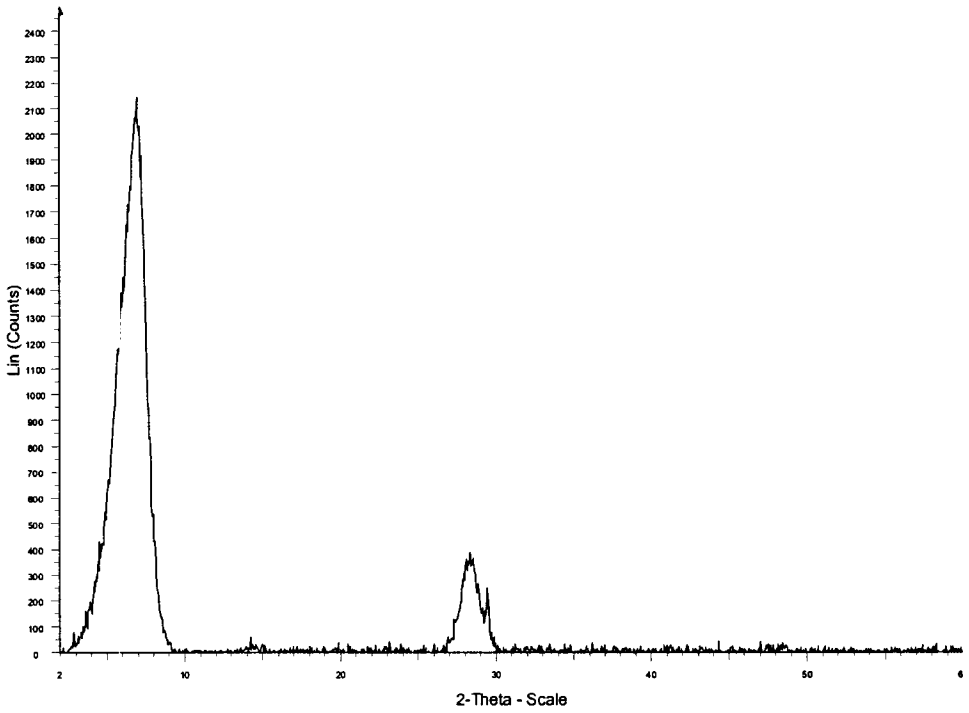

Figure 48 – X-ray Diffraction of Purified Hectorite

The XRD of the purified hectorite yields a peak at low angle corresponding to an interlayer spacing of 12.9 Å. Lithiation of the hectorite is afforded by mixing purified hectorite with a saturated solution of LiCl which is changed once a day, for three days. Natural hectorite contains ions such as sodium and magnesium in its interlayer so this process is essentially an ion exchange reaction driven by the large excess of lithium ions in solution. Upon completion of the lithiation a somewhat more rigid flaky material is obtained. XRD of this material, shown in figure 49, indicates a decrease in interlayer spacing of 1Å.

Reproduced with permission of the copyright owner. Further reproduction prohibited without permission.

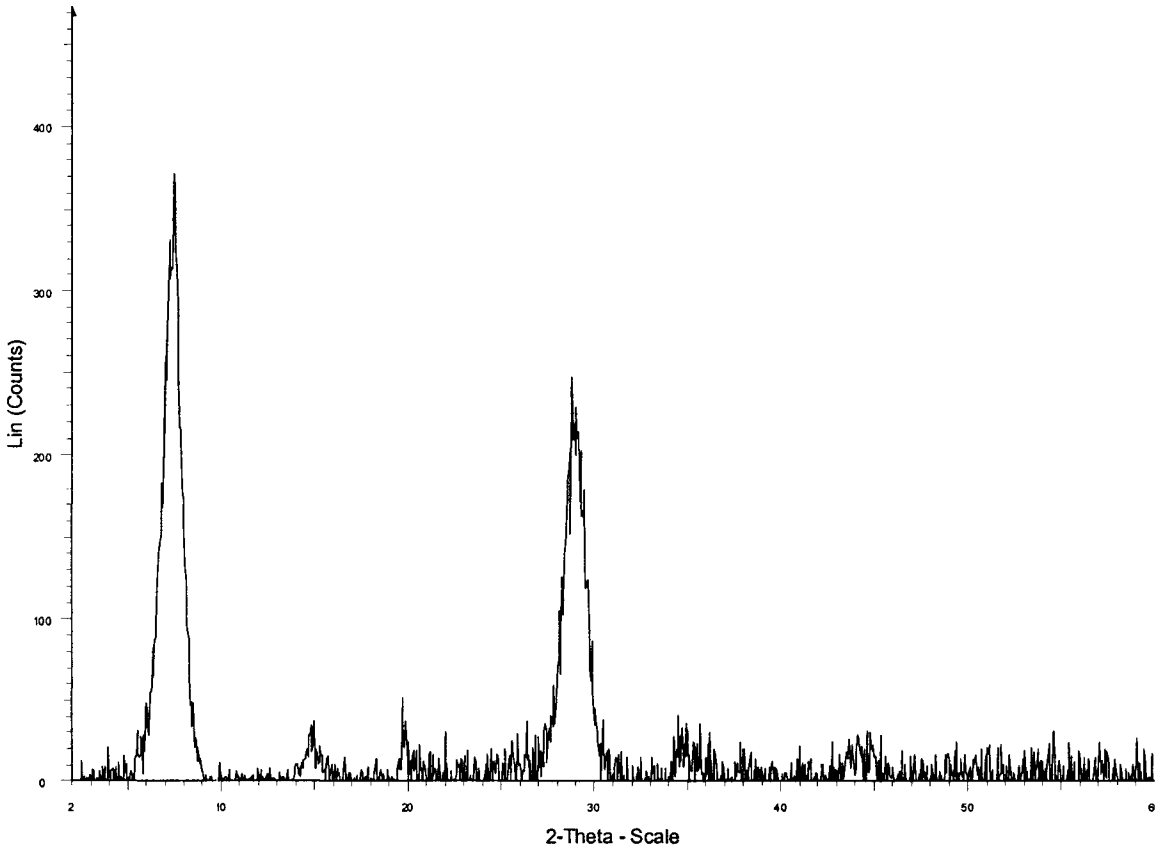

Figure 49 – X-ray Diffraction of LiHectorite

The observed decrease in interlayer spacing is very small and could be due to a change in atmospheric humidity more than a change of intercalated ions between the layers.

Variable temperature ionic conductivity measurements were taken on this material such that the conductivity was measured parallel to the stacking plane of the layers. The sample was prepared by painting silver electrodes on a glass slide and casting a suspension of Lithium hectorite over the electrodes. Wires were then attached to these electrodes so that measurements could be taken. Measurements were performed under vacuum to ensure that moisture was not contributing to the conductivity and the samples

Reproduced with permission of the copyright owner. Further reproduction prohibited without permission.

were dried at 100°C under dynamic vacuum prior to measurement. Impedance measurements yielded typical plots for ionic conductors. As sample of the raw impedance data for lithium hectorite is shown in figure 50.

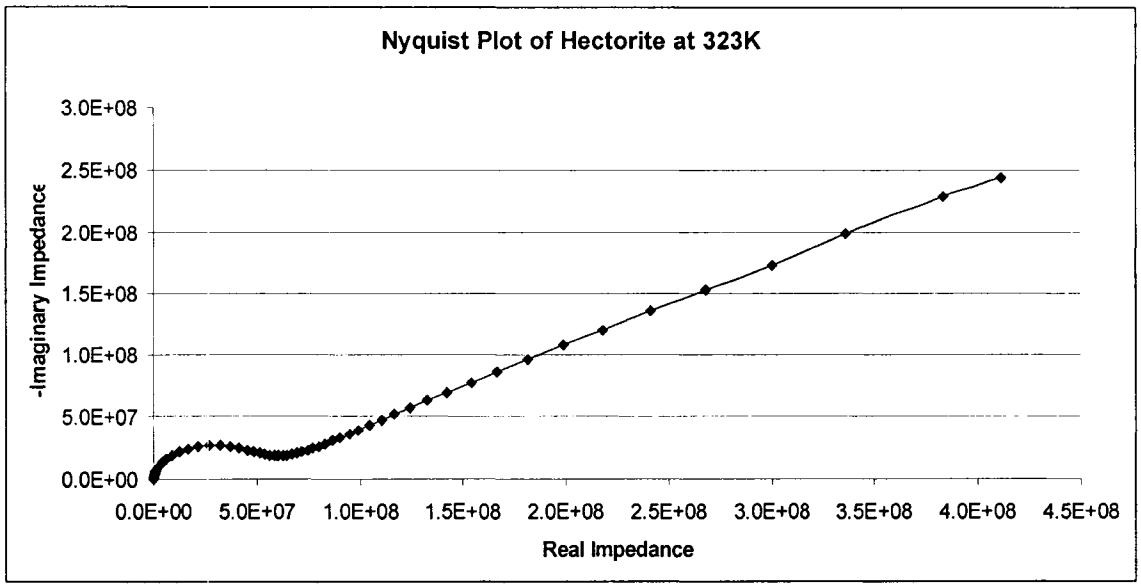

Figure 50 - Nyquist Plot of Lithium Hectorite at 323K

A fitting program was then used to fit this data to an equivalent electrical circuit. Essentially, the program determines an electrical circuit which will emulate the behavior of the material. From this circuit the bulk resistance of the sample can be determined and with the geometry of the sample being known the resistivity is calculated. This procedure is repeated at different temperatures and a set of resistivities as a function of temperature are obtained which are easily converted into conductivity by taking the reciprocal. The temperature dependence of lithium hectorite's conductivity is shown in figure 51.

Reproduced with permission of the copyright owner. Further reproduction prohibited without permission.

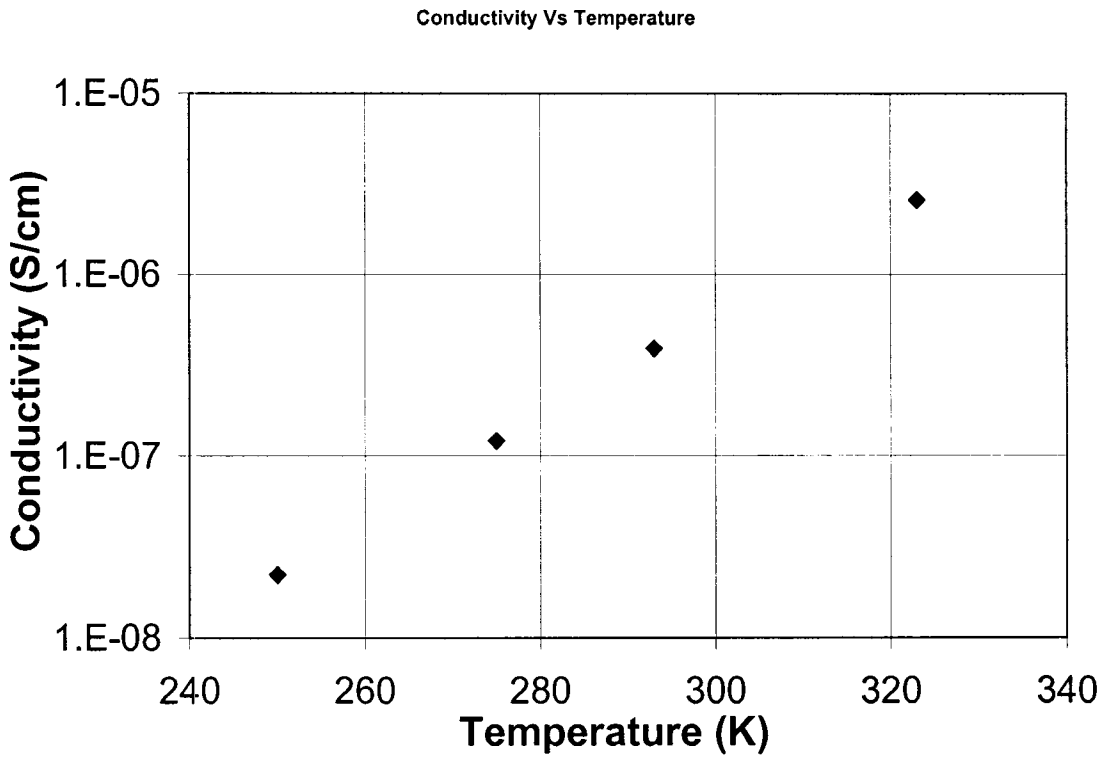

Figure 51 – Conductivity Vs Temperature of Lithiuim Hectorite

From this data the room temperature conductivity of lithium hectorite was found to be 3.91 x 10^{-7} S/cm. It is clear from figure 51 that the ionic conductivity of the material increases linearly with increasing temperature indicating that the conductivity is thermally activated. The measured room temperature ionic conductivity for solid lithium hectorite is quite good considering PEO_4LiOTf only displays room temperature conductivities on the order of 10^{-8} S/cm [147].

Reproduced with permission of the copyright owner. Further reproduction prohibited without permission.

Chapter 4 – Conclusions and Future Work

4.1 FeOCl

A series of anilines substituted in the two position have been intercalated between the layers of FeOCl. This work illustrates that FeOCl has the ability to polymerize substituted anilines *in situ* to yield polymer intercalated nanocomposites. The inclusion of polyanilines between the layers of FeOCl results in a large increase in conductivity allowing it to be considered for testing as a cathode material for lithium ion batteries. Future work on the FeOCl system should involve a study of the lithium intercalating properties of the polymer/FeOCl nanocomposites. The construction of small test cells using the nanocomposites as a cathode materials should also be explored to investigate the utility of substituted polyanilines intercalated FeOCl as cathode materials.

4.2 Titanate

The intercalation of ionically conductive polymers into layered titanate appears to be difficult due to the lack of specific attraction between the neutral polymers and negatively charged titanate layers. Attempts to charge the polymer chains by protonation failed due to reformation of layered $HTiO_2$ which appears to be a very stable phase. The $HTiO_2$ acts as a solid acid and as such can react with bases such as aniline. The inclusion of aniline between the layers has been successful and the subsequent polymerization of the intercalated aniline can be afforded by heating of the material in air. Attempts to polymerize the aniline with chemical oxidizers such as ammonium peroxydisulfate did not result in the formation of a polyaniline/$HTiO_2$ composites. Investigation of the effect, if any, polyaniline has on the band gap of $HTiO_2$ could be of interest towards solar cell or other semiconductor applications. While the intercalation of ionically conductive

Reproduced with permission of the copyright owner. Further reproduction prohibited without permission.

polymers was unsuccessful using a protonation method, several other techniques such as melt intercalation or perhaps coordination with lithium salts could be investigated to lead to inclusion of these polymer species.

4.3 Graphite Oxide

Lithiated MEEP has been complexed with graphite oxide to yield an exfoliated nanocomposite.

4.4 Lithium Hectorite

Natural hectorite has been ion exchanged with lithium ions to produce lithium hectorite. Ionic conductivity measurements on this layered system indicate surprisingly good ionic conductivities at room temperature with no presence of a polymer. While the conductivities are nowhere near good enough for use as an electrolyte directly, the inclusion of ionically conductive polymers between the layers of lithiated hectorite could produce highly ionically conductive materials. Future work should focus on the intercalation of ionically conducting polymers, such as MEEP, between the layers of lithium Hectorite.

Reproduced with permission of the copyright owner. Further reproduction prohibited without permission.

References

[1] Meyer, H. Wolfgang, *Adv. Mater.* **1998**, *10*, 6, 439.

[2] Buchmann, I. *Batteries in a Portable World: A Handbook on Rechargeable Batteries for Non-Engineers*. 2nd Ed. Cadex Electronics, 2001

[3] Singleton, V. Voltaic Cell. [Online Image] (17/2/2007). http://home.att.net/~v.d.singleton/genchem/voltaic.gif

[4] McMurry, J. and Fay, R. C. *Chemistry*. 3rd Ed. New Jersey: Prentice Hall, 2001.

[5] Ruetschi, P.; Meli, F.; Desilvestro, J. *J. Power Sources* **1995**, *57*, 85.

[6] Croce, F.; Appetecchi, G. B.; Persi, L.; Scrosati, B. *Nature* **1998**, *394*, 456.

[7] Bazito, F. F. C. and Torresi, R. M. *J. Braz. Chem. Soc.* **2006**, *17*, 4, 627.

[8] Tirado, J. L. *Materials Science and Engineering R.* **2003**, *40*, 103.

[9] Foster, M. S.; Crouthamel, C. E.; Wood, S. E. *J. Phys. Chem.* **1966**, *70*, 3042.

[10] Wen, C. J. and Huggins, R. A. *J. Electrochem. Soc.* **1981**, *128*, 1181.

[11] Beauliue, L. Y.; Eberman, K. W.; Turner, R. L.; Krause, L. J.; Dahn, J. R. *Electrochem. Solid State* **2001**, *4*, A137.

[12] Kasavajjula, U.; Wang, C.; Appleby, A. J. *J. Power Sources* **2007**, *163*, 1003.

[13] Denis, S.; Beudrin, E.; Touboul, M.; Tarascon, J. M. *J. Electrochem. Soc.* **1997**, *144*, 4099.

[14] Kim, S. S.; Ikuta, H.; Wakihara, M. *Solid State Ionics* **2001**, *139*, 57.

[15] Kim, S. S.; Ogura, S.; Ikuta, H.; Uchimoto, Y.; Wakihara, M. *Solid State Ionics* **2002**, *146*, 249.

[16] Whittingham, M. S. *Chem. Rev.* **2004**, *104*, 4271.

[17] Gamble, F. R.; Osiecki, J. H.; Cais, M.; Pishardy, R.; Disalvo, F. J.; Geballe, T. H. *Science* **1971**, *174*, 493.

Reproduced with permission of the copyright owner. Further reproduction prohibited without permission.

[18] Whittingham, M. S. *J. Chem. Soc., Chem. Commun.* **1974**, 328.

[19] SubbaRao, G. V.; Tsang, J. C. *Mater. Res. Bull.* **1974**, *9*, 921.

[20] Whittingham, M. S. *Science* **1976**, *192*, 1126.

[21] Whittingham, M. S. *Chemtech* **1979**, *9*, 766.

[22] Whittingham, M. S.; Chianelli, R. R. *J. Chem. Educ.* **1980**, *57*, 569.

[23] Holleck, G. L.; Driscoll, J. P. *Electrochim. Acta* **1977**, *22*, 647.

[24] Whittingham, M. S. *J. Electrochem. Soc.* **1976**, *123*, 315.

[25] Rao, B. M. L.; Francis, R. W.; Christopher, H. A. *J. Electrochem. Soc.* **1977**, *124*, 1490.

[26] Whittingham, M. S. *J. Electrochem. Soc.* **1976**, *123*, 315.

[27] Dampier, F. W. *J. Electrochem. Soc.* **1974**, *121*, 656.

[28] Whittingham, M. S.; Dines, M. B. *J. Electrochem. Soc.* **1977**, *124*, 1387.

[29] Delmas, C.; Cognac-Auradou, H.; Cocciantelli, J. M.; Menetrier, M.; Doumerc, J. P. *Solid State Ionics* **1994**, *69*, 257.

[30] Zhang, F.; Zavalij, P. Y.; Whittingham, M. S. *Mater. Res. Bull.* **1997**, *32*, 701.

[31] Zhang, F.; Zavalij, P. Y.; Whittingham, M. S. *Mater. Res. Soc. Proc.* **1998**, *496*, 367.

[32] Zhang, F.; Whittingham, M. S. *Electrochem. Commun.* **2000**, *2*, 69.

[33] Torardi, C. C.; Miao, C. R.; Lewittes, M. E.; Li, Z. *Electrochem. Soc. Proc.* **2000**, *2000-21*, 68.

[34] Torardi, C. C.; Miao, C. R.; Lewittes, M. E.; Li, Z. *J. Solid State Chem.* **2002**, *163*, 93.

[35] Mitzushima, K.; Jones, P. C.; Wiseman, P. J.; Goodenough, J. B. *Mater. Res. Bull.* **1980**, *15*, 783.

Reproduced with permission of the copyright owner. Further reproduction prohibited without permission.

[36] Nagaura, T.; Tozawa, K. *Prog. Batteries Solar Cells* **1990**, *9*, 209.

[37] Ozawa, K. *Solid State Ionics* **1994**, *69*, 212.

[38] Levasseur, S.; Menetrier, M.; Suard, E.; Delmas, C. *Solid State Ionics* **2000**, *128*, 11.

[39] Cho, J.; Kim, G. Electrochem. *Solid State Lett.* **1999**, *2*, 253.

[40] Cho, J.; Kim, C.; Yoo, S. I. *Electrochem. Solid State Lett.* **2000**, *3*, 362.

[41] Cho, J.; Kim, Y. J.; Park, B. *Chem. Mater.* **2000**, *12*, 3788.

[42] Cho, J.; Kim, Y. J.; Park, B. *J. Electrochem. Soc.* **2001**, *148*, A1110.

[43] Cho, J.; Kim, Y. J.; Kim, J. T.; Park, B. *Angew. Chem., Int. Ed.* **2001**, *40*, 3367.

[44] Padhi, A. K.; Nanjundaswamy, K. S.; Goodenough, J. B. *J. Electrochem. Soc.* **1997**, *144*, 1188.

[45] Yang, S.; Song, Y.; Zavalij, P. Y.; Whittingham, M. S. *Electrochem. Commun.* **2002**, *4*, 239.

[46] Yang, S.; Zavalij, P. Y.; Whittingham, M. S. *Electrochem. Commun.* **2001**, *3*, 505.

[47] Yang, S.; Song, Y.; Ngala, K.; Zavalij, P. Y.; Whittingham, M. S. *J. Power Sources* **2003**, *119*, 239.

[48] Yamada, A.; Chung, S. C.; Hinokuma, K. *J. Electrochem. Soc.* **2001**, *148*, A224.

[49] Andersson, A. S.; Kalska, B.; Haggstrom, L.; Thomas, J. O. *Solid State Ionics* **2000**, *130*, 41.

[50] Andersson, A. S.; Thomas, J. O.; Kalska, B.; Haggstrom, L. *Electrochem. Solid-State Lett.* **2000**, *3*, 66.

[51] Ravet, N.; Goodenough, J. B.; Besner, S.; Simoneau, M.; Hovington, P.; Armand, M. *Electrochem. Soc. Abstr.* **1999**, *99-2*, 127.

[52] Huang, H.; Yin, S.-C.; Nazar, L. F. *Electrochem. Solid State Lett.* **2001**, *4*, A170.

Reproduced with permission of the copyright owner. Further reproduction prohibited without permission.

[53] Prosini, P. P.; Zane, D.; Pasquali, M. *Electrochim. Acta* **2001**, *46*, 3517.

[54] Yang, S.; Song, Y.; Zavalij, P. Y.; Whittingham, M. S. *Mater. Res. Soc. Proc.* **2002**, *703*, V7.9.

[55] Chung, S.-Y.; Bloking, J. T.; Chiang, Y.-M. *Nat. Mater.* **2002**, *1*, 123.

[56] Herle, P. S.; Ellis, B.; Coombs, N.; Nazar, L. F. *Nat. Mater.* **2004**, *3*, 147.

[57] Croce, F.; Epifanio, A. D.; Hassoun, J.; Deptula, A.; Olczac, T.; Scrosati, B. *Electrochem. Solid State Lett.* **2002**, *5*, A47.

[58] Okada, S.; Sawa, S.; Egashira, M.; Yamaki, J.-i.; Tabuchi, M.; Kageyama, H.; Konishi, T.; Yoshino, A. *J. Power Sources* **2001**, *97-98*, 430.

[59] Morcrette, M.; Wurm, C.; Masquelier, C. *Solid State Sci.* **2002**, *4*, 239.

[60] Masquelier, C.; Padhi, A. K.; Nanjundaswamy, K. S.; Goodenough, J. B. *J. Solid State Chem.* **1998**, *135*, 228.

[61] Song, Y.; Yang, S.; Zavalij, P. Y.; Whittingham, M. S. *Mater. Res. Bull.* **2002**, *37*, 1249.

[62] Masquelier, C.; Reale, P.; Wurm, C.; Morcrette, M.; Dupont, L.; Larchera, D. *J. Electrochem. Soc.* **2002**, *149*, A1037.

[63] Hong, Y.-S.; Ryu, K. S.; Park, Y. J.; Kim, M. G.; Leeb, J. M.; Chang, S. H. *J. Mater. Chem.* **2002**, *12*, 1870.

[64] Linden, D.; Reddy, T. B. *Handbook of Batteries*, 3rd ed.; McGraw-Hill: New York, 2002.

[65] Besenhard, J. O. Editor, *Handbook of Battery Materials*; Wiley-VCH: Weinheim, Germany, 1999.

[66] Arora, P.; Zhang, Z. *Chem. Rev.* **2004**, *104*, 4419.

Reproduced with permission of the copyright owner. Further reproduction prohibited without permission.

[67] Wakihara, M. *Mater. Sci. Eng. R Rep.* **2001**, *33*, 4, 109.

[68] Matsuda, M.; Morita, M.; Tachihara, F. *Bull. Chem. Soc. Jpn.* **1986**, *59*, 1967.

[69] Arakawa, M.; Yamaki, J. *J. Electronal. Chem.* **1987**, *219*, 273.

[70] Aubach, D.; Ein-Eei, Y.; Markovski, B.; Zaban, A.; Luski, S.; Carmeli, Y.; Yamine, H. *J. Electrochem. Soc.* **1995**, *142*, 2882.

[71] Iijima, T.; Suzuki, K.; Matsuda, Y. *Synth. Met.* **1995**, *73*, 9.

[72] Ohta, A.; Koshina, H.; Okuno, H.; Murai, H. *J. Power Sources* **1995**, *54*, 6.

[73] Buchmann, I. *Powerpulse.net* Will Lithium-Ion Batteries Power the New Millennium? Darnell.com Inc., California, 2000.

[74] Takahashi, T. Silver ion conducting solid electrolytes, in: Z. Munshi Ed., *Handbook of Solid State Batteries and Capacitors*, World Scientific, Singapore, 1995, Ch. 4.

[75] Dias, F. B.; Plomp, L.; Veldhuis, J. B. J. *J. Power Sources* **2000**, *88*, 169.

[76] Riley, M.; Fedkiw, P. S.; Khan, S. A. *J. Electrochem. Soc.* **2002**, *149*, 6, A667

[77] Fenton, D. E.; Parker, J. M.; Wright, P. V. *Polymer* **1973**, *14*, 589.

[78] Wright, P. V. *Br. Polym. J.* **1975**, *7*, 319.

[79] Armand, M. B.; Chabagno, S. M.; Duclot, M., in: Second International Meeting on Solid Electrolytes, St. Andrews, Scotland, Extended Abstracts, 20-22 Sept., 1978.

[80] Hutchinson, J. C.; Bissessur, R.; Shriver, D. F. *Chem. Mater.* **1996**, *8*, 1597.

[81] Feullade, G.; Perche, P. *J. Appl. Electrochem.* **1975**, *5*, 63.

[82] Abraham, K. M.; Alamgir, M. *J. Electrochem. Soc.* **1990**, *137*, 1657.

[83] Croce, F.; Gerace, F.; Dautzenberg, G.; Passerini, S.; Appetecchi, G. B.; Scrosati, B. *Electrochim. Acta.* **1994**, *39*, 2187.

[84] Sung, H. Y.; Wang, Y. Y.; Wan, C. C. *J. Electrochem. Soc.* **1998**, *145*, 1207.

Reproduced with permission of the copyright owner. Further reproduction prohibited without permission.

[85] Stephan, A. M. and Nahm, K. S. *Polymer* **2006**, *47*, 5952.

[86] Appetecchi, G. B.; Croce, F,; Persi, L.; Ronci, F.; Scrosati, B. *J Electrochem. Soc.* **2000**, *147*, 4448.

[87] Bronstein, L. M.; Karlinsey, R. L.; Ritter, K.; Joo, C. G.; Stein, B., Zw, J. W. *J. Mater. Chem.* **2004**, *14*, 1812.

[88] Weston, J. E.; Steele, B. C. H. *Solid State Ionics* **1982**, *7*, 75.

[89] Itoh, T.; Miyamura, Y.; Iohikawa, Y.; Uno, T.; Kubo, M.; Yamamoto, O. *J. Power Sources* **2003**, *119-121*, 403.

[90] Kaarup, S. S.; West, K.; Christiansen, Z. B. *Solid State Ionics* **1980**, *28-30*, 375.

[91] Wieczorek, W. *Mater. Sci. Eng. B* **1992**, *15*, 108.

[92] Capuoano, F.; Croce, F.; Scrosati, B. *J Electrochem. Soc.* **1991**, *138*, 1918.

[93] Cho, J. P.; Liu, M. L. *Electrochim. Acta* **1997**, *42*, 10, 1481.

[94] Mustarelli, P.; Quartarone, E.; Tomasi, C.; Magistris, A. *Solid State Ionics* **1996**, *86-88*, 347.

[95] Appetecchi, G.B.; Croce, F.; Persi, L.; Ronci, F.; Scrosati, B. *Electrochim Acta* **2000**, *45*, 1481.

[96] Wasiucionek, M.; Breiter, M. W. in: Broadhead, J. and Scrosati, B. (Eds.) *Lithium Polymer Batteries,* Proceedings Vol. 96/17, The Electrochemical Society, NJ, 1997, 241.

[97] Dresselhaus, M. S. and Dresselhaus, G. *Advances in Physics* **1981**, *30*, 2, 139.

[98] Ouvrard, G.; Wu, Z. *Nucl. Instr. Meth. Phys. Res. B.* **1997**, *133*, 120.

[99] Ray, S. S.; Okamoto, M. *Prog. Polym. Sci.* **2003**, 1539.

[100] Benavente, E.; Santa Ana, M. A.; Mendizabal, F.; Gonzalez, G. *Coord. Chem. Rev.*

Reproduced with permission of the copyright owner. Further reproduction prohibited without permission.

2002, *224*, 87.

[101] Goldstaub, S. *Bull. Soc. Fr. Mineral.* **1935**, *58*, 49.

[102] Pieczko, M. E. and Breen, J. J. *Langmuir* **1995**, *11*, 1412.

[103] Armand, M.; Coic, L.; Palvadeau, P.; Rouxel, J. *J. Power Sources* **1978**, *3*, 137.

[104] Herber, R. H.; Cassell, R. A. *J. Chem. Phys.* **1981**, *75*, 4669.

[105] Halbert, T. R.; Johnston, D. C.; McCandlish, L. E.; Thompson, A. H.; Scanlon, J. C.; Dumesic, J. A. *Physica* **1980**, *99B*, 128.

[106] Hagenmullere, V. P.; Portier, J.; Barbe, B.; Bouclier, P. Z. *Anorg. Allg. Chem.* **1967**, *355*, 209.

[107] Kanamaru, F.; Yamanaka, S.; Koizumi, M.; Nagi, S. *Chem. Lett.* **1974**, 373.

[108] Kanamaru, F.; Shimada, M.; Koizumi, M.; Takano, M.; Kakada, T. *J. Solid State Chem.* **1973**, *7*, 297.

[109] Herber, R. H.; Maeda, Y. *Physica* **1981**, *105B*, 243.

[110] Kauzlarich, S. M.; Stanton, J. L.; Faber, J. Jr.; Averill, B. A. *J. Am. Chem. Soc.* **1986**, *108*, 7946.

[111] Kanatzidis, M. G.; Tonge, L. M.; Marks, T. J.; Marcy, H. O.; Kannewurf, C. R. *J. Am. Chem. Soc.* **1987**, *109*, 12, 3797.

[112] Kanatzidis, M. G.; Marcy, H. O.; McCarthy, W. J.; Kannewurf, C. R.; Marks, T. J. *Solid State Ionics.* **1989**, *32-33*, 594.

[113] Kanatzidis, M. G.; Wu, C. G.; Marcy, H. O.; DeGroot, D. C.; Kannewurf, C. R. *Adv. Mater.* **1990**, *2*, 8, 364.

Reproduced with permission of the copyright owner. Further reproduction prohibited without permission.

[114] Wu, C. G.; DeGroot, D. C.; Marcy, H. O.; Schindler, J. L.; Kannewurf, C. R.; Bakas, T.; Papaefthymiou, V.; Hirpo, W.; Yesinowski, J. P.; Liu, Y. J.; Kanatzidis, M. G. *J. Am. Chem. Soc.* **1995**, *117*, 9229.

[115] Sakaebe, H.; Higuchi, S.; Kanamura, K.; Fujimoto, H.; Takehara, Z. *J. Power Sources* **1995**, *56*, 165.

[116] Sagua, A.; Moran, E.; Alario-Franco, M. A.; Rivera, A.; Leon, C.; Santamaria, J.; Sanz, J. *Int. J. Inorg. Mat.* **2001**, *3*, 293.

[117] Bavykin, D. V.; Friedrich, J. M.; Walsh, F. C. *Adv. Mater.* 2006, 18, 2807.

[118] Kosmulski, M. *Adv. Coll. Inter. Sci.* **2002**, *99*, 255.

[119] Izawa, H.; Kikkawa, S.; Koizumi, M. *J. Phys. Chem.* **1982**, *86*, 25, 5023.

[120] Izawa, H.; Kikkawa, S.; Koizumi, M. *Polyhedron* **1983**, *2*, 741.

[121] Sasaki, T.; Watanabe, M.; Hashizume, H.; Yamada, H.; Nakazawa, H. *J. Am. Chem. Soc.* **1996**, *118*, 8329.

[122] Sasaki, T. and Watanabe, M. *J. Am. Chem. Soc.* **1998**, *120*, 4682.

[123] Sukpiron, N. and Lerner, M. M. *Chem. Mater.* **2001**, *13*, 2179.

[124] Huang H.; Kelder E.; Jak M.; Schoonman J. *Solid State Ionics.* **2001**, *139*, 67.

[125] Xu J.; Hu Y.; Song L.; Wang Q.; Fan W. *Mater. Res. Bul.* **2001**, *36*, 1833.

[126] Xu J.; Hu Y.; Song L.; Wang Q.; Fan W.; Liao G.; Chen Z. *Poly. Deg. Stab.* **2001**, *73*, 29.

[127] Hung, C. and Corbin, J. *Carbon.* **1999**, *37*, 701.

[128] Wu, J.; Zou, Y.; Li, X.; Liu, H.; Shen, G.; Yu, R. *Sensors Actuators B.* 2004.

[129] Lerf, H.; Heyong, H.; Forster, M.; linowski, J. *J. Phys. Chem. B.* **1998**, *102*, 4477.

[130] Bissessur, R.; Liu, P. K. Y.; White, W.; Scully, S. F. *Langmuir* **2006**, *22*, 4, 1729.

Reproduced with permission of the copyright owner. Further reproduction prohibited without permission.

[131] Bissessur, R.; Liu, P. K. Y.; Scully S. F. *Synthetic Metals* **2006**, *156*, 16-17, 1023.

[132] Bissessur, R. and Scully, S. F. *Solid State Ionics* 2007, *Accepted.*

[133] Madejova, J.; Bujdak, J.; Janek, M.; Komadel, P. *Spectrochimica Acta A* **1998**, *54*, 1397.

[134] Sandi, G.; Kizilel, R.; Carrado, K. A.; Fernandez-Saavedra, R.; Castagnola, N. *Electrochim. Acta* **2005**, *50*, 3891.

[135] Ray, S. S. and Okamoto, M. *Prog. Polym. Sci.* **2003**, *28*, 1539.

[136] Nicholas, C. V.; Wilson, D. J.; Booth, C.; Giles, J. R. M. *Br. Polym. J.* **1988**, *20*, 3, 289.

[137] *Chen*-Yang, Y. W.; Hwang, J. J.; Huang, A. Y. *Macromolecules* **2000**, *33*, 4, 1237.

[138] Bissessur, R.; DeGroot, D. C.; Schindler, J. L.; Kannewurf, C. R.; Kanatzidis, M. G. *J. Chem. Soc. Chem. Commun.* **1993**, *8*, 687.

[139] Liu, P.; Ong, K.; Xiao, P.; Xiao, M. *J. Mater. Chem.* **2000**, *10*, 933.

[140] Kloprogge, J. T.; Frost, R. L.; Hickey, L. *Thermochim. Acta.* **2000**, *345*, 145.

[141] Meyer, H.; Weiss, A.; Besenhard, J. O. *Mat. Res. Bull.* **1978**, *13*, 913.

[142] Liu, Z-H; Wang, Z-M; Yang, X.; Ooi, K. *Langmuir* **2002**, *18*, 4926.

[143] Paulsdorf, J.; Burjanadze, M.; Hagelschur, K.; Wiemhofer, H.-D. *Solid State Ionics* **2004**, *169*, 25.

[144] Nakajima, T.; Mabuchi, A.; Hagwara, R. *Carbon* **1988**, *26*, 357.

[145] Hutchison, J. C.; Bissessur, R.; Shriver, D. F. *American Chemical Society Symposium Series on "Nanotechnology-Molecularly Designed Material"* **1996**, *622*, 264.

Reproduced with permission of the copyright owner. Further reproduction prohibited without permission.

[146] Scully, S. F., Synthesis and Characterization of Hectorite and Graphite Oxide Nanocomposite Materials. *Honours Thesis*, UPEI, **2005**.

[147] Acosta, J. L. and Morales, E. *J. Appli. Polym. Sci.* **1996**, *60*, 8, 1185.

Reproduced with permission of the copyright owner. Further reproduction prohibited without permission.

Appendix

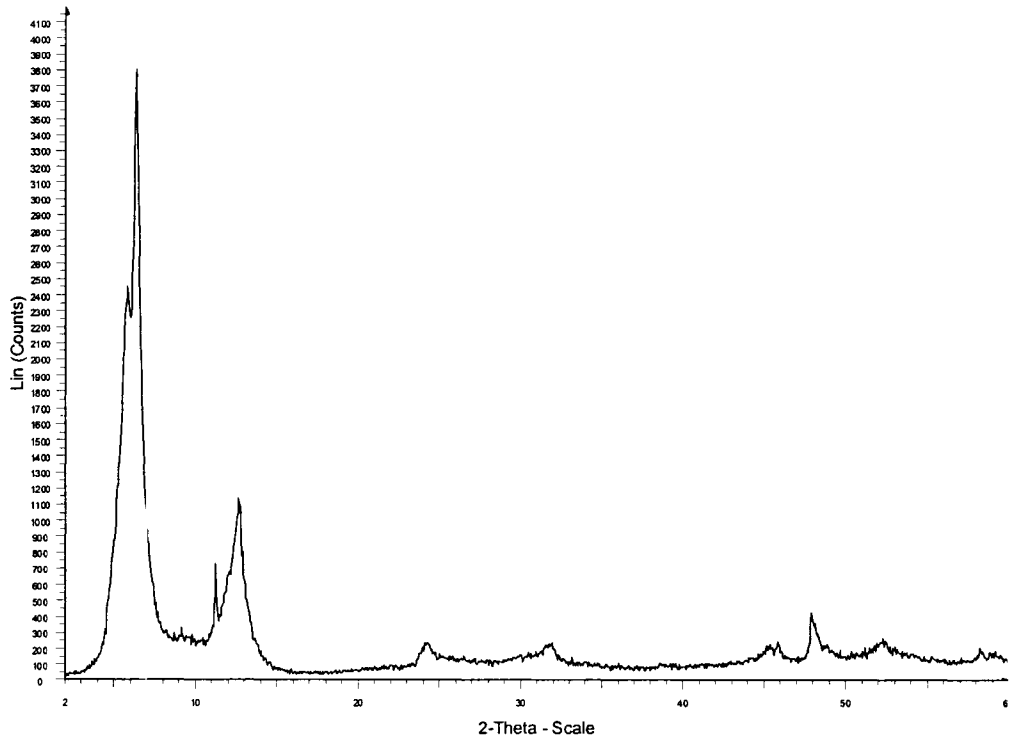

Figure A1 – XRD of Poly(2-methylaniline)/FeOCl

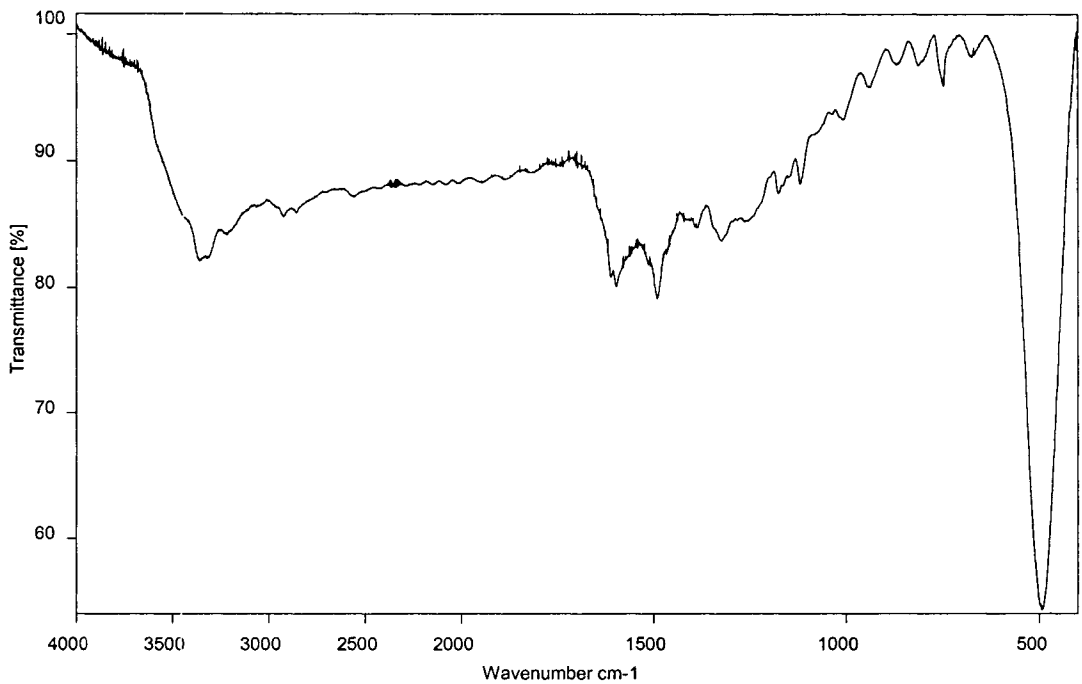

Figure A2- FTIR of Poly(2-methylaniline)/FeOCl

Reproduced with permission of the copyright owner. Further reproduction prohibited without permission.

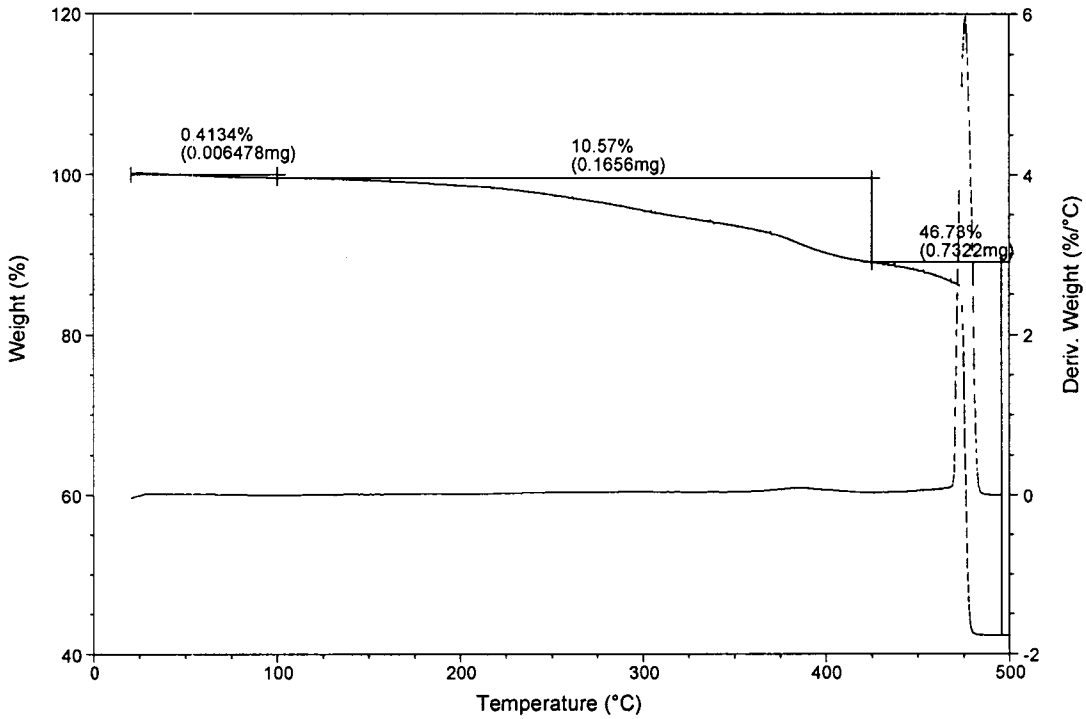

Figure A3 – TGA of Poly(2-methylaniline)/FeOCl

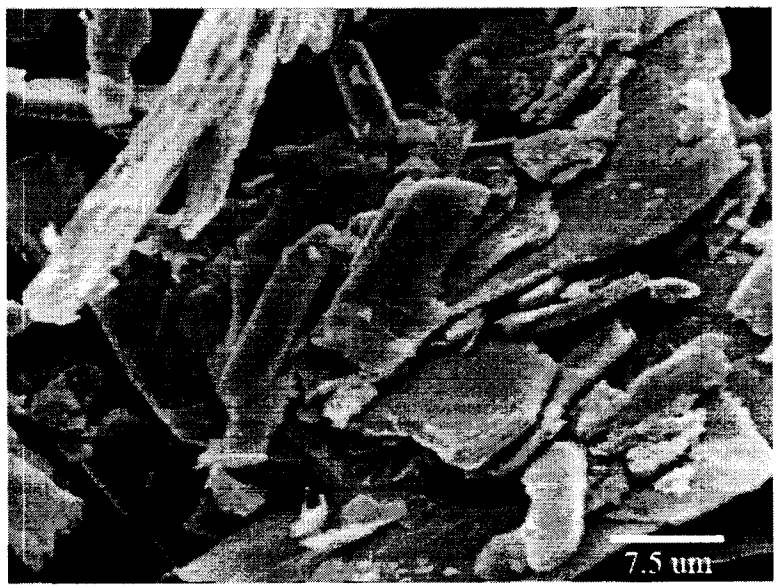

Figure A4 – SEM of Poly(2-methylaniline)/FeOCl (2000x)

Reproduced with permission of the copyright owner. Further reproduction prohibited without permission.

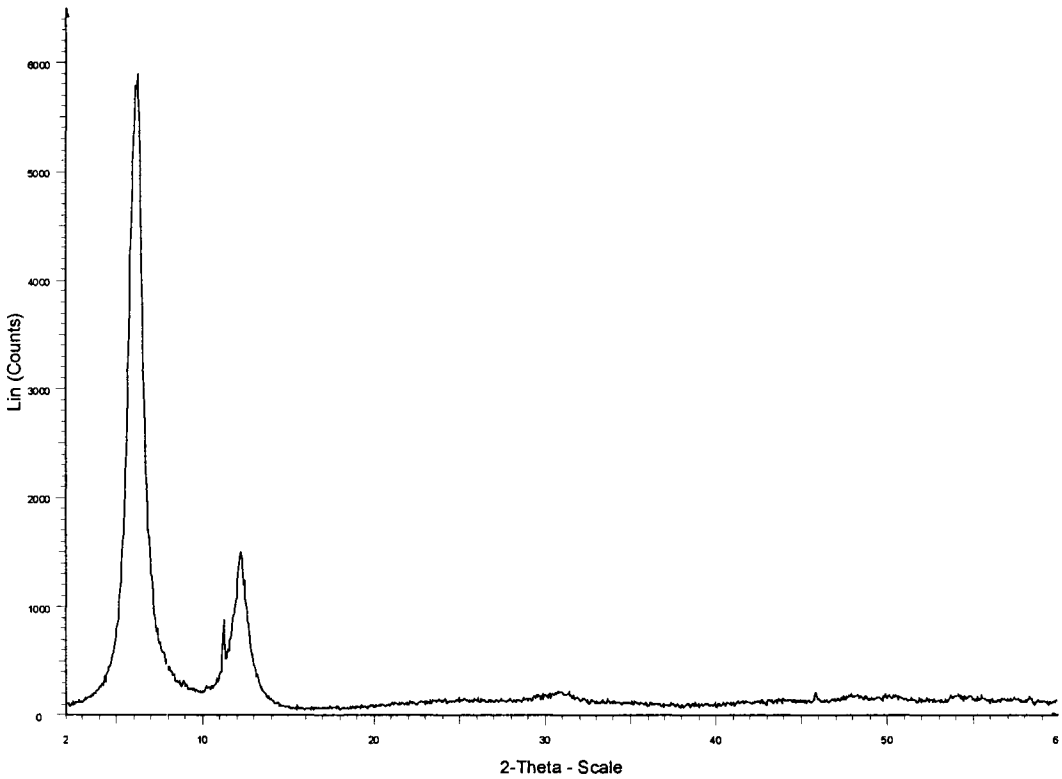

Figure A5 – X-ray Diffraction of Poly(2-ethylaniline)/FeOCl

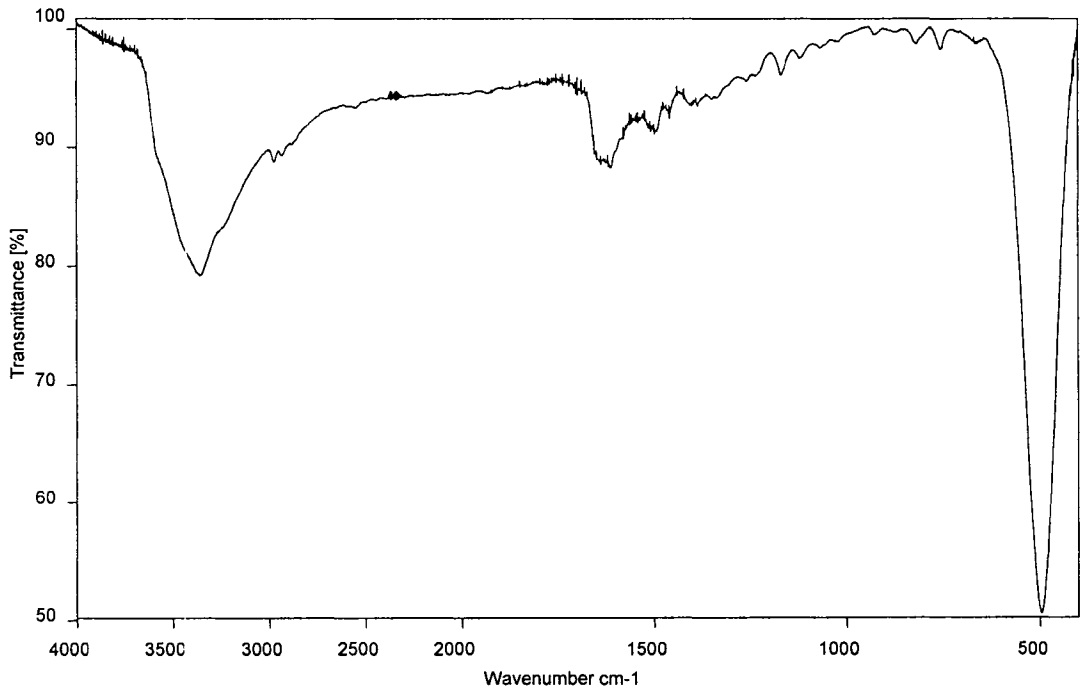

Figure A6 – FTIR of Poly(2-ethylaniline)/FeOCl

Reproduced with permission of the copyright owner. Further reproduction prohibited without permission.

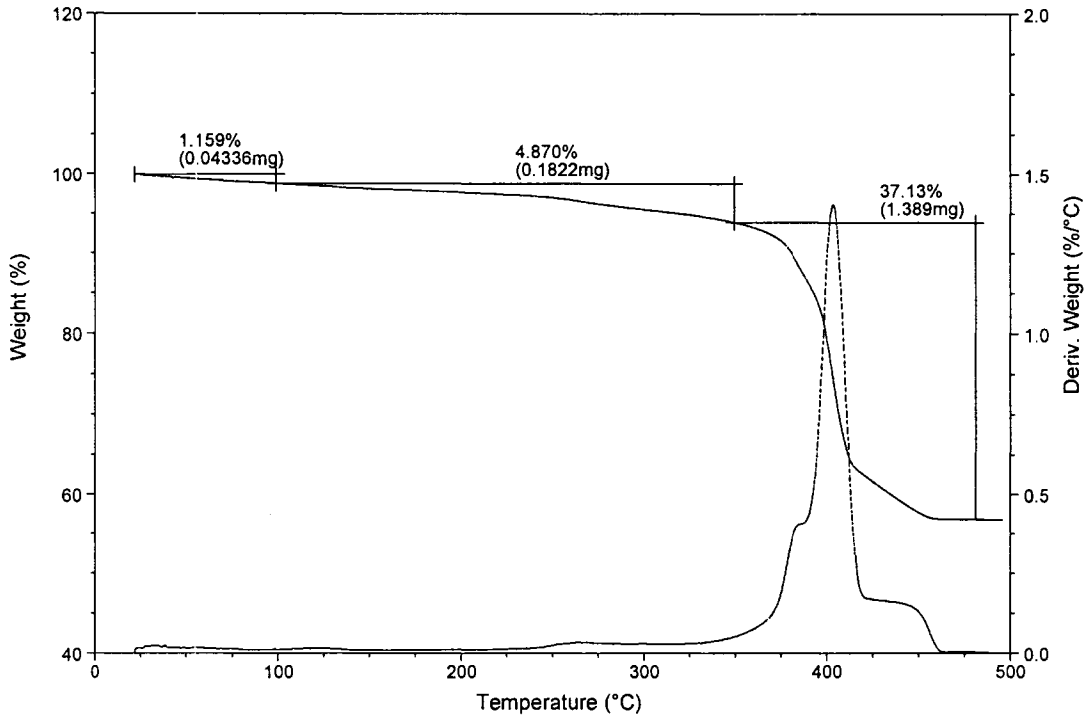

Figure A7 – TGA of Poly(2-ethylaniline)/FeOCl

Figure A8 – SEM of Poly(2-ethylaniline)/FeOCl (2000x)

Reproduced with permission of the copyright owner. Further reproduction prohibited without permission.

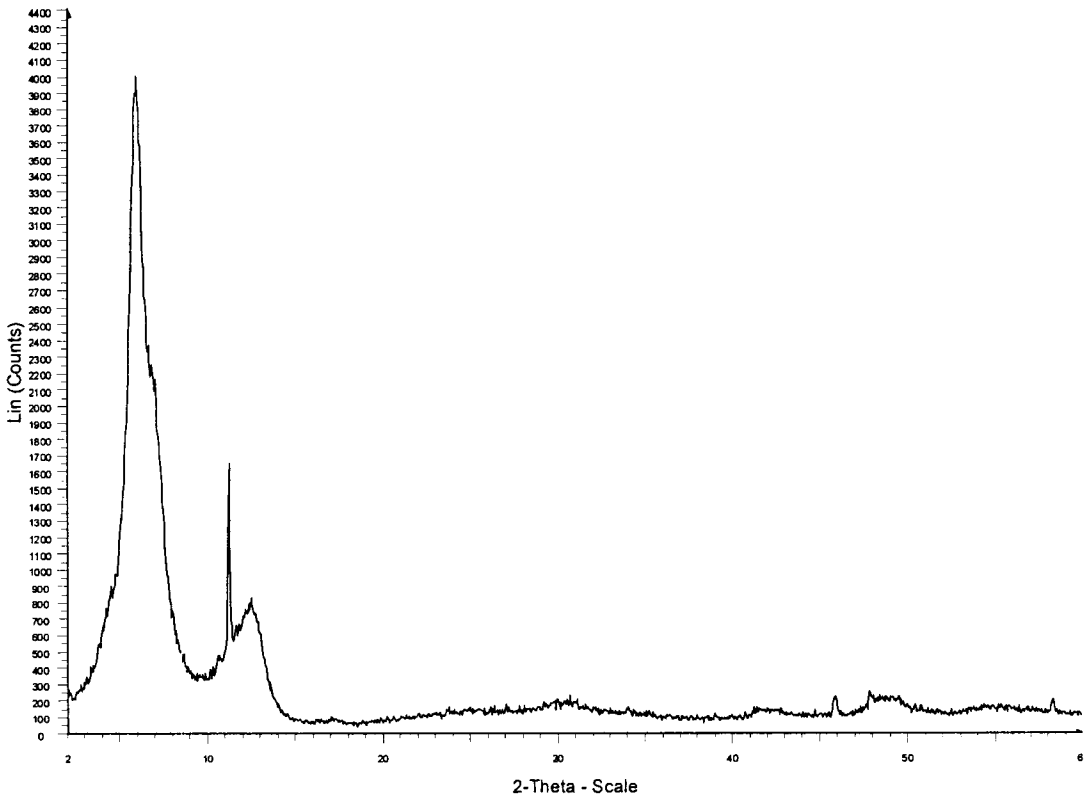

Figure A9 – X-ray Diffraction of Poly(2-propylaniline)/FeOCl

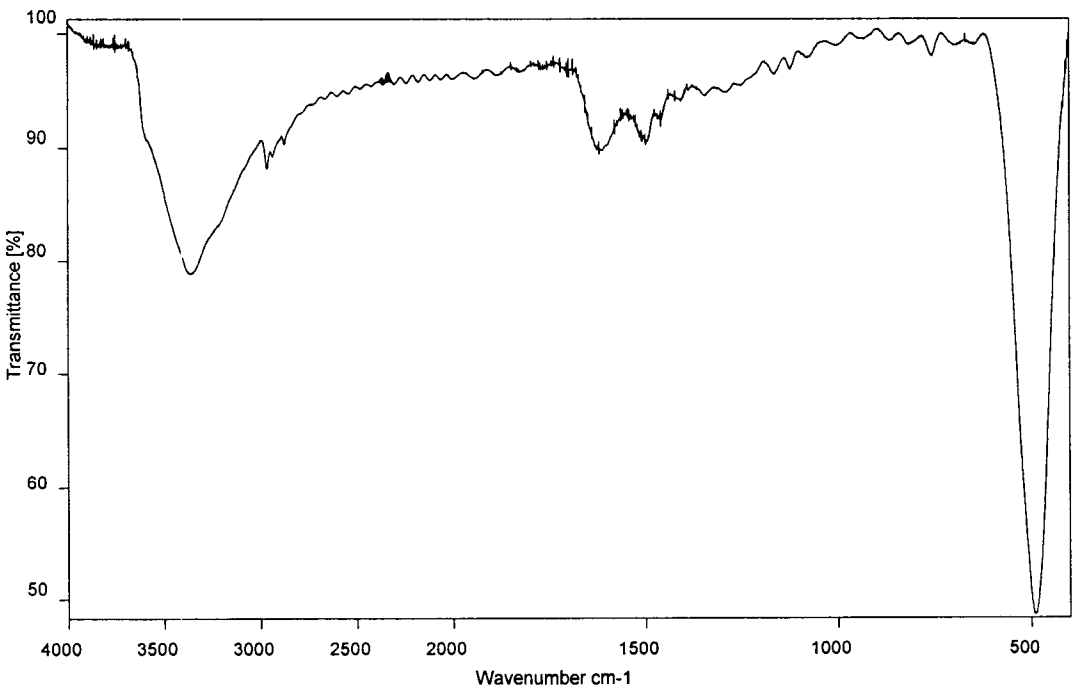

Figure A10 – FTIR of Poly(2-propylaniline)/FeOCl

Reproduced with permission of the copyright owner. Further reproduction prohibited without permission.

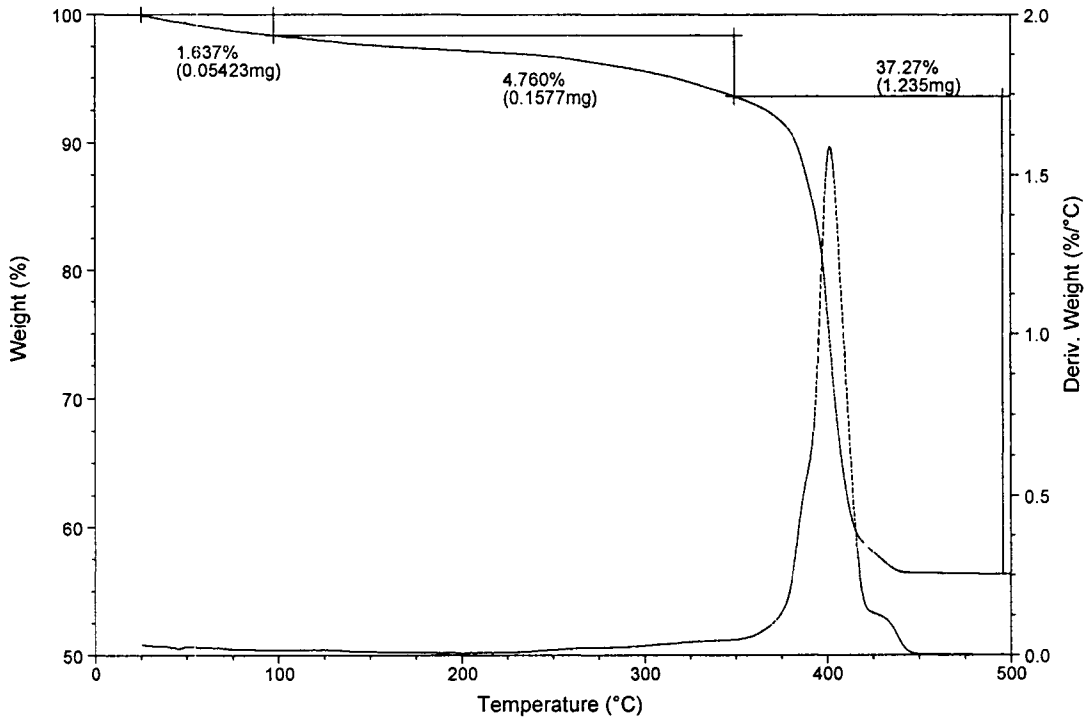

Figure A11 – TGA of Poly(2-propylaniline)/FeOCl

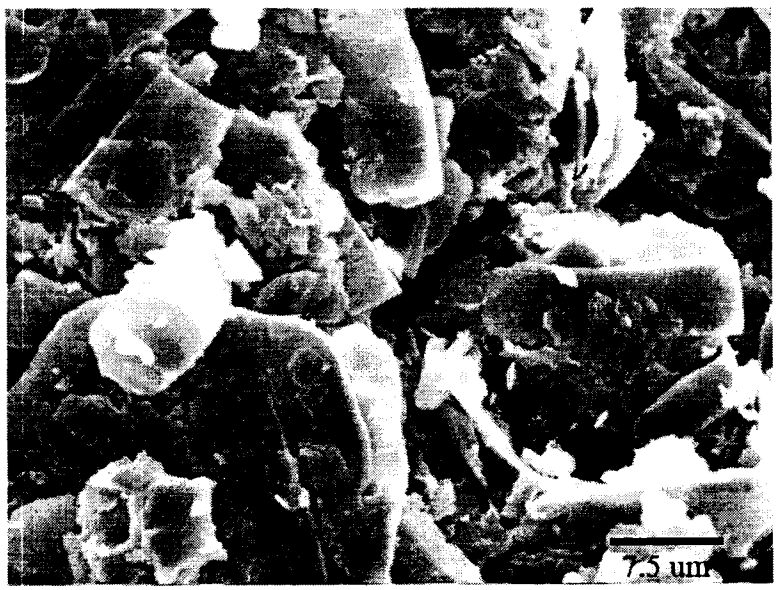

Figure A12 – SEM of Poly(2-propylaniline)/FeOCl (2000x)

Reproduced with permission of the copyright owner. Further reproduction prohibited without permission.